TRPV1 Sensitization in Primary Sensory Neurons

TRPV1 Sensitization in Primary Sensory Neurons

A dissertation presented

by

Jared Sprague

to

The Biological Sciences of Dental Medicine Program

in partial fulfillment of the requirements

for the degree of

Doctor of Philosophy

in the subject of

Biological Sciences of Dental Medicine

Harvard University

Cambridge, Massachusetts

May 2014

Dissertation Advisor: Professor Clifford J. Woolf Jared Sprague

TRPV1 Sensitization in Primary Sensory Neurons

Abstract

Pain is a major personal and community burden throughout the world with currently limited treatment options for persistent pain due to unacceptable side effects, dependence or frank inefficacy. It is necessary to understand the anatomical and molecular pathways leading to pain to better cope with the current challenge of treating it.

TRPV1 is a ligand-gated ion channel primarily expressed in small fiber sensory neurons and is important for the transmission of pain sensation in the nociceptors. TRPV1 is activated in response to painful heat and is sensitized through various internal signaling mechanisms. The sensitization of this channel has never been studied in a high-throughput un-biased approach. We developed a method using primary sensory murine neurons in a high-throughput apparatus to examine the sensitization of TRPV1. We applied this method to examine sensitization of TRPV1 over a 24-hour period to discover TRPV1 sensitization following many different compounds, including bortezomib, a proteasome inhibitor used to treat multiple myeloma. This compound frequently causes painful neuropathy in patients. The mechanism of this is unknown, even as it is a dose-limiting effect of this important cancer treatment. As demonstrated further via traditional cell-focused calcium-imaging experiments, bortezomib sensitizes TRPV1 *in vitro.* These results highlight a hypothetical mechanism of the painful aspects of bortezomib-induced polyneuropathy that is TRPV1-sensitization dependent. More pivotally, TRPV1 hyperfunction could drive a calcium-induced toxicity leading to the neuropathy itself.

We additionally investigate experimental approaches for accessing nociceptor inputs via optochemical means as discovered in a zebrafish behavioral assay as well as using a neuronal silencing strategy to show that histamine-dependent and histamine-independent itch are mediated by a separate population of neurons.

Table of Contents

Tables and Figures

Acknowledgments

It would have been impossible to do this work without the help of many incredible people. I thank Dan Smith, Edward Krupat, Bruce Donoff, Howard Howell, Bjorn Olsen, Peter Hauschka, and David Guthrie for early support. My dissertation advisor, Clifford Woolf, has cultivated a perfect place to discover and provided invaluable encouragement and direction. In the lab, I must particularly thank Ajay Yekkirala. As well I thank Christian von Hehn, Cleverton Kleiton Freitas de Lima, Michio Painter, David Roberson, Enrique Jose Cobos del Moral, Takao Omura, Alban Latremoliere, Mike Costigan, Cynita Blalock, Rebecca Innis, Brian Wainger, Liam Browne, Seungkyu Lee, Sebastien Talbot, Cassidy Mellin, Sun Wook Hwang, Lee Barrett, Gabriel Corfas, Robin Kleiman, Seog Bae Oh, David Kokel, Randall Peterson, Johnathan Tran, Cara Piccoli, Elizabeth Buttermore, Wardiya Afshar Saber, Isaac Chiu, Nader Ghasemlou, Christian Brenneis, Sebastien Talbot, Catherine Ward, Nick Andrews, Yung-Chih “Inge” Cheng, Amanda Strominger, Talia Patapoutian, Octavio Viramontes, and Navid Soltani for assistance, advice and help in the lab. Additional thanks to Mik Rinne for helpful discussion. My dissertation advisory committee: Rachelle Gaudet, Gary Yellen and Qiufu Ma, were a great help. I also thank the National Institute of Dental and Craniofacial Research for their support through a Ruth L. Kirschstein National Research Service Award (DE023033-02).

Many thanks to Jonathan Perrino who served as an excellent coach, my parents, parents-in-law and siblings who have all supported and encouraged me and to my children who have cheered for me. And mostly I thank my wife, Laura. She has been there through it all.

Dedication

Dedicated to E, M and Z. Keep discovering.

Introduction

Pain is a massive burden, both for individuals and for society. A recent report of the economic burden of pain estimated indirect and direct costs at over $500 billion per year in the United States[1]. However, personal, non-financial costs can not even be estimated. Activities of daily living are disrupted or altogether stopped. Pain treatment is still inadequate.

The network of neurons that senses, transmits and processes painful or noxious stimuli is a dynamic system. It helps us respond to the environment appropriately, and it also responds to the environment. The cells responsible for initiating nociception are spread throughout the body, maintaining sensitive nerve endings to detect harmful substances. These are primary sensory neurons. Upon recognition of an offending agent, they pass a signal along to cells in the spinal cord, which again relay a message to various cells that traverse the spinal cord and go to the brainstem and brain, or sometimes double back immediately along motor neuron tracks to affect muscle contraction locally.

The neurons that initiate this response are dependent for their function on discrete receptors. These molecular receptors are tiny, but quite effective and include among them TRPV1 (Transient Receptor Potential Vanilloid type 1). These molecular receptors specifically respond to an array of temperatures, chemical stimuli, and mechanical perturbations, initiating a signal which we can interpret with enough resolution to know what is hurting us (whether sharp, hot or cold, for instance) and where.

Our system for sensation can be drastically modulated. At times, the pain we feel is disproportionate to the insult. Wearing a shirt, for instance, after a bad sunburn can be quite painful. Fortunately for us, the painful effects of a sunburn are quite transient. Yet, some people suffer from chronic neuropathic pain due to damaged nerves and may experience pain much more severe than a sunburn to a typically-innocuous insult. The effects of constant or chronic pain are debilitating.

The complexity and variety of natural experience in pain modulation indicates that many pathways regulate the perception of pain. Pain can not be treated based on the intensity alone, but rather, it needs to be treated based on the actual mechanism. Understanding these mechanisms is at the core of my research in the Woolf lab and is an important step to properly treating pain. Over the years, careful observations have built a roster of key receptors, ion channels, soluble mediators, signaling peptides, enzymes, internal signaling pathways, nerve networks, and effector cells in pain biology. Undoubtedly, there are still many more to discover. We have explored many of these connections and pathways even when not specifically focused on pain because we know that biological systems are interconnected. Itch, as an example, is a system that shares common pathways with pain.

Lidocaine is a compound used in dental offices around the world as a local anesthetic. Its primary mode of action is by crossing into the nerve and blocking sodium channels from the inside, preventing the nerve's ability to relay information. In the lab, we have used a compound very similar to lidocaine in its nerve blocking properties with the exception of one: it can not get into a nerve on its own. This makes it a useful experimental tool as it will only get into nerves that are made susceptible to allowing the compound in, determined by the researcher[2]. Using this approach, we were able to explore the anatomical differences

between histamine-dependent and independent itch, showing that these were distinct populations of cells[3].

Understanding the role of cells and pathways in the nervous system has also been studied through the use of a technique call optogenetics. Optogenetics utilizes a *non-native* light-sensitive receptor to make a nerve active[4]. One great advantage of this approach is that a researcher can use a beam of light to activate one nerve at a time, and by watching the downstream effects, come to a conclusion as to what makes that particular nerve important. Optopharmacology is a variation on that theme, combining light with chemicals to activate *native* receptors to better understand the role of those receptors in their natural context. We developed and characterized an optopharmacological tool to activate an ion channel that is important for pain and itch and showed that it works in both fish and mice[5].

Being able to better understand how ion channels contribute to the signals leading to pain is a fundamental part of pain biology. TRPV1 is important for pain activation and also plays a role in itch. It resides in the membrane of a nerve, is opened to allow ions such as calcium or sodium to move across that membrane, generating an electrical signal. It opens in response to heat, acid and also a chemical in hot chili peppers called capsaicin.

Studying TRPV1 biological function is very important for understanding pain. TRPV1 is tuned to become hypersensitive by inflammatory mediators and might become more sensitive in other painful conditions such as neuropathic pain caused by chemotherapy treatment. To contribute to the current understanding of TRPV1 function, we tried a novel approach using primary sensory neurons. We examined these cells in a high-throughput

system to take advantage of the natural expression and signaling pathways of TRPV1 in these native nerves.

We used this approach to ask more of TRPV1 sensitization, but in an unbiased manner. We discovered that TRPV1 function is modulated in response to several different chemotherapeutic agents, including some that have never previously been reported to sensitize TRPV1. The implication of this finding is that TRPV1 may be more responsible for neuropathic pain and neuropathy than previously appreciated following chemotherapy.

Works Cited

1. Gaskin, D. J. & Richard, P. in Reli. Pain Am. A Bluepr. Transform. Prev. Care, Educ. Res. (Committee on Advancing Pain Research, Care, and E. B. on H. S. P.) 259–305 (National Academies Press, 2011).

2. Binshtok, A. M., Bean, B. P. & Woolf, C. J. Inhibition of nociceptors by TRPV1-mediated entry of impermeant sodium channel blockers. Nature 449, 607–10 (2007).

3. Roberson, D. P. et al. Activity-dependent silencing reveals functionally distinct itch-generating sensory neurons. Nat. Neurosci. 16, 910–8 (2013).

4. Boyden, E. S., Zhang, F., Bamberg, E., Nagel, G. & Deisseroth, K. Millisecond-timescale, genetically targeted optical control of neural activity. Nat. Neurosci. 8, 1263–8 (2005).

5. Kokel, D. et al. Photochemical activation of TRPA1 channels in neurons and animals. Nat. Chem. Biol. 9, 257–63 (2013).

Chapter 1: Chemotherapy-induced neuropathy and TRPV1

Chemotherapy-induced neuropathy is a burgeoning health problem. It is a common manifestation of neurotoxicity following treatment for malignancy. One estimate of the prevalence states 1/3 of all patients who have chemotherapy experience chemotherapy-induced neuropathy[1]. The actual symptoms and clinical signs are dependent on the chemotherapeutic agent used, dosing regimen, and previous underlying conditions. The distribution of effects can generally be classified by the types of nerves involved, whether sensory, motor or autonomic. Where sensory nerves are involved, the condition can be quite painful, requiring modification of treatment dose or outright cessation[2]. For some patients, the pain can be severe enough to require cessation of treatment; potentially quite consequential from the perspective of cancer treatment outcomes. The mechanisms of this painful neuropathy are highly varied, and there is no effective treatment.

The modern era has seen dramatic improvements in cancer treatment, extending many lives[3]. The degree to which a cancer therapeutic is effective is wildly dependent on the type of cancer and the stage of progression. Consider metastatic, recurring head and neck cancers as an example: the median survival if left untreated is estimated at about 3-4 months[4], while the effect of treatment on median survival appears to add only an additional 2-3 months of time[5]. Testicular cancer, on the other hand, by natural course a severe cancer in young men (90% 5 year *mortality* rate), currently has a 5-year *cure* rate of 80%[6]. However, with the positive gains in treatment, additional problems surface due to adverse effects of these treatments. Psychological, digestive, hair/skin-related, fatigue, nausea, fertility-related, sleep-disturbance, and taste/oral-changes are just a few types of problems that occur following treatment[8-14]. The prevalence of chemotherapy-induced neuropathy presents a new challenge to understand and

treat the adverse effects of chemotherapeutics without compromising the anti-tumor efficacy of these compounds.

There are several major classes of chemotherapeutics that cause chemotherapy-induced neuropathy. Antibiotic compounds (e.g. doxorubicin, actinomycin D), platinum based compounds (cisplatin, carboplatin, oxaliplatin), alkylating agents (e.g. thiotepa, ifosfamide), antimetabolites (e.g. 5-fluoruracil, tegafur), mitotic spindle inhibitors (e.g. vincristine, taxol), proteasome inhibitors (bortezomib), topoisomerase I inhibitors (e.g. topotecan, irinotecan), and others (e.g. thalidomide, suramin) are many of the different classes of chemotherapeutic agents that cause neuropathy[6].

The actual signs and symptoms can vary dramatically based on the drug of offense. For instance, thalidomide frequently causes a large-fiber neuropathy and axonal degeneration, bortezomib preferentially targets the small fibers with less axonal degeneration, but more direct toxicity on the dorsal root ganglia (DRG) themselves[7]. Paclitaxel-induced neuropathy sometimes comes with the added complication of extreme pruritis, and lenalidomide, a recently introduced analog of thalidomide, does not appear to even be neurotoxic[6,15,16]. For many drugs, actual neuropathy-based effects are still unclear; either potential direct autonomic effects (e.g. sexual dysfunction, orthostatic hypotension, bradycardia, constipation) are attributed to something else, or clinical examinations are not rigorous enough to find the signs of neurological deficits[7]. Neurological symptoms can include numbness, paresthesias, allodynia, hyperalgesia, burning, shooting, and/or lightning-like pain through sensory neuron involvement, ataxia, muscle weakness, and/or tremors through motor fibers, and constipation, impotence, orthostasis, and/or bradycardia via autonomic fiber neuropathy[2,7].

Patients receiving these drugs can first begin to experience symptoms within days to months following the induction of a treatment regime[7]. Once the drug is stopped, the symptoms will typically abate. Notable exceptions to this being the platinum-based compounds as well as thalidomide. In cases from the late 1950's and early 1960's when thalidomide was a popular nocturnal sedative, thalidomide-induced neuropathy persisted following cessation of treatment for three years or more[17].

Neuropathy is coincident with many conditions, not only chemotherapy treatment. Diabetes mellitus is the most common risk factor for neuropathy in general[18]. Roughly a quarter to a third of all persons with diabetes have neuropathy. Based on the estimate of people to have diabetes in the year 2030 of 366 million, more than 80 million will live with neuropathy as a result of diabetes alone[19,20]. Other risk factors and causes for neuropathy include nerve trauma, nerve entrapment, multiple sclerosis, postherpetic neuralgia, stroke, alcoholism, neoplasms, non-alcoholic liver disease, systemic amyloidosis, Sjögren's syndrome, environmental and pharmacological toxins, HIV, hereditary conditions, Lyme disease, hemochromatosis, vitamin B6 toxicity, thyroid disfunction, and gammopathies[21-23].

Presumably, a better understanding of why peripheral neurons are so susceptible to toxicity as well as the mechanisms of various neuropathies will lead to increasing treatment success. Anatomically, peripheral sensory neurons are very unique. Instead of being protected by the blood-brain barrier, these cells are highly susceptible to compounds in the blood and extracellular space. A highly fenestrated capillary network surrounds and bathes dorsal root ganglia neurons in the contents of the blood[24]. Additionally, neurons in the periphery are highly susceptible to disruptions in the energy supply chain due to their length, which can be over a meter. The peripheral terminal of nerve fibers are highly susceptible to neuropathy and also

heavily dependent on mitochondrial power. The elevated energy demands of distal epidermal nerve fibers could be due to the necessity to constantly break down and remodel in the context of tissue (skin) which renews itself every two weeks[25].

Small-fiber neuropathy can be severely painful. Usually, the onset is length-dependent, meaning that the distal tips of the longest nerves are affected first. A typical presentation begins as 'pins and needles' or parasthesias in the toes and then later the hands. The next longest sensory neurons are the intercostal nerves innervating the sternum, the third likeliest place for length-dependent pain. But, the pain can begin in less canonical locations as well[22]. Eventually, this develops into a 'burning', or 'lightning-like' dysesthetic pain and then perhaps severe numbness[26,27]. The occurrence of small-fiber neuropathy does not preclude involvement with the larger fibers (motor or sensory). Interestingly, 25% or more of the time, the actual cause or underlying risk factor of a neuropathy may be completely unknown[28], indicating an opportunity to discover exceptional and specific causal mechanisms.

Do agents or conditions that lead to neuropathy cause a gain-of-function in a similar manner as has been demonstrated with heritable mutations? There are several ion channels that are common on peripheral small-fibers that could be modified to cause pain or perhaps neuropathy when induced by chemotherapy. TRPA1, $Na_V1.7$, and $Na_V1.8$ have been shown to have a role in pain production in models of diabetic neuropathy via activation and modulation by methylglyoxal [29-31]. Evidence has accumulated for the role of TRPA1 and sodium channels in instances of oxaliplatin- and bortezomib-induced cold allodynia[32-34]. Paclitaxel-induced mechanical allodynia is partially blocked by the TRPA1 antagonist, HC-030031 and partially blocked by the TRPV4 antagonist, HC-067047, suggesting that both ion channels play a role in the painful phenotype following paclitaxel therapy[35].

These studies demonstrate the importance of ion channel function in the context of neurotoxicity. Ion channels play a key role in sensory transduction including in the detection of noxious stimuli such as extreme heat, cold, or mechanical insults. The TRP (Transient Receptor Potential) channels include a diverse array of sensation-capable structures. They play roles in vision, smell, hearing, touch, and pain[36,37]. The TRP vanilloid type 1 (TRPV1) is widespread among sensory neurons, is a non-selective cation channel that responds to heat, protons, capsaicin (the pungent ingredient of chili peppers), and other substances[38]. TRPV2, TRPV3, and TRPV4 also play a role in thermal sensation. TRPA1, which comes from the ankyrin transmembrane protein related group of channels (TRPAs) has a critical for chemosensation in nociceptors. It responds to a variety of pungent compounds such as mustard oil and wasabi[39]. TRPM8 (melastatin related TRP) responds to noxious cold[40]. Other channels are important as well for the transmittance of sensory signals such as voltage-gated sodium channels, $Na_V1.7$ and $Na_V1.8$, mentioned previously.

As one of the main complaints of small-fiber neuropathy is pain, it is relevant to look at these particular channels in the context of pain, both chemotherapy-related and otherwise. The *in vitro* function of naturally occurring mutated versions of $Na_V1.7$, for instance, correlates with several atypical conditions and the levels of pain experienced. Nonsense mutations within this gene cause a complete insensitivity to pain[41-43], while gain-of-function mutations result in conditions marked by spontaneous, extreme pain[44]. Examining the mutated versions of these channels in a heterologous expression system showed characteristics diagnostic of hypersensitivity, either impaired inactivation of sodium currents, increased resurgent currents, or the neurons had depolarized resting potentials, rendering them hyperexcitable[28].

Pain is not the only thing connected to malfunctioning ion channels. In the case of $Na_v1.7$ and $Na_v1.8$, it appears as though there is some overall role of the channel in the development of neuropathy itself, perhaps by depolarizing resting membrane potentials or a generally incrased excitability of sodium currents[28,45,46]. Blocking these channels with tetrodotoxin confers neuroprotective effects, possibly by limiting their activity and preventing subsequent apoptotic pathways from activating[47].

Ion channel disturbances have been directly connected with neuropathy. Recent work has connected cases of idiopathic small-fiber neuropathy with malfunctioning $Na_v1.7$ and $Na_v1.8$ channels. Previously it was shown that $Na_V1.7$ gain-of-function mutations result in painful conditions known as paroxysmal extreme pain disorder and inherited erythromelalgia[48]. The function of these sodium channels alone predicted hypo- or hyper-sensitivity to pain. Depolarized resting membrane potentials and general hyperexcitability of sodium currents could initiate apoptotic pathways if additional metabolic demand is added on top, and again, using TTX (tetrodotoxin) to block sodium channels conferred protection on these cells[47].

Another channel that was mentioned previously and extensively-studied in the context of heat hypersensitivity is TRPV1. It has not, however, been so explored in the context of chemotherapy-induced neuropathy. TRPV1 is expressed in a large proportion of the peptidergic small-diameter c-fibers, with cell bodies located in the dorsal root and trigeminal ganglia of the peripheral nervous system and fiber endings spread throughout the skin, joints, muscles and visceral tissue[49]. TRPV1 is also located centrally in the thalamus, locus coeruleus, periaqueductal grey, and cortex[51-54]. As was mentioned previously, TRPV1 is responsive to noxious heat, pH changes, and various endogenous and exogenous ligands.

Due to TRPV1's ability to detect a variety of noxious stimulants, it is referred to as a 'gateway' to the pain pathway or as a coincidence detector[55,56].

Additional evidence of the importance of TRPV1 in painful conditions is the demonstrated increase of TRPV1 protein expression following experimental inflammatory conditions[57] as well as the increased expression in the case of painful clinical conditions such as esophageal inflammation, irritable bowel syndrome or interstitial cystitis[58,59]. Moreover, knocking out or knocking down TRPV1 partially protects animals from mechanical, thermal and chemical pain[60-65]. As well, blocking TRPV1 pharmacologically with antagonists results in a similar reduction of pain-like behaviors in animal models of pain[66-68].

The implication of TRPV1 in the development of burning pain following chemotherapeutic treatment is intellectually satisfying, but its role is still largely unknown in the context of chemotherapy-induced neuropathy. TRPV1 has been shown to be necessary for heat hyperalgesia for a cisplatin-induced *in vivo* neuropathy animal model[**69**], while an earlier study showed that TRPV1 knockout animals were not less, but more susceptible to a cisplatin-induced model of thermal and mechanical hyperalgesia[**60**]. In a cisplatin-induced hearing loss model, knocking down TRPV1 did confer some benefit to the animal's ability to hear, suggesting that TRPV1 malfunction contributes to neurotoxicity[70]. Other cases indicate a sensitization of TRPV1 function following chemotherapy such as increased CGRP release following capsaicin-stimulation of neurons in culture and increased expression levels along with paclitaxel-induced thermal hyperalgesia reversed by TRPV1 antagonists[71,72]. The mechanical-, cold- and heat hyperalgesia following paclitaxel treatment are mediated via mast cell-based sensitization of TRPV1 among other TRP channels V4 and A1[73].

If TRPV1 plays a key role in the development of pain and/or neuropathy following chemotherapy, then a diverse array of modulators exists already as treatment options[74]. While TRPV1 antagonists have not been particularly effective analgesics[75], there have been promising advances in development that are still playing out[76]. An additional, more tangential strategy for dampening the role of TRPV1 in pain is by modifying or reducing its capacity for sensitization. Interfering with an important TRPV1 scaffolding protein diminishes pain behaviors in a formalin-injection model of spontaneous pain[77]. The scaffolding protein involved, AKAP79/150, was previously shown to be a convergent pathway of sensitization for PKA, PKC, and PIP2 based modulation of TRPV1[78-81].

There is no single pathway for pain processing; in the brain or in the periphery. It is important to note, some of the most painful conditions may actually be independent of 'normal' nociceptors, instead coming through the large, myelinated and fast Aβ fibers (trigeminal neuralgia, for instance[82]). After nociceptors synapse onto neurons within the central nervous system, neurons traversing the spinothalamic and spinoreticulothalamic tracts pass along pain signal to the thalamus and brainstem[83]. There are many different regions involved in the processing of pain, all receiving parallel inputs[84,85]. In similar fashion, there are multiple pathways to neuropathy following chemotherapy. And likely, of necessity, many pathways to treatment, some effective under some conditions, and some in others.

Conclusion

Pain and nociception typically serve a vital and useful purpose. Aberrant nociceptive feedback in the case of neuropathic pain can be severely debilitating, as is the case with peripheral small-fiber painful neuropathy due to chemotherapy. The increasing incidence of chemotherapy-induced neuropathy calls for a deeper understanding of the mechanisms of

pathology. Increasing our understanding of the roles of ion channels on neuronal function in health and disease is an important piece in grasping the big picture of neuropathy.

Chemotherapeutic-induced pathology represents a relatively recent and shifting set of scientific problems. A clearer understanding of the pathology and progression of symptoms following chemotherapy could aid in the development of suitable countermeasures for patients. Additional awareness of chemotherapy-induced neuropathy during the development could help find drugs that have similar cancer treatment profiles as drugs already in use, but without the adverse effects, although it is difficult to imagine. Fortunately, there appears to be no limit to the options ahead of us[86,87]. Neuropathic pain is one example of the dreadful impact of chemotherapy treatment. It is still not well understood how the particular chemotherapeutics lead to the development of pain or neuropathy. Mitigating the development or blocking the pain would have a profound impact on quality of life in cancer patients. In a respect, as pain can be dose-limiting, properly dealing with it may have an impact on survival-based outcomes. TRPV1 function is potentially an important part of the development of neuropathy following treatment by certain chemotherapeutics.

Works Cited

1. Bhagra, A. & Rao, R. D. Chemotherapy-induced neuropathy. Curr. Oncol. Rep. 9, 290–299 (2007).

2. Han, Y. & Smith, M. T. Pathobiology of cancer chemotherapy-induced peripheral neuropathy (CIPN). Front. Pharmacol. 4, 156 (2013).

3. American Cancer Society. Cancer Facts & Figures 2014. (2014).

4. Murphy, B. A. To treat or not to treat: balancing therapeutic outcomes, toxicity and quality of life in patients with recurrent and/or metastatic head and neck cancer. J. Support. Oncol. 11, 149–159 (2013).

5. Morton, R. P. et al. Cisplatinum and Bleomycin for advanced or recurrent squamous cell carcinoma of the head and neck: a randomised factorial phase III controlled trial. Cancer Chemother. Pharmacol. 15, 283–289 (1985).

7. Delforge, M. et al. Treatment-related peripheral neuropathy in multiple myeloma: the challenge continues. Lancet Oncol. 11, 1086–95 (2010).

8. Olver, I. N. Update on anti-emetics for chemotherapy-induced emesis. Intern. Med. J. 35, 478–481 (2005).

9. Carey, M. P. & Burish, T. G. Etiology and treatment of the psychological side effects associated with cancer chemotherapy: a critical review and discussion. Psychol. Bull. 104, 307–25 (1988).

10. Roscoe, J. a et al. Cancer-related fatigue and sleep disorders. Oncologist 12 Suppl 1, 35–42 (2007).

11. Sonis, S. T. Mucositis as a biological process: a new hypothesis for the development of chemotherapy-induced stomatotoxicity. Oral Oncol. 34, 39–43 (1998).

12. Lampe, H., Horwich, a, Norman, a, Nicholls, J. & Dearnaley, D. P. Fertility after chemotherapy for testicular germ cell cancers. J. Clin. Oncol. 15, 239–45 (1997).

13. Goldberg Arnold, R. J. et al. Clinical implications of chemotherapy-induced diarrhea in patients with cancer. J. Support. Oncol. 3, 227–232 (2005).

14. Hofman, M. et al. Cancer patients' expectations of experiencing treatment-related side effects: a University of Rochester Cancer Center--Community Clinical Oncology Program study of 938 patients from community practices. Cancer 101, 851–7 (2004).

15. Briani, C. et al. Lenalidomide in patients with chemotherapy-induced polyneuropathy and relapsed or refractory multiple myeloma: results from a single-centre prospective study. J. Peripher. Nerv. Syst. 18, 19–24 (2013).

16. Glantz, M. J. et al. Phase I study of weekly outpatient paclitaxel and concurrent cranial irradiation in adults with astrocytomas. J. Clin. Oncol. 14, 600–9 (1996).

17. Fullerton, P. M. & O'Sullivan, D. J. Thalidomide neuropathy: a clinical electrophysiological, and histological follow-up study. J. Neurol. Neurosurg. Psychiatry 31, 543–51 (1968).

18. Baldereschi, M. et al. Epidemiology of distal symmetrical neuropathies in the Italian elderly. Neurology 68, 1460–7 (2007).

19. Wild, S., Sicree, R., Roglic, G., King, H. & Green, A. Global prevalence of diabetes: estimates for the year 2000 and projections for 2030. Diabetes Care 27, 1047–1053 (2004).

20. Callaghan, B. C., Cheng, H. T., Stables, C. L., Smith, A. L. & Feldman, E. L. Diabetic neuropathy: clinical manifestations and current treatments. Lancet Neurol. 11, 521–34 (2012).

21. Freeman, R. Not all neuropathy in diabetes is of diabetic etiology: differential diagnosis of diabetic neuropathy. Curr. Diab. Rep. 9, 423–31 (2009).

22. Lacomis, D. Small-fiber neuropathy. Muscle Nerve 26, 173–88 (2002).

23. Bouhassira, D. et al. Development and validation of the Neuropathic Pain Symptom Inventory. Pain 108, 248–57 (2004).

24. Olsson, Y. Topographical Differences in the Vascular Permeability of the Peripheral Nervous System. Acta Neuropathol. 10, 26–33 (1968).

25. Bennett, G. J., Liu, G. K., Xiao, W. H., Jin, H. W. & Siau, C. Terminal arbor degeneration--a novel lesion produced by the antineoplastic agent paclitaxel. Eur. J. Neurosci. 33, 1667–76 (2011).

26. Devigili, G. et al. The diagnostic criteria for small fibre neuropathy: from symptoms to neuropathology. Brain 131, 1912–25 (2008).

27. Colvin, L. A., Johnson, P. R. E., Mitchell, R., Fleetwood-Walker, S. M. & Fallon, M. From Bench to Bedside: A Case of Rapid Reversal of Bortezomib-Induced Neuropathic Pain by the TRPM8 Activator, Menthol. J. Clin. Oncol. 26, 4519–4520 (2008).

28. Faber, C. G. et al. Gain of function Nav1.7 mutations in idiopathic small fiber neuropathy. Ann. Neurol. 71, 26–39 (2012).

29. Eberhardt, M. J. et al. Methylglyoxal activates nociceptors through transient receptor potential channel A1 (TRPA1): a possible mechanism of metabolic neuropathies. J. Biol. Chem. 287, 28291–306 (2012).

30. Andersson, D. a et al. Methylglyoxal evokes pain by stimulating TRPA1. PLoS One 8, e77986 (2013).

31. Bierhaus, A. et al. Methylglyoxal modification of Nav1.8 facilitates nociceptive neuron firing and causes hyperalgesia in diabetic neuropathy. Nat. Med. 18, 926–33 (2012).

32. Trevisan, G. et al. Novel therapeutic strategy to prevent chemotherapy-induced persistent sensory neuropathy by TRPA1 blockade. Cancer Res. 73, 3120–31 (2013).

33. Nassini, R. et al. Oxaliplatin elicits mechanical and cold allodynia in rodents via TRPA1 receptor stimulation. Pain 152, 1621–31 (2011).

34. Adelsberger, H. et al. The chemotherapeutic oxaliplatin alters voltage-gated Na(+) channel kinetics on rat sensory neurons. Eur. J. Pharmacol. 406, 25–32 (2000).

35. Materazzi, S. et al. TRPA1 and TRPV4 mediate paclitaxel-induced peripheral neuropathy in mice via a glutathione-sensitive mechanism. Pflugers Arch. 463, 561–9 (2012).

36. Corey, D. P. et al. TRPA1 is a candidate for the mechanosensitive transduction channel of vertebrate hair cells. Nature 432, 723–30 (2004).

37. Minke, B. & Cook, B. TRP channel proteins and signal transduction. Physiol. Rev. 82, 429–72 (2002).

38. Lee, Y., Lee, C. & Oh, U. Painful Channels in Sensory Neurons. Mol. Cells 20, 315–324 (2005).

39. da Costa, D. S. M. et al. The involvement of the Transient Receptor Potential A1 (TRPA1) in the maintenance of mechanical and cold hyperalgesia in persistent inflammation. Pain 148, 431–7 (2010).

40. Dhaka, A. et al. TRPM8 is required for cold sensation in mice. Neuron 54, 371–8 (2007).

41. Cox, J. J. et al. An SCN9A channelopathy causes congenital inability to experience pain. Nature 444, 894–8 (2006).

42. Goldberg, Y. P. et al. Loss-of-function mutations in the Nav1.7 gene underlie congenital indifference to pain in multiple human populations. Clin. Genet. 71, 311–9 (2007).

43. Ahmad, S. et al. A stop codon mutation in SCN9A causes lack of pain sensation. Hum. Mol. Genet. 16, 2114–21 (2007).

45. Persson, A.-K. et al. Sodium channels contribute to degeneration of dorsal root ganglion neurites induced by mitochondrial dysfunction in an in vitro model of axonal injury. J. Neurosci. 33, 19250–61 (2013).

46. Hoeijmakers, J. G. J. et al. Small nerve fibres, small hands and small feet: a new syndrome of pain, dysautonomia and acromesomelia in a kindred with a novel NaV1.7 mutation. Brain 135, 345–58 (2012).

47. Banasiak, K. J., Burenkova, O. & Haddad, G. G. Activation of voltage-sensitive sodium channels during oxygen deprivation leads to apoptotic neuronal death. Neuroscience 126, 31–44 (2004).

48. Dib-Hajj, S. D., Cummins, T. R., Black, J. a & Waxman, S. G. Sodium channels in normal and pathological pain. Annu. Rev. Neurosci. 33, 325–47 (2010).

49. Szallasi, A. & Blumberg, P. M. Vanilloid (Capsaicin) receptors and mechanisms. Pharmacol. Rev. 51, 159–212 (1999).

51. Sasamura, T., Sasaki, M., Tohda, C. & Kuraishi, Y. Existence of capsaicin-sensitive glutamatergic terminals in rat hypothalamus. Neuroreport 9, 2045–2048 (1998).

52. Tóth, A. et al. Expression and distribution of Vanilloid Receptor 1 (TRPV1) in the adult rat brain. Brain Res. Mol. Brain Res. 135, 162–8 (2005).

53. McGaraughty, S. et al. Antagonism of TRPV1 receptors indirectly modulates activity of thermoregulatory neurons in the medial preoptic area of rats. Brain Res. 1268, 58–67 (2009).

54. Roberts, J. C., Davis, J. B. & Benham, C. D. [3H]Resiniferatoxin autoradiography in the CNS of wild-type and TRPV1 null mice defines TRPV1 (VR-1) protein distribution. Brain Res. 995, 176–183 (2004).

55. Caterina, M. J. & Julius, D. The vanilloid receptor: a molecular gateway to the pain pathway. Annu. Rev. Neurosci. 24, 487–517 (2001).

56. Ramsey, I. S., Delling, M. & Clapham, D. E. An introduction to TRP channels. Annu. Rev. Physiol. 68, 619–47 (2006).

57. Ji, R.-R., Samad, T. A., Jin, S.-X., Schmoll, R. & Woolf, C. J. p38 MAPK activation by NGF in primary sensory neurons after inflammation increases TRPV1 levels and maintains heat hyperalgesia. Neuron 36, 57–68 (2002).

58. Homma, Y. et al. Increased mRNA expression of genes involved in pronociceptive inflammatory reactions in bladder tissue of interstitial cystitis. J. Urol. 190, 1925–31 (2013).

59. Akbar, A. et al. Increased capsaicin receptor TRPV1-expressing sensory fibres in irritable bowel syndrome and their correlation with abdominal pain. Gut 57, 923–9 (2008).

60. Bölcskei, K. et al. Investigation of the role of TRPV1 receptors in acute and chronic nociceptive processes using gene-deficient mice. Pain 117, 368–76 (2005).

61. Everaerts, W. et al. The capsaicin receptor TRPV1 is a crucial mediator of the noxious effects of mustard oil. Curr. Biol. 21, 316–21 (2011).

62. Chen, Y., Willcockson, H. H. & Valtschanoff, J. G. Influence of the vanilloid receptor TRPV1 on the activation of spinal cord glia in mouse models of pain. Exp. Neurol. 220, 383–90 (2009).

63. Katanosaka, K. et al. Contribution of TRPV1 to the bradykinin-evoked nociceptive behavior and excitation of cutaneous sensory neurons. Neurosci. Res. 62, 168–75 (2008).

64. Banik, R. K. & Brennan, T. J. Trpv1 mediates spontaneous firing and heat sensitization of cutaneous primary afferents after plantar incision. Pain 141, 41–51 (2009).

65. Christoph, T. et al. Silencing of vanilloid receptor TRPV1 by RNAi reduces neuropathic and visceral pain in vivo. Biochem. Biophys. Res. Commun. 350, 238–43 (2006).

66. Lehto, S. G. et al. Antihyperalgesic Effects of (R,E)-N-(2-Hydroxy-2,3-dihydro-1 H-acrylamide (AMG8562), a Novel Transient Receptor Potential Vanilloid Type 1 Modulator That Does Not Cause Hyperthermia in Rats. J. Pharmacol. Exp. Ther. 326, 218–229 (2008).

67. Honore, P. et al. Repeated dosing of ABT-102, a potent and selective TRPV1 antagonist, enhances TRPV1-mediated analgesic activity in rodents, but attenuates antagonist-induced hyperthermia. Pain 142, 27–35 (2009).

68. Ghilardi, J. R. et al. Selective blockade of the capsaicin receptor TRPV1 attenuates bone cancer pain. J. Neurosci. 25, 3126–31 (2005).

69. Ta, L. E. et al. Transient Receptor Potential Vanilloid 1 is essential for cisplatin-induced heat hyperalgesia in mice. Mol. Pain 6, 15 (2010).

70. Mukherjea, D. et al. Short interfering RNA against Transient Receptor Potential Vanilloid 1 attenuates cisplatin-induced hearing loss in the rat. J. Neurosci. 28, 13056–65 (2008).

71. Pittman, S. K., Gracias, N. G., Vasko, M. R. & Fehrenbacher, J. C. Paclitaxel alters the evoked release of calcitonin gene-related peptide from rat sensory neurons in culture. Exp. Neurol. 253C, 146–153 (2013).

72. Hara, T. et al. Effect of paclitaxel on Transient Receptor Potential Vanilloid 1 in rat dorsal root ganglion. Pain 154, 882–889 (2013).

73. Chen, Y., Yang, C. & Wang, Z. J. Proteinase-activated Receptor 2 sensitizes Transient Receptor Potential Vanilloid 1, Transient Receptor Potential Vanilloid 4, and Transient Receptor Potential Ankyrin 1 in paclitaxel-induced neuropathic pain. Neuroscience 193, 440–451 (2011).

74. Kym, P. R., Kort, M. E. & Hutchins, C. W. Analgesic potential of TRPV1 antagonists. Biochem. Pharmacol. 78, 211–6 (2009).

75. Kort, M. E. & Kym. in Prog. Med. Chem. (Lawton, G. & Witty, D. R.) 57–68 (Elsevier B.V., 2012).

76. Reilly, R. M. et al. Pharmacology of modality-specific Transient Receptor Potential Vanilloid-1 antagonists that do not alter body temperature. J. Pharmacol. Exp. Ther. 342, 416–28 (2012).

77. Fischer, M. J. M., Btesh, J. & McNaughton, P. A. Disrupting Sensitization of Transient Receptor Potential Vanilloid Subtype 1 Inhibits Inflammatory Hyperalgesia. J. Neurosci. 33, 7407–7414 (2013).

78. Schnizler, K. et al. Protein kinase A anchoring via AKAP150 is essential for TRPV1 modulation by forskolin and prostaglandin E2 in mouse sensory neurons. J. Neurosci. 28, 4904–17 (2008).

79. Jeske, N. A., Patwardhan, A. M., Henry, M. A. & Milam, S. B. Fibronectin stimulates TRPV1 translocation in primary sensory neurons. J. Neurochem. 108, 591–600 (2009).

80. Zhang, X., Li, L. & McNaughton, P. a. Proinflammatory mediators modulate the heat-activated ion channel TRPV1 via the scaffolding protein AKAP79/150. Neuron 59, 450–61 (2008).

81. Jeske, N. A. et al. A-kinase anchoring protein 150 mediates Transient Receptor Potential family V type 1 sensitivity to phosphatidylinositol-4,5-bisphosphate. J. Neurosci. 31, 8681–8 (2011).

82. Bowsher, D. Trigeminal neuralgia: an anatomically oriented review. Clin. Anat. 10, 409–415 (1997).

83. Basbaum, A. I., Bautista, D. M., Scherrer, G. & Julius, D. Cellular and molecular mechanisms of pain. Cell 139, 267–84 (2009).

84. Peyron, R. et al. Mechanical allodynia in neuropathic pain. Where are the brain representations located? A positron emission tomography (PET) study. Eur. J. Pain 17, 1327–37 (2013).

85. Apkarian, A. V., Bushnell, M. C., Treede, R.-D. & Zubieta, J.-K. Human brain mechanisms of pain perception and regulation in health and disease. Eur. J. Pain 9, 463–84 (2005).

86. Cragg, G. M., Grothaus, P. G. & Newman, D. J. Impact of natural products on developing new anti-cancer agents. Chem. Rev. 109, 3012–43 (2009).

87. Harvey, A. L. Natural products in drug discovery. Drug Discov. Today 13, 894–901 (2008).

Chapter 2: Kinetic high-throughput imaging of primary sensory neurons*

Abstract

We describe a dynamic high-throughput paradigm to identify small molecules and peptides that target murine primary sensory neurons. The method allows for the study of protein targets in their native cells, improving on current methods focused on heterologous expression systems. These approaches are flexible as a primary screen, or they can be used to study additional functional characteristics of neurons, while profoundly reducing the time and effort spent in conducting traditional microscopy-based experiments.

Introduction

There has been an explosion of various “omics” datasets that presents a complex network of protein and pathway interactions in systems neurobiology[1]. To explore this complexity, there is a pressing need to study receptor-ligand interactions in concert with their pathways in an efficient and high-throughput fashion. In the past decade, the emergence of high-throughput screening (HTS) technologies that utilize sophisticated robots and process ~100,000 reactions a day has had a profound impact on basic biology and drug discovery[2]. However, these endeavors have been limited to heterologous expression systems, commonly in HEK or CHO cells for at least two reasons: 1) these cell lines are easily scalable to an experiment requiring large amounts of cells, and 2) a specific target protein can be expressed in these cells to study its effects individually. However, such an approach requires that the experimenter knows the target *a priori* and the artificial environment does not lead to spurious results. By using primary neurons, there is an additional world of potential targets, that can lead to the study of

---

* Work attribution - This work was done in close collaboration with Ajay Yekkirala. We jointly performed the dissections and optimization of the imaging technology together. Takao Omura and Michio Painter provided sciatic nerve crush pre-conditioned animals and neurons for measuring neurite outgrowth.

physiologically relevant pathways and signal cascades. An additional advantage of using primary neurons is the existence of a native 'supporting cast' of scaffolds, signaling molecules, etc., ensuring the most appropriate post-translational state (**Table 2.1**). Hence, a method to study receptors and pathways in primary cultured neurons is highly desirable. To address this critical issue, we describe a dynamic high-throughput paradigm that can be applied to primary sensory neurons; we show that it is feasible, robust, versatile, and efficient.

Methods

Dissection and culture

Male adult C57Bl/6 mice were purchased from Jackson Laboratories and housed in the animal facilities of Children's Hospital Boston on a 12 hour alternating light-dark cycle. Animals for imaging were dissected after 7 weeks of age. After CO_2 asphyxiation and cervical translocation, and following spinal laminectomy, the left and right dorsal root ganglia (DRG) from the whole spine were removed and placed in 4ºC Hanks buffered saline solution without calcium and magnesium (HBSS, Life Technologies). After the DRG were collected and spun down for 3 minutes at 1000 rpm (150 g), they were placed in a collagenase/dispase solution (3 mg/mL dispase II and 1 mg/mL collagenase A, Roche Applied Science) and allowed to incubate at 37°C for 90 minutes. After incubation the cells were washed in Dulbecco's Modified Eagle's Medium (DMEM, Life Technologies), fortified with 4.5 g/L D-glucose, L-glutamine, 110 mg/L sodium pyruvate, 10% fetal bovine serum (Life Technologies), penicillin (500 U/mL, cellgro), and streptomycin (500 μg/mL, cellgro). DNAse (125 U/mL, Sigma) was then added and the solution was triturated using successively smaller caliber flame-polished pasteur pipettes. This solution was gently layered onto a bovine serum albumin gradient (10% albumin from bovine serum, Sigma in PBS, Life Technologies) and spun at 150 g for 12 minutes. After removal of the supernatant, the cells were washed again in DMEM, suspended

in neurobasal medium (Life Technologies) supplemented with L-glutamine (20 mM, Life Technologies), B-27 supplement (Life Technologies), penicillin (500 U/mL, cellgro), and streptomycin (500 μg/mL, cellgro) and then plated onto laminin-treated (1 mg/mL, Sigma) 15 mm glass-bottom dishes (MatTek Corporation), and then placed in an incubator at 37°C (5% CO2) overnight. All imaging was performed one day post-dissection and culture.

Calcium Imaging

DRG neurons were imaged on a Nikon Ti Eclipse inverted microscope. Fura-2, AM (Life Technologies) was loaded into the neurons for 30 minutes (room temperature, 4 μg/mL). After washing with standard extracellular solution (Boston BioProducts), the cells were imaged using a QImaging EXi Aqua cooled camera and data was collected and analyzed using NIS Elements software (AR 3.10). Neurons were selectively exposed to various solutions via a gravity-assisted perfusion system. Responses were included if they were 20% greater than baseline.

Statistical parameters for assay development

The Z-factor is a statistical measure to determine the suitability of a high-throughput assay for finding 'hits'. It incorporates the variability of both positive and negative controls to determine how 'good' an assay is. We used the Z-factor merely to determine an optimal number of cells to use for this assay. It is calculated with the mean values and standard deviations from positive (μ_p and σ_p) and negative (μ_n and σ_n) controls. Developed by Zhang and colleagues[14], it uses the following formula:

$$Z = 1 - \frac{(3\sigma_p + 3\sigma_n)}{|\mu_p - \mu_n|}.$$

We used the Z-factor to gauge the best number of cells to use per well as a way to optimize the assay for direct activation using the best case scenario KCl as an indication of response.

Calcium flux protocol – Hamamatsu

DRG neurons were dissected from adult (~8 week old) C57Bl/6 mice as described above. After dissociation, cells were seeded into 384 well plates coated with laminin (Greiner, Inc.) at 2000 cells/well in a volume of 25 mL/well of neurobasal medium and incubated overnight at 37°C and 5% CO2. The plates were assayed for calcium flux using the FLIPR calcium-5 kit (Molecular devices) in an FDSS-7000Ex apparatus (Hamamatsu) with increasing concentrations of the test ligands. The response was measured in relative fluorescence units (RFU) and the ratio of change in well fluorescence ($Ratio_{max}$ - $Ratio_{min}$)was computed over time. The data was then analyzed as percent of Basal RFU = $(Ratio_{max}\text{-}Ratio_{min})_{treatment/}$ $(Ratio_{max}\text{-}Ratio_{min})_{control}$ x 100 and plotted using Prism 4.0 analysis software (GraphPad, Inc.). For sensitization assays, the potentiation of CAP 100 nM response was computed as % potentiation over control = $((Ratiomax)_{treatment}$ - $(Ratiomax)_{control})/(Ratiomax)_{control}$ x 100 and presented in Prism 4.0.

HT neurite outgrowth assay:

DRG neurons were dissected from naïve and injured Thy1-YFP mice (~8 weeks old) expressing the YFP reporter as described above. After dissociation, cells were seeded into 384 well plates coated with laminin (Greiner, Inc.) at 2000 cells/well in neurobasal media (50 mL/well) and incubated overnight at 37°C and 5% CO_2. The plates were then assayed for YFP reporter expression (Ex/Em = 488 nm/509 nm) in an FDSS-7000Ex apparatus (Hamamatsu) after adding 5mL of trypan blue to quench any well autofluorescence. The response was measured as Relative Fluorescence Units (RFU) and plotted using Prism 4.0 analysis

software (GraphPad, Inc.).

Sciatic nerve crush

Surgeries for peripheral injury were performed as published previously[3]. The sciatic nerve was clamped with a smooth forceps (5/45, Fine Scientific Tools) for 30s at the level of the proximal thigh, to inflict injury. A 10-0 nylon suture was knotted to the epineurium to mark the crush site. All procedures were performed under anesthesia.

Efficiency Model

We used three main components to estimate the amount of time per mouse. They are: time for dissection (T_d), time for culture (T_c), and time for imaging (T_i). Each component occupies its own amount of time dependent on the method of imaging employed. In the high-speed format, equation (1) can approximate the amount of time (hours) by each set of mouse DRG neurons included in the experiment:

$$t = \frac{m}{2} + \frac{1}{2}\left\lceil \frac{m}{3} \right\rceil + 3\left\lceil \frac{m}{3} \right\rceil + \left\lceil \frac{26m}{384} \right\rceil + \frac{1}{15}\left\lceil \frac{26m}{384} \right\rceil \qquad (1)$$

If m = the number of mice used for dissections, $T_d = \frac{m}{2} + \frac{1}{2}\left\lceil \frac{m}{3} \right\rceil$, $T_c = \left\lceil \frac{26m}{384} \right\rceil$ and

$T_i = \left\lceil \frac{26m}{384} \right\rceil + \frac{1}{15}\left\lceil \frac{26m}{384} \right\rceil$.

Comparing this model with traditional microscopy-based experiments, the main differences are in the T_i parameter. Assuming *t(m)* is the total time required as a function of number of mice, the model is shown by the following formula (2):

$$t = m + 3m + \frac{1}{2}\left(\frac{26m}{3}\right) + \frac{1}{4}(26m) \qquad (2)$$

The greatest difference between these two models is the necessity of imaging experiments in series in the traditional calcium imaging setup, while such experiments can be done in parallel in the high-throughput method. However, there are additional time-based advantages aside from this, including the increased efficiency of dissecting and culturing of DRG neurons from several mice in one session.

Results

The first step towards establishing this method required insight into the practical issue of numerical feasibility. For HTS experiments with cultured cells in 384-well plates, cells are typically seeded at a density of around 20,000 cells/ well. However, given that we typically

Mammalian cell lines	Primary sensory neurons
Immortal and can be passaged	Cannot be passaged; single use
Easy to grow in large numbers	Smaller numbers (~50K neurons/ mouse); dissections and cultures require skilled technicians
Easy to introduce protein target of interest	Contains the full complement of receptors and signaling molecules
Artificial environment: untenable for studying pathways due to potential spurious interactions	Native environment: amenable for studying cellular pathways and downstream signaling events
Artificial environment: limited testing capability	Native environment: cells can be used to test multiple endpoints - calcium flux, neurite outgrowth, ion channel sensitization, etc.

Table 2.1 - Comparison between mammalian cell line and primary sensory neurons.

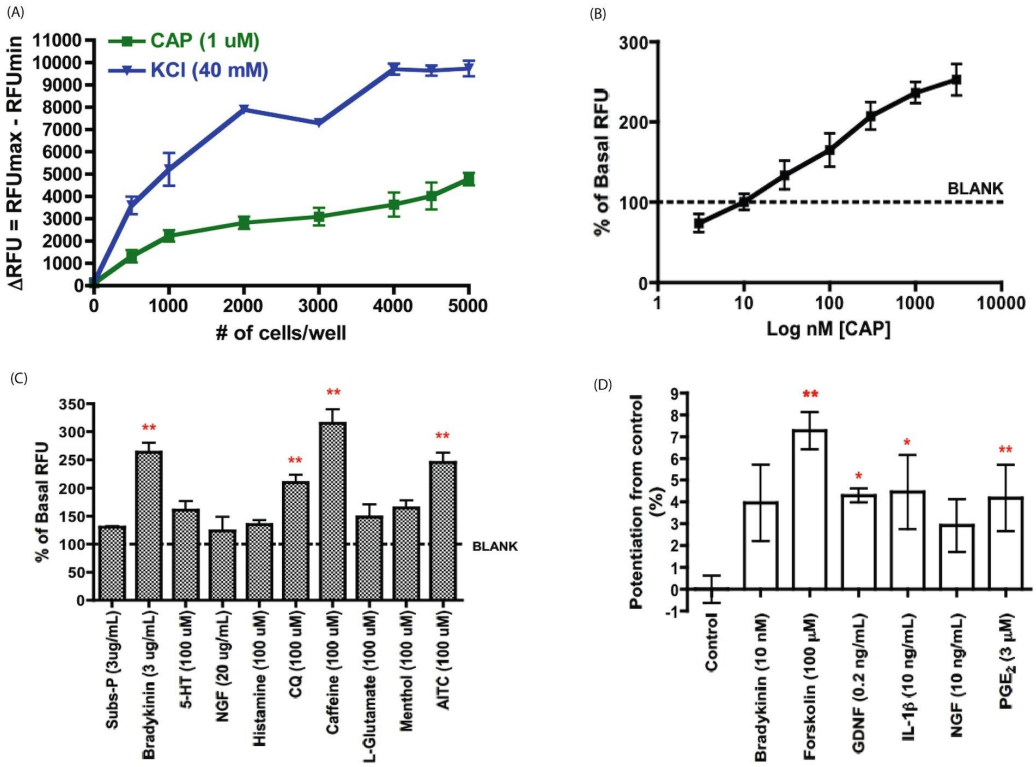

Figure 2.1 - Calcium flux method was established for DRG neurons in a 384-well format. (A) Cells were seeded in a range of 0 to 6000 cells/well in 384-well black, clear-bottom plates and tested for calcium flux with KCl and capsaicin. 2000 neurons/well provided robust calcium flux responses for both KCl and capsaicin and became our default cell density for the procedure. (B) Capsaicin concentration-response curve was generated for DRG neurons with an EC_{50} of 121 nM. (C) Small scale screening experiments were performed with a few peptide ligands and small molecules to identify direct activators of sensory neurons. (D) Functional sensitization of TRPV1 channels was interrogated with a 10 minute incubation of known potentiators preceding application of capsaicin (100 nM). Several ligands produced strong potentiation of capsaicin-induced calcium flux. All experiments were performed with three biological replications. Potentiation from control indicates the change (%) of overall signal. One-way ANOVA was performed followed by Dunnett's post-hoc test to evaluate the significance of the results (** denotes $p<0.001$, * denotes $p<0.05$).

extract ~50,000 DRG neurons per adult mouse, we set out to determine the least possible cell density that would provide robust and reproducible calcium ion fluxes. Utilizing the FLIPR calcium 5 kit (Molecular Devices) we seeded freshly-dissociated DRG neurons in increasing density, ranging from 500 cells to 5000 cells/well in a black, clear-bottom 384 well plate (Greiner) treated with laminin (1 mg/mL) (Sigma). After 24 hours, the cells were tested with 40 mM KCl to induce calcium flux in all neurons and 1 μM capsaicin, a transient-receptor

potential vanilloid-1 (TRPV1) receptor agonist[4], in an FDSS 7000ex apparatus (Hamamatsu). Both KCl and capsaicin produced robust calcium flux and clear, cell density-dependent responses (**Figure 2.1a**). We show that 2000 cells is sufficient to achieve a robust Z-score with direct activation using 40 mM KCl[14] (**Supplementary Figure 2.1 and Supplementary Figure 2.2**), increasing our confidence that 2000 cells per well was an appropriate choice for cell density in the case of direct activation. Importantly, since we were able to use as few as 2000 neurons/well we were convinced that, indeed, using primary neurons in an HTS-based experimental setup is quite feasible.

To better understand the optical sensitivity of the cells in individual wells of a 384-well plate, we measured the coverage area of the cultured neurons and response percentage of capsaicin (1 μM), and KCl (40 mM) by using an inverted microscope (Nikon Ti Eclipse) (**Figure 2.2a-c**). Roughly half of all neurons were activated by capsaicin (42 ± 5.3%), corresponding to ~6% of the surface area of the well (**Figure 2.2d**). To further see how the system handles a dynamic range of calcium fluxes, we generated a concentration response curve (CRC) for capsaicin. After four independent biological replicate experiments we calculated an EC_{50} of 127.2 nM (**Figure 2.1b**), which is comparable to the EC_{50} described for capsaicin in cultured cells stably expressing TRPV1 (99-900 nM; ref. 4-6) and in cultured murine neurons (200 nM; ref. 7).

The fact that we are using primary neurons allows for testing receptors and pathways in their native environment - a major advantage when compared with artificial expression in heterologous cell lines. We explored this versatility by assaying for neuronal direct activation and TRPV1 sensitization, as both phenomena have been shown to play important roles in nociception. We observed that several ligands produced visible calcium fluxes upon addition

(**Figure 2.1c**). Moreover, known sensitizers of TRPV1 such as forskolin (100 μM)[8], IL-1β (10 ng/mL), GDNF (0.2 ng/mL), and prostaglandin E_2 (PGE_2) (3 μM)[9] produced statistically significant sensitization of a low capsaicin (100 nM) response after a 10 minute incubation period (**Figure 2.1d**).

Aside from direct activation studies and sensitization, DRG neurons are also frequently assayed for neurite outgrowth in the context of peripheral nerve regeneration and neuropathies[10]. We wanted to gauge if we could rapidly track changes in neurite-outgrowth of DRG neurons in a high-throughput format. A pre-conditioning crush injury to the sciatic nerve

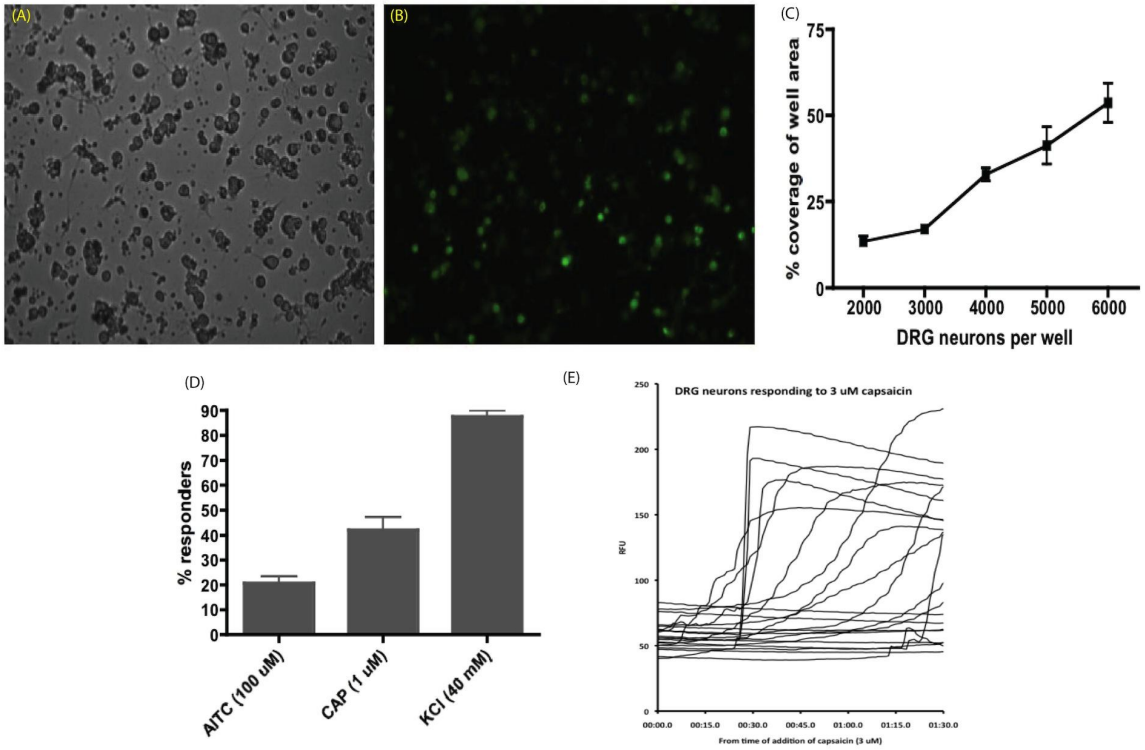

Figure 2.2 - Characteristics of plate coverage and activation. (A) Brightfield image of dorsal root ganglia cells plated at 2000 cells per well. (B) Dorsal root ganglia cells plated and loaded with FLIPR calcium-5 dye (Molecular Devices) viewed by fluorescence at same magnification as in (A). (C) % coverage of well area as calculated using ImageJ software. (D) Complete response percentages among DRG cells for TRPA1 (AITC), TRPV1 (CAP = capsaicin) and KCl (all responsive neurons). (E) representative traces of individual neurons responding to capsaicin (3 μM).

results in increased neurite outgrowth in culture[11]. This phenomenon can be readily observed *in vitro* after plating DRG neurons isolated from L3-L5 ganglia of yellow fluorescent protein (YFP) -reporter mice (Thy1-YFP)[12] with and without sciatic nerve injury. The neurons after preconditioning injury show a marked enhancement in neurite outgrowth, presumably leading to increased well fluorescence (**Figure 2.3a, b**). We again found a cell density of 2000 cells/ well to be optimal for examination of both enhancers and inhibitors of neurite outgrowth (**Figure 2.3c**). At this cell density we observe ~90% increase in well fluorescence from neurons after pre-conditioning injury when compared with neurons from naive mice (**Figure 2.3d**). In addition to this experiment showing increased neuronal growth, we were able to

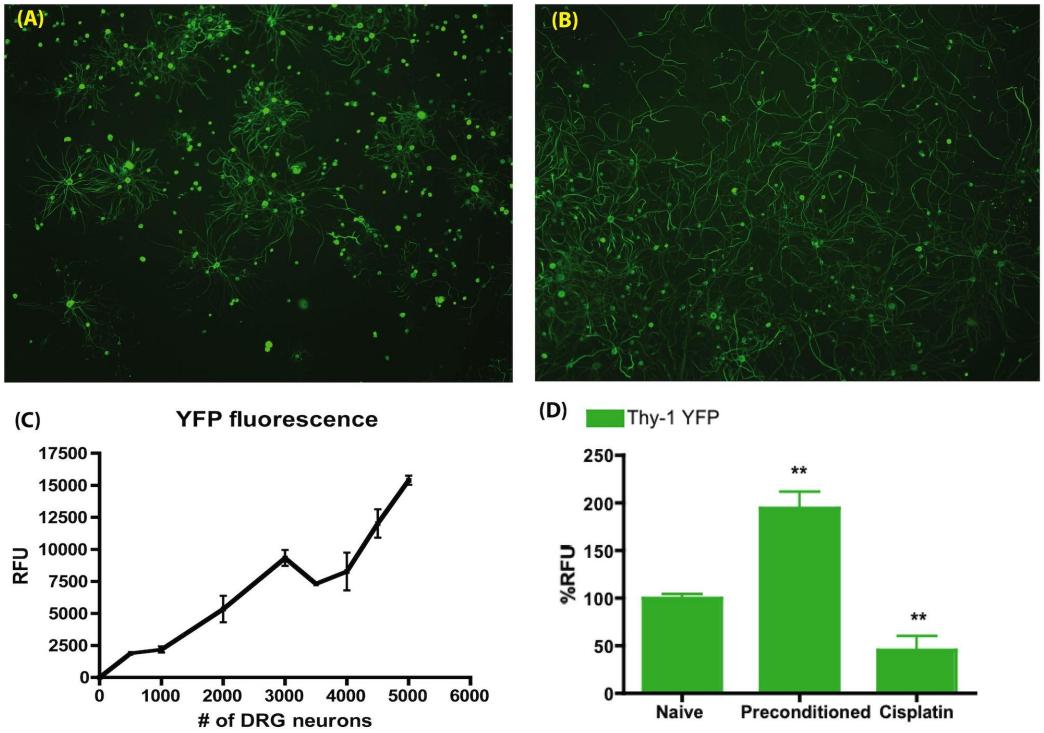

Figure 2.3 - High-throughput neurite outgrowth assay. Purified DRG neurons from a reporter line that labels mechanoreceptors (Thy1-YFP) were seeded into 384-well black clear-bottom plates (Greiner Inc.) before (A, D) and 5 days after a 'preconditioning' sciatic nerve injury (B, D). Eighteen hours later, total well fluorescence was quantified in an FDSS-7000 apparatus (Hamamatsu) and preconditioned neurons showed >90% increase in fluorescence when compared with naïve neurons. Treatment with cisplatin (1 μM), a chemotherapeutic agent, produced ~70% reduction in well fluorescence that correlates well with the loss of neurites; asterisk, P <0.001 (ANOVA followed by Dunnett's test). (C) We quantified the fluorescence intensity vs cell number to identify the number of neurons required for robust response.

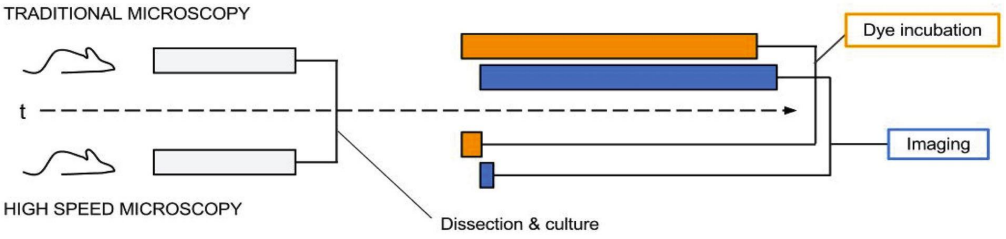

# of Compounds	Mice		Hours	
10	2	2	6	24
30	4	5	10	60
100	12	16	24	190
300	35	48	64	569
1000	116	158	203	1870
3000	347	474	603	5610
10000	1155	1582	2003	17916
	high speed		high speed	

Chart 2.1 - Comparative analysis between traditional and high-throughput imaging methods. The proposed method provides ~ 6-8-fold advantage in total time spent to study similar number of compounds without the need for additional dissections.

reproduce cisplatin-induced reduction of neurite outgrowth (**Figure 2.3d**) as an example of chemotherapeutic-induced neuropathy[13].

The hallmark of this method is the fact that it is a directed approach to study a complex cellular subtype that are sensory neurons in an unbiased, high-throughput format. In generating a concentration response curve for capsaicin, we estimate that we saved over 16 hours of experimentation time. Based on our model of workflow and output, for simple experiments such as direct activation, sensitization or the generation of concentration response curves, this system is extremely time economical (for more complete details on model, see methods section). Importantly, there is little difference in the number of mice that need to be dissected to screen a given number of compounds, but the similarities end there as

we can incubate all the wells in a plate with dye, and read the entire plate at the same time (**Chart 2.1**).

Due to the fact that the output signal in this system is an integrated and simplified trace for a whole population of heterogenous neurons, it is important to note the lack of neuron-specific information. For instance, we are unable to identify the specific percentage or populations (such as small, medium or large) of neurons that are contributing to the measured fluorescence output parameters. An important consideration particularly when DRG neurons are used, is that any non-neuronal cell in culture with DRG neurons can contribute to calcium signals indiscriminately. We propose that these methods be utilized as a primary screen, taking advantage of the speed and volume of compounds that can be tested with relative ease in a primary sensory neuron. The best hits and controls should then be tested by utilizing conventional microscopy techniques, thus serving to validate the data from the unbiased high-throughput method.

Conclusions

Primary sensory neurons provide an intact neuronal environment, independent of heterologous expression, for unbiased screening approaches. Signaling pathways, scaffold proteins, and other necessary molecules are in place to provide proper support for interrogating cellular function, allowing a platform for elemental and unbiased discovery. Indeed, DRG neurons have been used extensively for neurobiological studies via traditional biochemical, microscope-based imaging, and electrophysiological techniques. Given that sensory neurons are of primary importance in heat, cold, pain and itch sensing, to name a few, this high-throughput method will serve to identify biologically relevant endogenous and exogenous ligands that modulate nociception and sensory perception, adding an additional

and important tool to the arsenal of analgesic drug discovery. Generating concentration response curves, assaying direct activation and sensitization, as well as neurite growth assays (even dynamic growth assays where the chamber is incubated) are all possible in primary sensory neurons in an efficient and large-scale manner. The additional context of an intact primary cell also makes this paradigm adaptable for interrogating the intracellular biology of any assay that can be performed, either by blocking specific pathways prior to functional analysis, and/or antagonizing receptor function via pharmacological means in a high-throughput fashion. Moreover, we suggest that our approaches should be utilized for their speed and relative ease to set up, as a primary screen, and then complemented with traditional microscope-based imaging, biochemical, and electrophysiological methods of interrogation. It is conceivable that such a tandem approach has tremendous potential to make quick and efficient neurobiological discoveries in the near future.

Works Cited

1. Joyce, A.R. & Palsson B.Ø. The model organism as a system: integrating 'omics' data sets. *Nat Rev Mol Cell Biol.* 7, 198-210 (2006).

2. Agresti, J.J., et al. Ultrahigh-throughput screening in drop-based microfluidics for directed evolution. *Proc Natl Acad Sci U S A.* 107, 4004-09 (2010).

3. Ma, C.H.E. et al. The BMP coreceptor RGMb promotes while the endogenous BMP antagonist noggin reduces neurite outgrowth and peripheral nerve regeneration by modulating BMP signaling. *J. Neurosci.* 31, 18391–400 (2011).

4. Caterina, M.J., et al. The capsaicin receptor: a heat-activated ion channel in the pain pathway. *Nature* 389, 816-24 (1997).

5. Iida, T., et al. TRPV1 activation and induction of nociceptive response by a non-pungent capsaicin-like compound, capsiate. *Neuropharmacology.* 44, 958-67 (2003).

6. Welch, J.M., Simon, S.A. & Reinhart, P.H. The activation mechanism of rat vanilloid receptor 1 by capsaicin involves the pore domain and differs from the activation by either acid or heat. *Proc Natl Acad Sci U S A.* 97, 13889-94 (2000).

7. Wood, J.N., et al. Capsaicin-induced ion fluxes in dorsal root ganglion cells in culture. *J Neurosci.* 8, 3208-20 (1988).

8. Lopshire, J.C. & Nicol, G.D. The cAMP transduction cascade mediates the prostaglandin E_2 enhancement of the capsaicin-elicited current in rat sensory neurons: whole-cell and single-channel studies. *J. Neurosci*. 18, 6081-6092 (1998).

9. Cheng, J.K. & Ji, R.R. Intracellular signaling in primary sensory neurons and persistent pain. *Neurochem. Res.* 33, 1970-1978 (2008).

10. Seijffers, R., Mills, C.D. & Woolf, C.J. ATF3 increases the intrinsic growth state of DRG neurons to enhance peripheral nerve regeneration. *J. Neurosci.* 27, 7911-7920 (2007).

11. Neumann S. & Woolf, C.J. Regeneration of dorsal column fibers into and beyond the lesion site following adult spinal cord injury. *Neuron*. 23, 83-91 (1999).

12. Nguyen, Q.T., Sanes, J.R. & Lichtman, J.W. Pre-existing pathways promote precise projection patterns. *Nat. Neurosci.* 5, 861-867 (2002).

13. Manji, H. Toxic neuropathy. *Curr. Op. Neurol.* 24, 484–490 (2011).

14. Zhang, J.-H., Chung, T. D. Y. & Oldenburg, K. R. A Simple Statistical Parameter for Use in Evaluation and Validation of High Throughput Screening Assays. J. Biomol. Screen. 4, 67–73 (1999).

Chapter 3: Proteasome inhibition sensitizes TRPV1 in DRG neurons*

ABSTRACT

TRPV1 is a ligand-gated ion channel primarily expressed in small fiber sensory neurons and is important for the transmission of pain sensation in the nociceptors. TRPV1 is activated in response to noxious heat (~42 °C) and is sensitized through various internal signaling mechanisms. The sensitization of this channel has never been studied in a high-throughput un-biased approach. We developed a method using primary sensory mouse neurons in a high-throughput apparatus to examine the sensitization of TRPV1. We applied this method to discover TRPV1 sensitization characteristics following many different compounds, including bortezomib, a proteasome inhibitor used to treat multiple myeloma. This compound frequently causes painful neuropathy in patients. The mechanism of this is unknown, even as it is a dose-limiting effect of this effective cancer treatment. As demonstrated further via traditional cell-focused calcium-imaging experiments, bortezomib sensitizes TRPV1 *in vitro.* These results highlight a hypothetical mechanism of the painful aspects of bortezomib-induced polyneuropathy that is TRPV1-sensitization dependent. More fundamentally, TRPV1 hyperfunction could drive a calcium-induced toxicity leading to the neuropathy itself.

INTRODUCTION

TRPV1 (transient receptor potential vanilloid type 1) is a non-selective cation channel that plays a critical role in the sensation of pain. In the peripheral nervous system it is directly activated by painful heat (~42 °C), protons, and the 'hot' ingredient in chilis, capsaicin[1].

---

* I performed the initial screen of this work jointly with Ajay Yekkirala with the assistance of Navid Soltani. I performed all rig-based calcium imaging and several additional FDSS 7000EX follow-up experiments, sometimes with the assistance of Ajay Yekkirala or Octavio Viramontes. I also performed the qPCR experiments and worked in collaboration with Nick Andrews, Alban Latremoliere, and Catherine Ward, who performed all the behavioral assays.

Functional TRPV1 is a tetrameric ion channel with 6 transmembrane domains for each subunit, plus one pore loop. TRP channels are a group of more than seven subfamilies of 28 different subunit proteins[2]. TRPA, TRPC, TRPL, TRPM, TRPN, TRPP, and TRPV are the various families belonging to the TRP channel group. The first TRP channel was discovered to be important in visual transduction in flies[3]. The particular functions of all members of the TRP family are highly varied, but some of the common elements include six transmembrane domains, the formation of tetramers, and all channels are cation-selective, although the balance between different cations varies[3]. Additional details such as ankyrin repeats and the 'TRP' domain are common elements but vary in details between channels[2-7].

TRPV1 is a remarkable protein for the variety of ways that it can be activated from outside the cell (heat, capsaicin and other compounds, acid), as well, TRPV1 is sensitive to modulation via internal phosphorylation events. PKC, PKA, PI3K, calcineurin, PDK1, and Cdk5 have all been shown to phosphorylate TRPV1 at specific serine and threonine residues[8], leading to attenuated responses[9-14]. Via sensitization, TRPV1 can become more responsive to noxious stimuli (hyperalgesia) or responsive to agonists that normally would not cause pain (hypoalgesia). Some of these agonists may be internal, such as heat or some known activators such as endogenous compounds: including the endocannabinoid, anandamide[15], lipoxygenase products 12-(S)-HPETE, 15-(S)-HPETE, 5-(S)-HETE, 15-(S)-HETE, leukotriene B_4[16], or DAG[17]. TRPV1 activity serves as an archetype for peripheral hypersensitivity; it becomes more responsive due to phosphorylation-based sensitization following NGF, GDNF, IL-1β, PGE_2 and bradykinin[18-22]. TRPV1 is sensitized in cell-based assays by various growth factors, internal signal arachidonic acid metabolites, lipids and other peptides. The sensitization of TRPV1 mirrors what actually happens when these same compounds are injected into the skin of human or animal test subjects; it causes pain hypersensitivity[23-26].

Studying TRPV1 sensitization *in vitro* in the traditional research paradigm has relied on an important cellular phenomenon of TRPV1: the development of short-term desensitization. When TRPV1 is exposed to capsaicin or other agonists it becomes desensitized to further activation by capsaicin in the short-term (minutes)[27]. This process is largely calcium-dependent, relying in part on the protein phosphatase, calcineurin, and calcium-binding protein calmodulin to inhibit TRPV1 activation during a latency phase[4,28-30]. Reverting this process is considered to be sensitization. Typically, blocking desensitization *in vitro* is accomplished by modifying the phosphorylation status of TRPV1[8]. While many compounds have been discovered that modulate the desensitization of TRPV1, it is not clear how these same compounds effect the sensitization of TRPV1 in the absence of desensitization. It is difficult to test multiple varied conditions at once and challenging to examine TRPV1 responsiveness following a lengthy sensitization period (hour+). To address some of these issues, we undertook the task of developing a high-throughput sensitization model of TRPV1 using primary sensory neurons taken from the dorsal root ganglia (DRG). Rather than relying on desensitization, this model would measure the sensitization of TRPV1 directly following exposure to a variety of compounds. Instead of comparing measurements from individual neuronal cells (highly heterogenous), we measured from a population of neurons (2000+ neurons), thus smoothing over any local heterogeneity issues. We utilized a 480-compound library of well-annotated bioactive molecules to look for TRPV1 sensitization following simultaneous exposure to a diverse set of molecules (ScreenWell® ICCB Known Bioactives Library).

We dissected and cultured primary sensory neurons from mice and assayed them in a 384-well format for sensitization of TRPV1 following 24 hour exposure to the 480 compounds in

the BioMol library. This system allows us to test several hundred compounds for TRPV1 sensitization; a phenotypic outcome, in an unbiased manner. By being able to directly assess TRPV1 sensitization independent of desensitization and using native neurons with native amounts of TRPV1 expression with signaling pathways and protein scaffolding intact, we can exploit an opportunity to uncover clinically relevant sensitizers of TRPV1. To our knowledge it is the first attempt to test so broadly for TRPV1 sensitization.

METHODS

Dissection and culture of DRG neurons

Male adult C57Bl/6 mice were purchased from Jackson Laboratories and housed in the animal facilities of Children's Hospital Boston on a 12 hour alternating light-dark cycle. Animals for imaging were dissected after 7 weeks of age similarly to the procedures outlined previously[31]. After CO_2 asphyxiation and cervical translocation, and following spinal laminectomy, the left and right dorsal root ganglia (DRG) from the whole spine were removed and placed in 4 ºC Hanks buffered saline solution (HBSS, Life Technologies). After the DRG were collected and spun down for 5 minutes at 1000 rpm (150 g), they were placed in a collagenase/dispase solution (3 mg/mL dispase II and 1 mg/mL collagenase A, Roche Applied Science) and allowed to incubate at 37°C for 90 minutes. After incubation the cells were washed in Dulbecco's Modified Eagle's Medium (DMEM, Life Technologies), fortified with 4.5 g/L D-glucose, L-glutamine, 110 mg/L sodium pyruvate, 10% fetal bovine serum (Life Technologies), penicillin (500 U/mL, cellgro), and streptomycin (500 μg/mL, cellgro). DNAse (125 U/mL, Sigma) was then added and the solution was triturated using successively smaller caliber flame-polished pasteur pipettes. This solution was gently layered onto a bovine serum albumin gradient (10% albumin from bovine serum, Sigma in PBS, Life Technologies) and spun at 150 g for 12 minutes. After removal of the supernatant, the cells were washed again in DMEM,

suspended in neurobasal medium (Life Technologies) supplemented with L-glutamine (20 mM, Life Technologies), B-27 supplement (Life Technologies), penicillin (500 U/mL, cellgro), and streptomycin (500 μg/mL, cellgro) and then plated onto PDL and laminin-treated (1 mg/mL, Sigma) 15 mm glass-bottom dishes (MatTek Corporation), or placed into laminin-treated 384-well optical plates (Greiner) and then placed in an incubator at 37 °C (5% CO_2) overnight. Plating density in the 15 mm optical plates was between 150-250 cells/μL, while in the 384-well optical plates was 80-120 cells/μL.

FDSS7000EX - 384-well imaging

Cells were plated at 2000 cells/25 μL/well in neurobasal medium (Life Technologies) in laminin-coated (1 mg/mL, Sigma) borosilicate glass-bottomed and black polystyrene cased 384-well plates (Sensoplate, Greiner). Within 3 hours of plating the cells, a 2.5 μL drop of the 384-well screening plate (ICCB, Screen-Well® Bioactive Molecules, plates 3402 and 3403) was added using the FDSS7000EX (Hamamatsu). After overnight incubation at 37 °C with 5% CO_2, the wells were then loaded with 20 μL of FLIPR 5 calcium dye (Molecular Devices). We preloaded all ligand solutions at 5x concentrations in individual v-shaped conical-bottomed 384-well polypropylene plates (Greiner) when we custom prepared the ligand plates. Library-based ligand plates were purchased from the Institute of Chemistry and Cell Biology (ICCB, Harvard Medical School) screening facility. Solutions were added following mechanical trituration from stages 1 and 2 at 10 and 12 μL, and 10 μL/s and 12 μL/s respectively. Solutions were added at a height of 2.4mm from the bottom of the assay plate. Primarily, the drop period with the following 20-30 seconds was sampled at 2.5 Hz, otherwise samples were taken at .33 Hz. The camera used is a digital CCD camera C9100-13 (Hamamatsu) with an exposure time of 200 ms with 2x2 binning. The light source is a LightningCure™ LC8 (Hamamatsu) bulb that was passed through a 472 nm excitation filter and collected at 540 nm.

Solutions of capsaicin (end concentration of 100nM - drop of 10 μL) and KCl (end concentration 5mM for sub-maximal and 40mM for maximal with drop of 12 μL) or HBSS (vehicle for all solutions) were added at various times. The responses were measured as relative fluorescence units, initially captured using FDSS7000EX/uCell software and analyzed on Excel (Microsoft) for area under the curve (AUC), plotted on Prism analysis and visualization software (Graphpad). Data points are collected as relative fluorescence and then are modified to ratio values post-collection. The first frame of each well equals the baseline, and all following responses are calculated as a ratio of the initial fluorescence (Ratio). Percent change of response was calculated as:

$$\frac{R_x - R_y}{R_y} \quad (1)$$

Where R_x is the fluorescence signal of all accumulated signal (AUC) of the treated well, and R_y is the AUC fluorescence ratio signal of the untreated well, but still activated with capsaicin.

In some experiments additional controls were used to calculate the actual % sensitization or desensitization. These required treated controls that, instead of capsaicin agonism following treatment were given vehicle control (HBSS). % sensitization is calculated by first subtracting the treated negative control (vehicle following treatment) from the treated and challenged wells and is referred to as the ΔRatio. The ΔRatio is used as in Formula (1) to calculate % change as an actual sensitization or desensitization of response.

Compound library

The ScreenWell™ ICCB Known Bioreactives Library (BioMol) was purchased through the Assay Development and Screening Facility Core at Boston Children's Hospital who worked with the Institute of Chemistry and Cell Biology at Harvard Medical School (Boston) to

formulate the plate. The BioMol library is a 480-compound library of well-annotated chemicals with diverse topologies and mechanisms of action. The complete list of compounds can be found here: http://iccb.med.harvard.edu/biomol-known-bioactives-2012-list-of-compounds/. The daughter library plate was formed by adding a 30 nL pin drop to 300 μL HBSS for a 10000-fold dilution. This library was kept at 4 °C for 2 weeks and used within that time. Many of the compounds in the Screen-Well® ICCB Known Bioactives (BioMol) Library activate specific signaling pathways and receptors as well-suited experimental compounds in addition to including a large proportion of compounds that are used in the clinic. Although this library is small by industry-standards, it offers a wide and diverse set of topologies and targets, well suited for an experiment in primary sensory neurons[32].

Calcium Imaging

DRG neurons were imaged on a Nikon Ti Eclipse inverted microscope. Fura-2, AM (Life Technologies) was loaded into the neurons for 30 minutes (room temperature, 4 μg/mL). After washing with standard extracellular solution (Boston BioProducts), the cells were imaged using a QImaging EXi Aqua cooled camera and data was collected and analyzed using NIS Elements software (AR 3.10). Neurons were selectively exposed to various solutions via a gravity-assisted perfusion system. Responses were included if they were 20% greater than baseline. The perfusion rate of the solutions was 0.6 mL $\cdot$ min^{-1} and the pencil tip was 150 μm away from the field of view.

Statistics

Comparisons between groups with respective n more than 8 were made using students' t-test. Comparisons of distributions were made using the Kolmogorov-Smirnov test in Stata (StataCorp LP). Quantile-quantile plots were derived in Excel (Microsoft) by interpolation.

RNA extraction

Cells were cultured under standard plating and imaging conditions. After treatment or control, the media is removed and 500 μL TRIzol® (Life Technologies) is added and cells are scraped off and mixed well, incubating at RT for 5 minutes before adding to a -80 °C freezer for at least 1 hour. After thawing, we add 100 μL chloroform to each sample, shake vigorously for 15 seconds, incubate at RT for 3 minutes, and then spin at 4 °C at 12000 g. The aqueous, chloroform phase we transfer to a fresh tube on ice and. 1 μL of GlycoBlue™ (Life Technologies) is added to each sample, then 250 μL of isopropanol is added, and then incubated at least an hour at -80 °C. After thawing, the samples are centrifuged at 12000 g at 4 °C for 20 minutes. The supernatant is removed and discarded and then the samples are washed with 500 μL 75% cold ethanol and then centrifuged at 7400 g at 4 °C for 15 minutes. The ethanol is removed and the pellet allowed to air dry. Each pellet is resuspended in 12.5 μL Nuclease-free water, incubated at RT for 3 minutes, placed on ice and quantified for RNA content using a Nanodrop spectrophotometer.

cDNA synthesis and qPCR

cDNA is prepared using the SuperScript® Vilo cDNA synthesis kit (Life Technologies) according to manufacturer's instructions. qPCR is performed using the TaqMan® probe set for mouse TRPV1 (Mm01246302_m1) and GAPDH (Mm03302249_g1) as control, following manufacturer's instructions (Life Technologies). Fold changes were calculated using the comparative C_T method[33]:

$2^{-(\Delta\Delta C_T)}$ such that $\Delta\Delta C_T$ = ($C_{treatment\_gene}$ - $C_{treatment\_standard}$) - ($C_{control\_gene}$ - $C_{control\_standard}$).

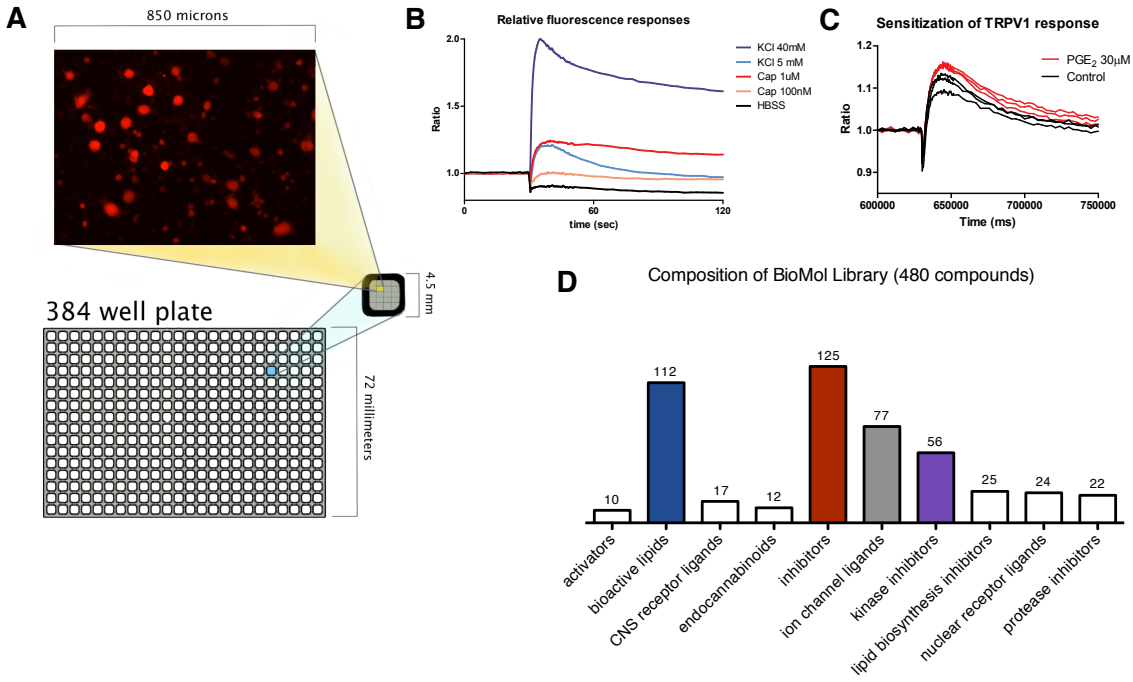

Figure 3.1 - High-throughput sensory neuron imaging. (A) The scale of the 384-well plate setup, showing a blown-up figure of DRG neurons illuminated by fluorescent dye in one portion of a dish. The cells are plated at 2000 neurons/well. (B) Representative traces of activation of wells using high and low capsaicin (1 μM, 100 nM) and KCl (40 mM, 5 mM). (C) Sensitization of capsaicin responses (100 nM) following short-term sensitization via PGE_2 (10 minutes at 30 μM). (D) Basic composition of the ScreenWell® ICCB Known Bioactives Library (BioMol).

RESULTS

TRPV1 activation and sensitization is detectable in a parallel-based imaging system

We examined the effectiveness of the FDSS7000EX (Hamamatsu) dynamic calcium-imaging machine in discerning the sensitization of TRPV1 *in vitro*. The advantage of using DRG neurons is the relatively intact signaling pathways with effector proteins as well as natural expression of TRPV1 on the membrane. Our plating strategy was based on previous experiments showing that 2000 cells per well and 100 nM - 1 μM capsaicin led to the highest calculated z-scores[35]. Hypothesizing that sensitization would cause not only increases in signal from those cells apt to respond, but also responses in cells that would normally not respond at lower concentrations, we used 100 nM capsaicin as the concentration at which we

interrogated our system. **Figure 3.1A** demonstrates the scale of this protocol. At a plating density of 2000 cells per well, we achieved discernible signal for low (100 nM) and high (1 μM) concentrations of capsaicin, as well as very strong responses to low (5 mM) and high (40 mM) KCl (**Figure 3.1B**). High KCl activates all neurons in culture, whereas capsaicin activates about half of neurons at the maximal concentration (1 μM).

We employed a novel approach in examining TRPV1 sensitization: combining parallel processing with a long-term pre-sensitization, independent of desensitization. To cover as much ground as possible, we initiated a 480-compound screen in our 384-well system of a diverse body of drugs, all with robust literature-based annotation associated with them (For general categories: **Figure 3.1D**, for complete list: http://iccb.med.harvard.edu/biomol-known-bioactives-2012-list-of-compounds/).

Many chemotherapeutic agents cause sensitization of TRPV1

Of particular note was the high prevalence of chemotherapeutic agents among the top sensitizing agents (**Figure 3.2C** and **Supplementary Figure 3.1**). This is particularly important in recognition of one of the common adverse events of many chemotherapeutics: neuropathy which is frequently painful. The mechanisms of chemotherapy-induced neuropathic pain are poorly understood and there is no effective treatment[36]. TRPV1 function has been implicated in part, but otherwise very little is known relative to TRPV1 activity in the context of chemotherapy-induced neuropathy[36,37].

Of three proteasome inhibitors included in the BioMol (MG-132, Z-Leu3-VS, and gliotoxin), all three were represented in the most likely candidates to cause sensitization of TRPV1 (**Figure 3.2B** and **Figure 3.3**)[38-40]. Bortezomib (AKA Velcade™ or PS-341) has recently been

approved by the FDA (2003) for the treatment of multiple myeloma and was the first-in-class

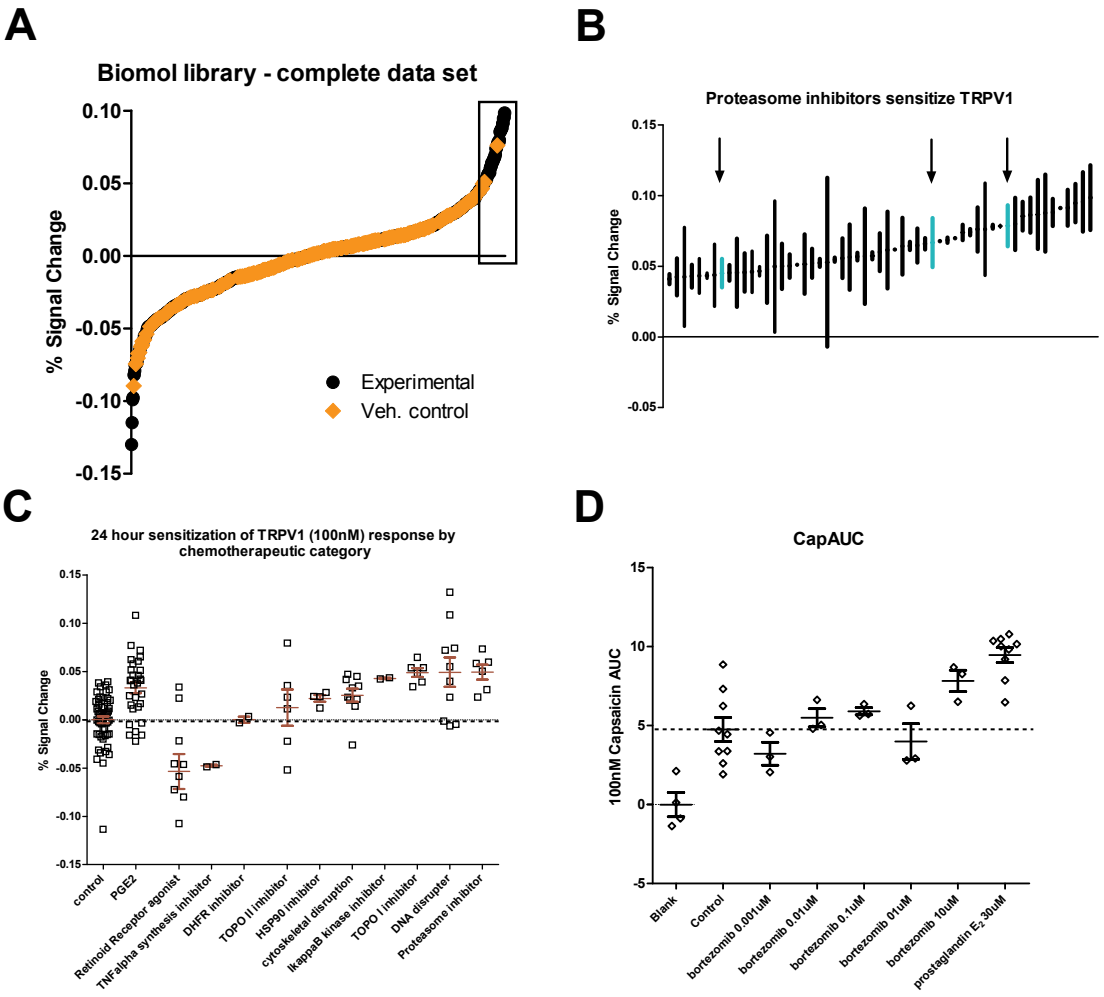

Figure 3.2 - Unbiased large-scale experiment uncovers the proteasome inhibition as potential mechanism for TRPV1 sensitization. (A) Complete, ranked results of well responses in FDSS7000EX. Each point is an average of the two experiments run after 24 hours of incubation with test compounds. % signal change represents the overall change in fluorescence intensity first normalized to initial intensity levels. (B) Closeup view of the top 8% of results showing top hits that are also chemotherapeutic agents. Proteasome inhibitors (Z-Leu3-VS (50 ng/mL), MG-132 (50 ng/mL), and gliotoxin (50 ng/mL)) are indicated by arrows. Bars connect both responses measured. (C) Grouped chemotherapeutic, or experimental analogs of chemotherapeutics modulate TRPV1 function. (D) Retrial of varying bortezomib concentrations demonstrates concentration response. PGE2 is a positive control for sensitization.

proteasome inhibitor allowed on the market[41]. Roughly half of all patients taking bortezomib develop neuropathy[43]. Bortezomib is a peptide boronic acid, analogous to a common class of protease inhibitors, aldehyde peptides[44]. It inhibits the 26S proteasome complex with a high

degree of specificity; its Ki is less than 1 nM (~0.6 nM)[44]. The proteasome complex is responsible for the degradation of many cell-cycle regulatory proteins including cyclins, tumor suppressor genes (e.g. p53), oncogenes like c-myc, IκB, p130, and enzymes such as topoisomerase inhibitors[44]. The increased buildup of these would-be breakdown products leads to an increase in apoptotic activation.

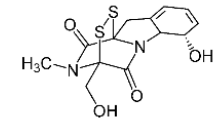

gliotoxin

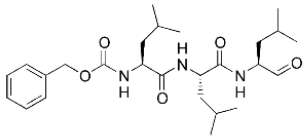

MG-132

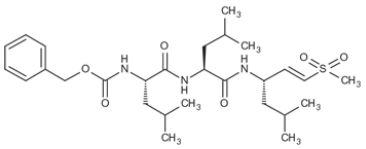

Z-Leu3-VS

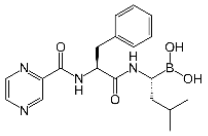

bortezomib

Figure 3.3 - Structures of proteasome inhibitors that cause TRPV1 sensitization. Gliotoxin (50 ng/mL), MG-132 (50 ng/mL), and Z-Leu3-VS (50 ng/mL) were in original screen and showed capsaicin-sensitization effect. Bortezomib is a clinical tool that also causes sensitization of TRPV1.

Fortunately neuropathy from bortezomib does resolve in most cases following cessation of treatment, however, the pain from the neuropathy frequently can be dose-limiting for cancer treatment[45].

Proteasome inhibition causes increased strength and amount of cells responding to low concentrations of capsaicin

Bortezomib was not included in the initial screen, but due to its high incidence of neuropathy as well as the consistent results among other proteasome inhibitors in the screen, we focused our attention on this compound. By repeated tests in the FDSS 7000EX (Hamamatsu) we see a concentration-dependent onset of TRPV1 sensitization (**Figure 3.2D**). Using traditional microscope-based calcium imaging with the ratiometric dye, fura-2, we saw marked changes in neuronal responses as well.

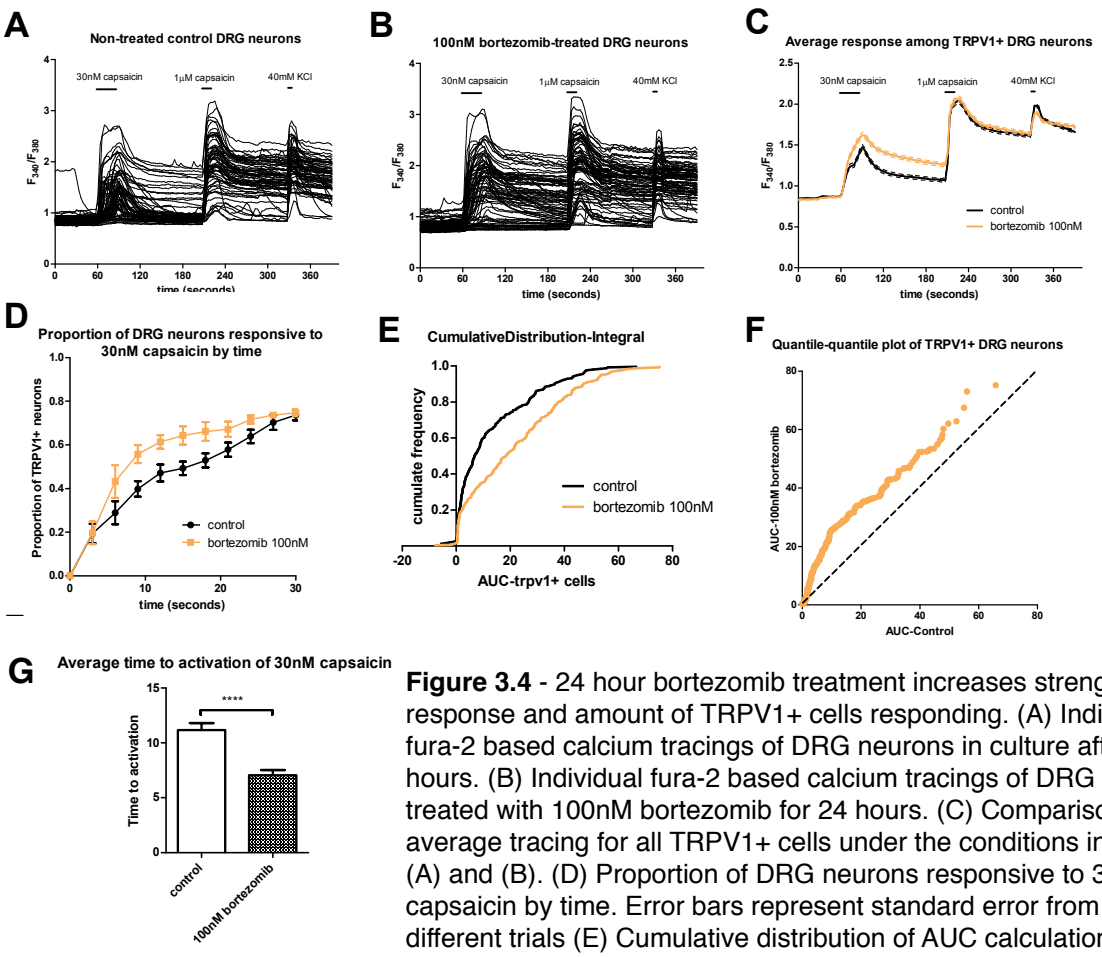

Figure 3.4 - 24 hour bortezomib treatment increases strength of response and amount of TRPV1+ cells responding. (A) Individual fura-2 based calcium tracings of DRG neurons in culture after 24 hours. (B) Individual fura-2 based calcium tracings of DRG neurons treated with 100nM bortezomib for 24 hours. (C) Comparison of average tracing for all TRPV1+ cells under the conditions in panels (A) and (B). (D) Proportion of DRG neurons responsive to 30 nM capsaicin by time. Error bars represent standard error from 3-4 different trials (E) Cumulative distribution of AUC calculations with capsaicin-based activation (30 nM). (F) Quantile-quantile plot demonstrating response increases across all quantiles when treated with bortezomib (100 nM). (G) The average time to respond among treated cells is significantly less than control ($p < 0.0001$ student's t-test, df = 392). Dashes represent standard error margins. Error bars in panels C and D represent SE. C averages all cells for each condition (Control n = 250, treated n = 283), while D is an average for 3 or 4 separate dishes.

By adding the compound, and then assessing TRPV1 sensitivity to a low-concentration capsaicin challenge (30 nM) 24 hours later, we examined strength of responses, amount of cells responding, and the time to activation of response. We used a concentration of bortezomib (100 nM) roughly equivalent to early plasma concentrations following administration of the drug in human patients[46]. We exposed the cells to a sub-maximal concentration of capsaicin (30 nM) and compared these responses to the response following a

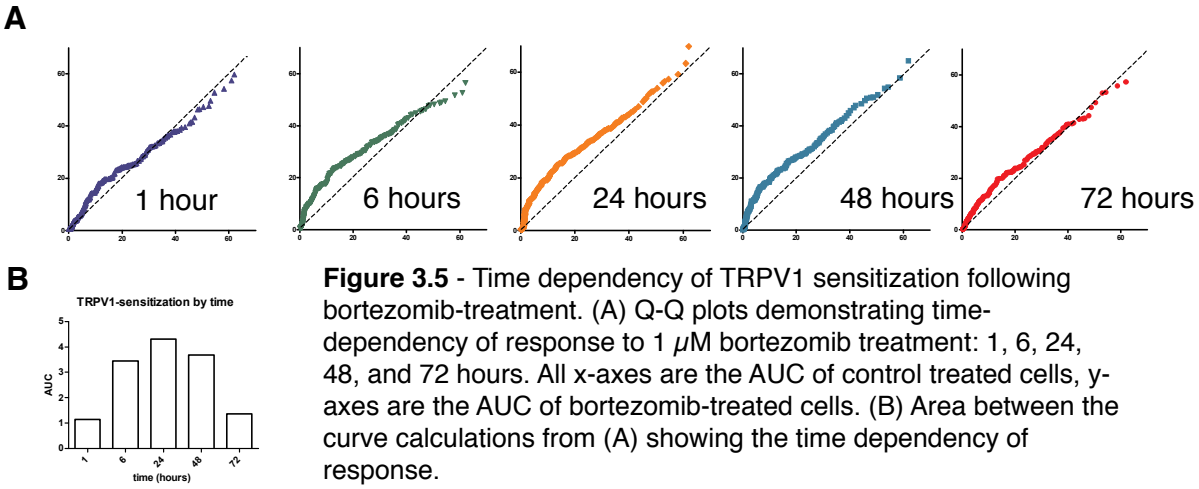

Figure 3.5 - Time dependency of TRPV1 sensitization following bortezomib-treatment. (A) Q-Q plots demonstrating time-dependency of response to 1 μM bortezomib treatment: 1, 6, 24, 48, and 72 hours. All x-axes are the AUC of control treated cells, y-axes are the AUC of bortezomib-treated cells. (B) Area between the curve calculations from (A) showing the time dependency of response.

high concentration of capsaicin (1 μM) after a brief wash-out period. **Figure 3.4** (**A** & **B**) shows representative traces from control-treated DRG neurons and traces from bortezomib-treated (100 nM) for 24 hours.

By averaging the TRPV1+ cells' responses, we see a markedly increased response to a low concentration of capsaicin following incubation with bortezomib (**Figure 3.4C**). Additionally, tracking the time at which each cell reaches a threshold response demonstrates the marked changes that bortezomib induces in DRG neurons (**Figure 3.4D**). The % response differences upon activation by 30 nM capsaicin across 30 seconds of activation in 3 second increments shows kinetic differences with the early differences in response % being the most striking. This difference in response kinetics can be summarized as a time to activation across all cells, which is nearly twice as fast among cells treated with bortezomib than those not treated (**Figure 3.4G**).

To gain a greater appreciation for the onset of the effect of TRPV1 sensitization following bortezomib treatment, we modified the amount of time for treatment. Using 1 μM bortezomib, the response of treated cells to capsaicin relative to control increases rapidly with time. The

maximal effect is seen at 24 hours of treatment compared with 1 hour and 6 hours (**Figure 3.5**). By 2 and 3 days, the difference between treated and untreated cells becomes much greater, however these changes are also marked by other effects on the culture as a whole. As DRG cultures are grown longer than a day, they typically become overrun by proliferating non-neuronal cells that also reside in the DRG. These cells are markedly reduced by bortezomib treatment (figure not shown). The timing and onset of sensitization and the additional effects of bortezomib on non-neuronal cells allows for the possibility of multiple mechanisms of action, direct and indirect. The elucidation of these mechanisms will be the focus of future studies. No expression level changes in mRNA were seen as assessed by qPCR for TRPV1 over these same time points (**Figure 3.6**).

To examine the specificity of TRPV1 sensitization, we examined TRPA1 modulation as well as voltage-gated calcium channels following treatment with bortezomib (**Figure 3.7**). KCl activates voltage-gated calcium channels activating all TRPV1+ neurons, while AITC (allyl-isothiocyanate, or mustard oil) activates the non-selective cation channel, TRPA1 (transient receptor potential ankyrin type 1) which is largely subsumed within the TRPV1+ population [47-49]. 100nM bortezomib over 24 hours causes a roughly 20% increase in TRPV1-specific sensitization, while AITC and KCl responses drop by more than 40%. The opposite effect of bortezomib treatment on AITC and KCl demonstrates the sensitization effect of bortezomib on calcium flux is at least specific for TRPV1 relative to TRPA1 and voltage-gated calcium channels.

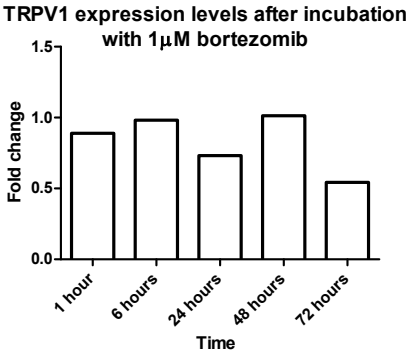

Figure 3.6 - TRPV1 mRNA expression levels unmodified following treatment with 1uM.

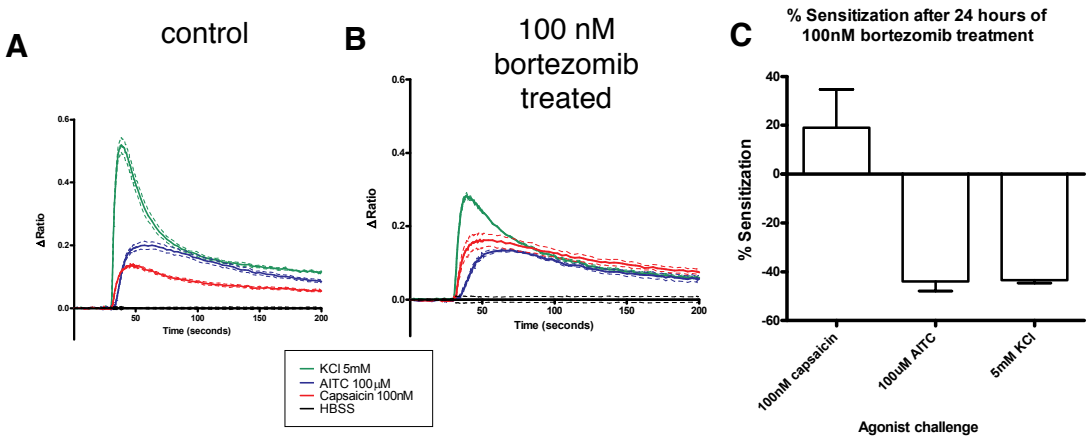

Figure 3.7 - 100nM bortezomib treatment desensitizes KCl and AITC responses. (A) Average traces of non-treated DRG neuronal responses as measured by the FDSS7000EX. (B) Average traces of DRG neuronal responses after 24 hour treatment with 100nM bortezomib. (C) % sensitization for each condition represented. Capsaicin responses were increased, while KCl and AITC responses are significantly desensitized. Error bars represent standard error.

Discussion

Neuropathy has been estimated to occur in 1/3 of all patients who take chemotherapy[50]. The symptoms can be quite severe, particularly when the neuropathy is painful. Burning, paroxysmal pain or extreme hypersensitivity as a result of chemotherapy can be dose-limiting[51]. Bortezomib affects about half of patients treated to varying levels of intensity, with 1 out of 5 or 6 patients having severe neuropathy[52,53]. About 70% of patients recover from the neuropathy following cessation of treatment[54,55].

Among the most common adjectives that patients use to describe the neuropathy following bortezomib treatment are: “numb”, “tingling”, “burning”, “cold”, “sharp” and “electric”[56]. It is noteworthy that patients actually become less sensitive to heat and more sensitive to cold, while “burning” is used to describe the pain in half of all patients. TRPV1, the heat channel is

potentially playing a central role in the genesis of the pain in this condition, as well as a role in the actual development of neuropathy.

We used a high-throughput and unbiased approach to discover that proteasome inhibitors, including the clinical compound, bortezomib, cause TRPV1 sensitization. The high rate of bortezomib-induced neuropathy is a serious clinical problem and needs further study. An immediate role for TRPV1 in the cause of pain can be established quickly by trying TRPV1 antagonists or agonists as a treatment. Perhaps more fundamental a question regarding the role of TRPV1 is whether TRPV1 plays a role in the pathogenesis of the bortezomib-induced neuropathy itself. Could calcium-overload via TRPV1 result in increased apoptosis? With bortezomib-use on the rise, understanding the mechanisms of neuropathy is a critical issue.

TRPV1 is a critical gateway for pain, and while not all pain travels down the same neuronal circuitry, previous experience with two other chemotherapeutics: cisplatin and paclitaxel, shows that TRPV1 plays a critical role in the painful aspects of chemotherapy-induced neuropathy[37,57-59]. The unbiased approach of using a high-throughput screening system has demonstrated here TRPV1 sensitization not only after bortezomib, but also following several different chemotherapeutics that cause neuropathy as well as a high proportion of the endpoint of TRPV1 following chemotherapeutic intervention, yet also demonstrates more of the function of TRPV1 sensitization. KCl activation has been used as an indicator in our experiments of overall cell health and viability. Chemotherapeutic agents drastically lower the responses within our system to KCl, while increasing responses through TRPV1. Does TRPV1 serve a role as warning sensor for internal damage and apoptosis driven by toxic chemicals or

otherwise? Or, is TRPV1 actually participating in the development of pain at the least, and possibly neuropathy itself? This is a particularly intriguing and important question.

Ionic disregulation, mitochondrial impairment and apoptotic pathway activation are all implicated in what is currently an unsorted and not completely clear view on the mechanisms of chemotherapy-induced neuropathy[60]. To the point of ionic disturbance in general as a mechanism for neuropathy is recent evidence arguing for a direct role of sodium channel mutations in the spontaneous development of neuropathy[61,62]. As for a greater role of TRPV1 sensitization in the pain and/or neuropathy generation, it is interesting to note that one of the effects of multiple myeloma, the primary indication for bortezomib treatment, is hypercalcemia[42]. Additionally, a small proportion of patients with multiple myeloma develop neuropathy without any chemotherapeutic intervention, inviting the question: how do plasma calcium levels in the face of multiple myeloma correlate with neuropathy during bortezomib-treatment? Perhaps it is the combination of calcium overload, TRPV1 sensitization and mitochondrial and ER stress (limiting the cellular capacity for calcium sequestration) that lead to selective damage of DRG neurons. It was previously shown that ruthenium red, a non-selective pore-blocker of TRP channels provides some cellular protection against apoptosis[63]. TRPV1, a sensitized non-selective cation channel could be the gate by which calcium initiates the apoptotic pathway, particularly in the case of mitotoxicity - leading to pain as well as neuropathy[64].

Additional experiments will be necessary to demonstrate the role of TRPV1 in bortezomib's neurotoxic effects. By comparing DRG neurons, axons, intra-epidermal nerve fibers, as well as the assortment of non-neuronal supporting cells in bortezomib-treated mice who are

TRPV1 deficient (pharmacologically or genetically) should lend useful insights to understanding the bortezomib-induced neuropathy.

We initiated the experiments described here by utilizing a high-throughput system to examine TRPV1 sensitization. In an unbiased manner, we found that several chemotherapeutic compounds cause TRPV1 sensitization, including bortezomib, a proteasome inhibitor. Hopefully, by following up on the other leads as well, we can develop a more complete picture of TRPV1 sensitization and relevance to disease.

Works Cited

1. Caterina, M. J. et al. The capsaicin receptor: a heat-activated ion channel in the pain pathway. Nature 389, 816–24 (1997).

2. Ramsey, I. S., Delling, M. & Clapham, D. E. An introduction to TRP channels. Annu. Rev. Physiol. 68, 619–47 (2006).

3. Montell, C., Birnbaumer, L. & Flockerzi, V. The TRP channels, a remarkably functional family. Cell 108, 595–8 (2002).

4. Lishko, P. V, Procko, E., Jin, X., Phelps, C. B. & Gaudet, R. The ankyrin repeats of TRPV1 bind multiple ligands and modulate channel sensitivity. Neuron 54, 905–18 (2007).

5. Liao, M., Cao, E., Julius, D. & Cheng, Y. Structure of the TRPV1 ion channel determined by electron cryo-microscopy. Nature 504, 107–12 (2013).

6. Cao, E., Liao, M., Cheng, Y. & Julius, D. TRPV1 structures in distinct conformations reveal activation mechanisms. Nature 504, 113–8 (2013).

7. Moiseenkova-Bell, V. Y., Stanciu, L. a, Serysheva, I. I., Tobe, B. J. & Wensel, T. G. Structure of TRPV1 channel revealed by electron cryomicroscopy. Proc. Natl. Acad. Sci. U. S. A. 105, 7451–5 (2008).

8. Winter, Z. et al. Functionally important amino acid residues in the Transient Receptor Potential Vanilloid 1 (TRPV1) ion channel--an overview of the current mutational data. Mol. Pain 9, 30 (2013).

9. Pareek, T. K. et al. Cyclin-dependent kinase 5 modulates nociceptive signaling through direct phosphorylation of Transient Receptor Potential Vanilloid 1. Proc. Natl. Acad.

Sci. U. S. A. 104, 660–5 (2007).

10. Wang, Y. The Functional Regulation of TRPV1 and Its Role in Pain Sensitization. Neurochem. Res. 33, 2008–2012 (2008).

11. Zhuang, Z.-Y., Xu, H., Clapham, D. E. & Ji, R.-R. Phosphatidylinositol 3-kinase activates ERK in primary sensory neurons and mediates inflammatory heat hyperalgesia through TRPV1 sensitization. J. Neurosci. 24, 8300–9 (2004).

12. Mandadi, S. et al. Activation of protein kinase C reverses capsaicin-induced calcium-dependent desensitization of TRPV1 ion channels. Cell Calcium 35, 471–8 (2004).

13. Zhu, W. & Oxford, G. S. Phosphoinositide-3-kinase and mitogen activated protein kinase signaling pathways mediate acute NGF sensitization of TRPV1. Mol. Cell. Neurosci. 34, 689–700 (2007).

14. Moriyama, T. et al. Sensitization of TRPV1 by EP1 and IP reveals peripheral nociceptive mechanism of prostaglandins. Mol. Pain 1, 3 (2005).

15. van der Stelt, M. et al. Anandamide acts as an intracellular messenger amplifying Ca2+ influx via TRPV1 channels. EMBO J. 24, 3026–37 (2005).

16. Hwang, S. W. et al. Direct activation of capsaicin receptors by products of lipoxygenases: endogenous capsaicin-like substances. Proc. Natl. Acad. Sci. U. S. A. 97, 6155–60 (2000).

17. Woo, D. H. et al. Direct activation of transient receptor potential vanilloid 1(TRPV1) by diacylglycerol (DAG). Mol. Pain 4, 42 (2008).

18. Zhang, X., Huang, J. & McNaughton, P. a. NGF rapidly increases membrane expression of TRPV1 heat-gated ion channels. EMBO J. 24, 4211–23 (2005).

19. Amaya, F. et al. NGF and GDNF differentially regulate TRPV1 expression that contributes to development of inflammatory thermal hyperalgesia. Eur. J. Neurosci. 20, 2303–10 (2004).

20. Obreja, O., Rathee, P. K., Lips, K. S., Distler, C. & Kress, M. IL-1 beta potentiates heat-activated currents in rat sensory neurons: involvement of IL-1RI, tyrosine kinase, and protein kinase C. FASEB J. 16, 1497–503 (2002).

21. Pitchford, S. & Levine, J. D. Prostaglandins sensitize nociceptors in cell culture. Neurosci. Lett. 132, 105–8 (1991).

22. Sugiura, T., Tominaga, M., Katsuya, H. & Mizumura, K. Bradykinin Lowers the Threshold Temperature for Heat Activation of Vanilloid Receptor 1. J Neurophysiol 88, 544–548 (2002).

23. McMahon, S. B. NGF as a mediator of inflammatory pain. Philos. Trans. R. Soc. Lond. B. Biol. Sci. 351, 431–40 (1996).

24. Ferreira, S. H., Lorenzetti, B. B., Bristow, A. F. & Poole, S. Interleukin-1beta as a potent hyperalgesic agent antagonized by a tripeptide analogue. Nature 334, 698–700 (1988).

25. Ferreira, S. H. Prostaglandins, aspirin-like drugs and analgesia. Nat. New Biol. 240, 200–203 (1972).

26. Ferreira, S. H., Nakamura, M. & de Abreu Castro, M. S. The hyperalgesic effects of prostacyclin and prostaglandin E2. Prostaglandins 16, 31–37 (1978).

27. Green, B. G. Capsaicin sensitization and desensitization on the tongue produced by brief exposures to a low concentration. Neurosci. Lett. 107, 173–8 (1989).

28. Cholewinski, A., Burgess, G. & Bevan, S. The role of calcium in capsaicin-induced desensitization in rat cultured dorsal root ganglion neurons. Neuroscience 55, 1015–1023 (1993).

29. Docherty, R. J., Yeats, J. C., Bevan, S. & Boddeke, H. W. Inhibition of calcineurin inhibits the desensitization of capsaicin-evoked currents in cultured dorsal root ganglion neurones from adult rats. Pflugers Arch. 431, 828–37 (1996).

30. Mohapatra, D. P. & Nau, C. Desensitization of capsaicin-activated currents in the vanilloid receptor TRPV1 is decreased by the cyclic AMP-dependent protein kinase pathway. J. Biol. Chem. 278, 50080–90 (2003).

31. Malin, S. A., Davis, B. M. & Molliver, D. C. Production of dissociated sensory neuron cultures and considerations for their use in studying neuronal function and plasticity. Nat. Protoc. 2, 152–60 (2007).

32. Shelat, A. A. & Guy, R. K. Scaffold composition and biological relevance of screening libraries. Nat. Chem. Biol. 3, 442–446 (2007).

33. Schmittgen, T. D. & Livak, K. J. Analyzing real-time PCR data by the comparative CT method. Nat. Protoc. 3, 1101–1108 (2008).

34. Hargreaves, K., Dubner, R., Brown, F., Flores, C. & Joris, J. A new and sensitive method for measuring thermal nociception. Pain 32, 77–88 (1988).

35. Zhang, J.-H., Chung, T. D. Y. & Oldenburg, K. R. A Simple Statistical Parameter for Use in Evaluation and Validation of High Throughput Screening Assays. J. Biomol. Screen. 4, 67–73 (1999).

36. Albers, J., Chaudhry, V., Cavaletti, G. & Rc, D. Interventions for preventing neuropathy caused by cisplatin and related compounds (Review). (2011).

37. Chen, Y., Yang, C. & Wang, Z. J. Proteinase-Activated Receptor 2 sensitizes Transient Receptor Potential Vanilloid 1, Transient Receptor Potential Vanilloid 4, and Transient Receptor Potential Ankyrin 1 in paclitaxel-induced neuropathic pain. Neuroscience 193, 440–51 (2011).

38. Ta, L. E. et al. Transient Receptor Potential Vanilloid 1 is essential for cisplatin-induced heat hyperalgesia in mice. Mol. Pain 6, 15 (2010).

39. Crawford, L. J. a et al. Comparative selectivity and specificity of the proteasome inhibitors BzLLLCOCHO, PS-341, and MG-132. Cancer Res. 66, 6379–86 (2006).

40. Kroll, M. et al. The secondary fungal metabolite gliotoxin targets proteolytic activities of the proteasome. Chem. Biol. 6, 689–698 (1999).

41. de Bettignies, G. & Coux, O. Proteasome inhibitors: Dozens of molecules and still counting. Biochimie 92, 1530–45 (2010).

42. Zeng, Z., Lin, J. & Chen, J. Bortezomib for patients with previously untreated multiple myeloma: a systematic review and meta-analysis of randomized controlled trials. Ann. Hematol. 92, 935–43 (2013).

43. Richardson, P. G. et al. Single-agent bortezomib in previously untreated multiple myeloma: efficacy, characterization of peripheral neuropathy, and molecular correlations with response and neuropathy. J. Clin. Oncol. 27, 3518–25 (2009).

44. Adams, J. & Kauffman, M. Development of the Proteasome Inhibitor Velcade™ (Bortezomib). Cancer Invest. 22, 304–311 (2004).

45. Colvin, L. A., Johnson, P. R. E., Mitchell, R., Fleetwood-Walker, S. M. & Fallon, M. From Bench to Bedside: A Case of Rapid Reversal of Bortezomib-Induced Neuropathic Pain by the TRPM8 Activator, Menthol. J. Clin. Oncol. 26, 4519–4520 (2008).

46. Papandreou, C. N. et al. Phase I trial of the proteasome inhibitor bortezomib in patients with advanced solid tumors with observations in androgen-independent prostate cancer. J. Clin. Oncol. 22, 2108–21 (2004).

47. Bandell, M. et al. Noxious cold ion channel TRPA1 is activated by pungent compounds and bradykinin. Neuron 41, 849–57 (2004).

48. Jordt, S., Bautista, D. M., Chuang, H., Meng, I. D. & Julius, D. Mustard oils and cannabinoids excite sensory nerve fibres through the TRP channel ANKTM1. Nature 427, 260–265 (2004).

49. Kobayashi, K. et al. Distinct expression of TRPM8, TRPA1, and TRPV1 mRNAs in rat primary afferent neurons with adelta/c-fibers and colocalization with trk receptors. J. Comp. Neurol. 493, 596–606 (2005).

50. Bhagra, A. & Rao, R. D. Chemotherapy-induced neuropathy. Curr. Oncol. Rep. 9, 290–299 (2007).

51. Han, Y. & Smith, M. T. Pathobiology of cancer chemotherapy-induced peripheral neuropathy (CIPN). Front. Pharmacol. 4, 156 (2013).

52. Broyl, A. et al. Mechanisms of peripheral neuropathy associated with bortezomib and vincristine in patients with newly diagnosed multiple myeloma: a prospective analysis of data from the HOVON-65/GMMG-HD4 trial. Lancet Oncol. 11, 1057–65 (2010).

53. Cata, J. P. et al. Quantitative sensory findings in patients with bortezomib-induced pain. J. Pain 8, 296–306 (2007).

54. Richardson, P. G. et al. Frequency, characteristics, and reversibility of peripheral neuropathy during treatment of advanced multiple myeloma with bortezomib. J. Clin. Oncol. 24, 3113–20 (2006).

55. Chaudhry, V., Cornblath, D. R., Polydefkis, M., Ferguson, A. & Borrello, I. Characteristics of bortezomib- and thalidomide-induced peripheral neuropathy. J. Peripher. Nerv. Syst. 13, 275–82 (2008).

56. Bölcskei, K. et al. Investigation of the role of TRPV1 receptors in acute and chronic nociceptive processes using gene-deficient mice. Pain 117, 368–76 (2005).

57. Pittman, S. K., Gracias, N. G., Vasko, M. R. & Fehrenbacher, J. C. Paclitaxel alters the evoked release of calcitonin gene-related peptide from rat sensory neurons in culture. Exp. Neurol. 253C, 146–153 (2013).

58. Hara, T. et al. Effect of paclitaxel on transient receptor potential vanilloid 1 in rat dorsal root ganglion. Pain 154, 882–889 (2013).

59. Zheng, H., Xiao, W. H. & Bennett, G. J. Mitotoxicity and bortezomib-induced chronic painful peripheral neuropathy. Exp. Neurol. 238, 225–34 (2012).

61. Faber, C. G. et al. Gain of function Nav1.7 mutations in idiopathic small fiber neuropathy. Ann. Neurol. 71, 26–39 (2012).

62. Szalai, G., Krishnamurthy, R. & Hajnóczky, G. Apoptosis driven by IP(3)-linked mitochondrial calcium signals. EMBO J. 18, 6349–61 (1999).

63. Persson, A.-K. et al. Sodium channels contribute to degeneration of dorsal root ganglion neurites induced by mitochondrial dysfunction in an in vitro model of axonal injury. J. Neurosci. 33, 19250–61 (2013).

64. Landowski, T. H., Megli, C. J., Nullmeyer, K. D., Lynch, R. M. & Dorr, R. T. Mitochondrial-mediated disregulation of Ca2+ is a critical determinant of Velcade (PS-341/bortezomib) cytotoxicity in myeloma cell lines. Cancer Res. 65, 3828–36 (2005).

Chapter 4: Photochemical activation of TRPA1 channels in neurons and animals* **

Abstract

Optogenetics is a powerful research tool because it enables high-resolution optical control of neuronal activity. However, current optogenetic approaches are limited to transgenic systems expressing microbial opsins and other exogenous photoreceptors. Here, we identify optovin, a small molecule that enables repeated photoactivation of motor behaviors in wild-type zebrafish and mice. To our surprise, optovin's behavioral effects are not visually mediated. Rather, photodetection is performed by sensory neurons expressing the cation channel TRPA1. TRPA1 is both necessary and sufficient for the optovin response. Optovin activates human TRPA1 via structure-dependent photochemical reactions with redox-sensitive cysteine residues. In animals with severed spinal cords, optovin treatment enables control of motor activity in the paralyzed extremities by localized illumination. These studies identify a light-based strategy for controlling endogenous TRPA1 receptors *in vivo*, with potential clinical and research applications in nontransgenic animals, including humans.

INTRODUCTION

One of the most influential recent innovations in neuroscience has been optogenetics, an approach for controlling neurons with exogenous microbial opsins or other ectopic

---

* The chemical and zebrafish work for this study was performed in the laboratory of Randall Peterson at Massachusetts General Hospital, Boston. I worked on confirming the specificity of optovin for activating TRPA1 in WT and TRPA1-/- primary dorsal root ganglia cells via calcium imaging that I dissected and cultured. I showed that optovin was not effective in activating 3CK mutant HEK cells with additional assistance from Ajay Yekkirala and Cleverton Kleiton Freitas de Lima. Additionally, I developed and performed the assay to see optovin-based behavioral responses in mice in the Woolf Laboratory at Children's Hospital, Boston with advice and assistance from Ajay Yekkirala and David Roberson.

** This chapter is a modified version of an article previously published as: Kokel, D., Cheung, C.Y.J., Mills, R., Coutinho-Budd, J., Huang, L., Setola, V., Sprague, J., Jin, S., Jin., Y.N., Huang, X-P., Bruni, G., Woolf, C.J., Roth, B.L., Hamblin, M.R., Zylka, M.J., Milan, D.J., & Peterson, R.J. Photochemical activation of TRPA1 channels in neurons and animals. Nat. Chem. Biol. 9, 257–63 (2013).

photosensitive channels[1–11]. Optogenetic techniques in model organisms are yielding remarkable new insights in neuroscience and medicine. However, current approaches do not address the unmet need for controlling endogenous neuronal proteins and neuronal signaling in nontransgenic animals with light.

Photochemical tools for controlling endogenous channels *in vivo* enable powerful approaches for neuroscience research and therapeutic intervention[12]. For example, photorelease of caged glutamate provides optical control of glutamate receptors in brain slices. Azobenzene-containing photoswitchable ligands also provide optical control of glutamate receptors and potassium channels[9,10,12–19]. However, virtually all prior work in chemical optogenetics has been limited to cultured cells, tissue slices and other *ex vivo* preparations because most existing techniques are not effective *in vivo*. Discovery of new compounds with higher potency and better *in vivo* properties would improve the photochemical ligand toolbox. Here, we used behavior-based chemical screening to identify optovin, a new photochemical switch compound with potent bioactivity in intact living animals.

Receptors in the transient receptor potential (TRP) family are attractive channels for bringing under optical control[20]. TRP channels are involved in diverse sensory systems including vision, taste, temperature and touch. TRPA1 signaling contributes to illnesses, including neuropathic pain and chronic inflammation[21–24]. Precise control of TRPA1 channels may be useful for understanding and treating these disorders. However, currently available TRPA1 ligands such as mustard oil and cinnamaldehyde provide imprecise spatiotemporal control of TRPA1 signaling.

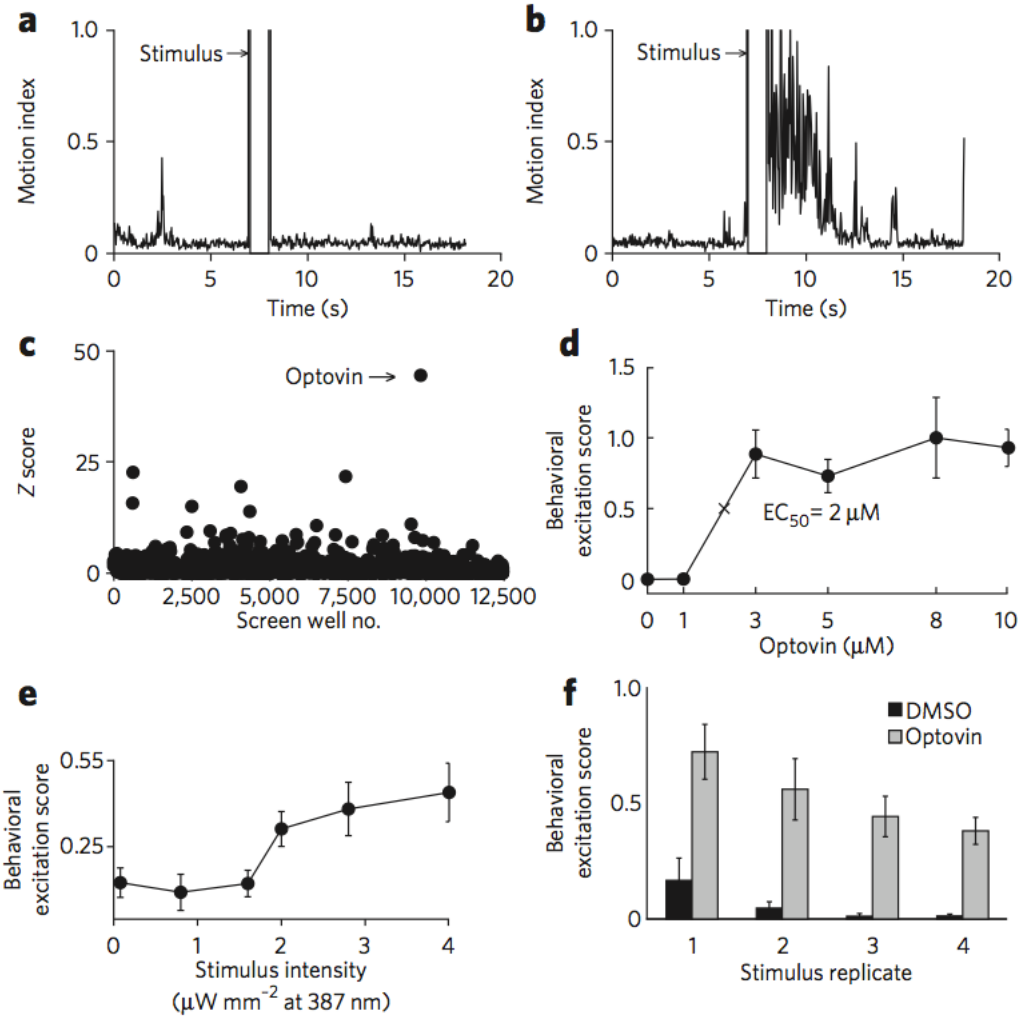

Figure 4.1 - Identification of optovin, a compound enabling light-mediated neuronal excitation. (a,b) Plots showing the zebrafish behavioral response of DMSO-treated (a) and optovin-treated (b) animals. The bar indicates the timing of a 1-s white light stimulus. (c) Scatter plot showing the behavioral excitation scores from chemicals in the screen (12,500 individual wells). The y axis represents the number of s.d. of each excitation score from the control mean (Z score). The labeled arrow indicates the well treated with optovin. (d) Dose response curve showing optovin's effects on animal behavior (EC50 = 2 M; n = 5). The difference between the 1-M and 3-M treatments is significant, $P < 0.001$. (e) Line plot showing excitation scores at the indicated stimulus intensities (n = 5). The difference between groups treated at 1.6 W mm–2 and 2 W mm–2 is significant, $P < 0.001$. (f) Bar plot showing behavioral responses to repeated light stimuli (n = 5). Differences between treated and untreated groups are significant, $P < 0.001$. Error bars represent s.d.

Here, we used a behavior-based chemical screening approach to identify optovin, a new neuroactive small molecule. Optovin is a TRPA1 ligand that can be reversibly photoactivated

by violet light. Optovin's behavioral effects depend on TRPA1 and it shows activity in zebrafish, mice, mouse neurons and recombinant human protein. The photochemical reaction mechanism most likely involves reversible covalent thioether bonding between TRPA1 and optovin. Optovin is the first known photochemical TRPA1 ligand, and it enables optical control of neurons that express this target in wild-type animals.

RESULTS

Behavior-based chemical screening identifies optovin

To identify small molecules for the optical control of endogenous channels, we screened for compounds that could drive light-dependent motor behaviors in wild-type zebrafish. Zebrafish embryos are uniquely well suited for phenotype-based chemical screens[25,26]. They are blind for the first 3 d of development, and, aside from a one-time motor response to the first light exposure in dark-adapted animals (the photomotor response (PMR)), zebrafish embryos are unresponsive to light[27,28] (**Figure 4.1a**). We screened a library of 10,000 structurally diverse synthetic small molecules for compounds that render zebrafish embryos responsive to light. Behavioral responses were measured for each well in comparison to a set of 2,500 DMSO-treated controls. This screen identified a single compound, optovin, which increased motor activity greater than 40 s.d. above the control mean (**Figure 4.1a–c**).

Optovin is a rhodanine-containing small molecule with no previously annotated biological activity. Whereas DMSO-treated animals do not respond to photic stimuli, optovin-treated animals respond to light with vigorous motor excitation at a half-maximum excitatory concentration (EC_{50}) of 2 μM (**Figure 4.1d**). Motor behavior in optovin-treated animals (387 nm) is elicited by stimulus intensities greater than 1.6 W mm^{-2} (**Figure 4.1e**). In treated

animals, multiple responses can be triggered with repeated light pulses (**Figure 4.1f**). To determine the effects of optovin exposure on development, behavior and survival, we analyzed zebrafish exposed to optovin (10 μM) for 96 h. We did not identify any differences in the appearance, touch response, heart rate, fin movements, morphology or percentage survival between the treated and untreated groups (data not shown). Thus, optovin is a new behavior-modifying compound that causes rapid and reversible motor excitation in response to violet light stimuli.

To gain initial insight into optovin's mechanism of action, we profiled optovin using the National Institute of Mental Health Psychoactive Drug Screening Program (NIMH PDSP) to determine its activities against a panel of human and rodent CNS receptors, channels and transporters. No submicromolar targets were identified (data not shown), suggesting that optovin may act through a mechanism of action not represented in the extensive NIMH PDSP collection.

TRPA1 is necessary and sufficient for optovin activity

Optovin-treated zebrafish embryos respond to light at very early stages of development, before the eye and vision develop. The observation that animals respond prior to the onset of vision suggests that the optovin response is a nonvisual behavior and that optovin acts on tissues other than the eye. To determine whether the eyes are necessary for the optovin response, we compared the responses of intact zebrafish embryos to the trunks of age-matched spinalized preparations transected posterior to the hindbrain. Sensory neurons in the trunk normally respond to various kinds of touch, stretch, temperature and pain but not to light. To our surprise, we found that optovin-treated spinalized preparations also responded to light (**Figure 4.2**). Using a 405-nm laser beam, we observed optovin-dependent motor responses to illumination of the trunk, tail and fins, which are all sites innervated by sensory neurons.

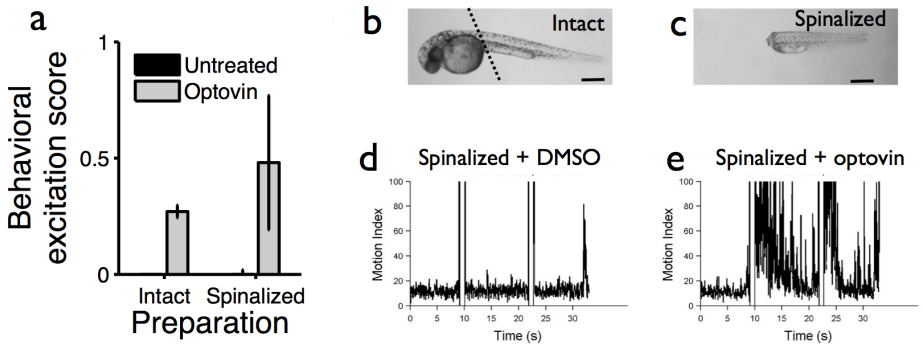

Figure 4.2 - Optovin-treated spinalized preparations respond to light. (a) Behavioral excitation scores of intact and spinalized zebrafish embryos (30 hpf). Differences between treated and untreated groups are significant, $p<0.001$. Photographs showing zebrafish embryos at 35hpf before (b) and after (c) transection posterior to the hindbrain as indicated by the dashed line. Scale bar, 150 µm. (d,e) Examples of how DMSO-treated (c) and optovin-treated (d) spinalized animals respond to light stimuli.

Together, these data indicate that visual pathways are not necessary for the optovin-induced light response and suggest that optovin may act on sensory neurons.

To determine whether optovin acts on sensory neurons, we used calcium imaging to compare the activity of treated and untreated dorsal root ganglia (DRG) sensory neurons isolated from wild-type mice. We found that optovin strongly activated 33% (35/105) of DRG neurons (**Figure 4.3a**). This activation did not occur when optovin treatment occurred in the dark (**Figure 4.4a–d**). To determine whether optovin activates neurons that also respond to known ligands, we treated the DRG neurons with mustard oil, a TRPA1 ligand[30]. We found that mustard oil activated 27% (28/105) of DRG neurons and that nearly all DRG sensory neurons that responded to mustard oil also responded to optovin (27/28; **Figure 4.4b,d,e**). These data suggest that optovin acts on a molecular target expressed in mustard oil–responsive mammalian DRG sensory neurons and perhaps on TRPA1 itself.

TRPA1 channels have important roles in detecting chemical, thermal and mechanical stimuli in a variety of organisms[31–33]. The zebrafish genome encodes two orthologs of the mammalian

TrpA1 gene, designated *trpa1a* and *trpa1b*, which have different expression patterns and functions[34]. To test the hypothesis that optovin acts on TRPA1, we analyzed the behavior of *trpa1a* and *trpa1b* mutant animals. As expected, we found that wild-type zebrafish responded to optovin and the 387-nm light stimulus with a prolonged motor excitation (**Figure 4.3b,c**). By contrast, mutant fish homozygous for *trpa1b* failed to respond (**Figure 4.3b,c**). Notably, dark-adapted *trpa1b* mutant fish still showed normal control behaviors, such as the PMR and the

Figure 4.3 - TRPA1 is necessary and sufficient for the optovin response. (a) Percentage of mouse DRG neurons responding to the indicated treatments. In the wild type (WT), the light stimulus activated 30% of neurons assayed (35/105). In the TRPA1 knockout (KO) neurons, the total percentage of responding neurons was 2.7% (8/291). MO, mustard oil. (b) Behavioral excitation scores during the optovin response for zebrafish 25 of the indicated genotypes. Het, heterozygous. (c) Behavioral excitation scores calculated for wild-type, heterozygous and homozygous TrpA1b mutant animals (n = 21, 23 and 16, respectively) during the PMR (control) and optovin response assays. Homozygous mutant animals show a significantly lower activity during the optovin response assay, $P < 0.001$. (d) Bar plot showing calcium indicator dye fluorescence in cells transfected with GFP or hTrpA1 before and after a 2-min treatment with optovin and light (n = 130 and 120 cells, respectively). The difference between treated and untreated hTRPA1-transfected cells is significant, $P < 0.001$.

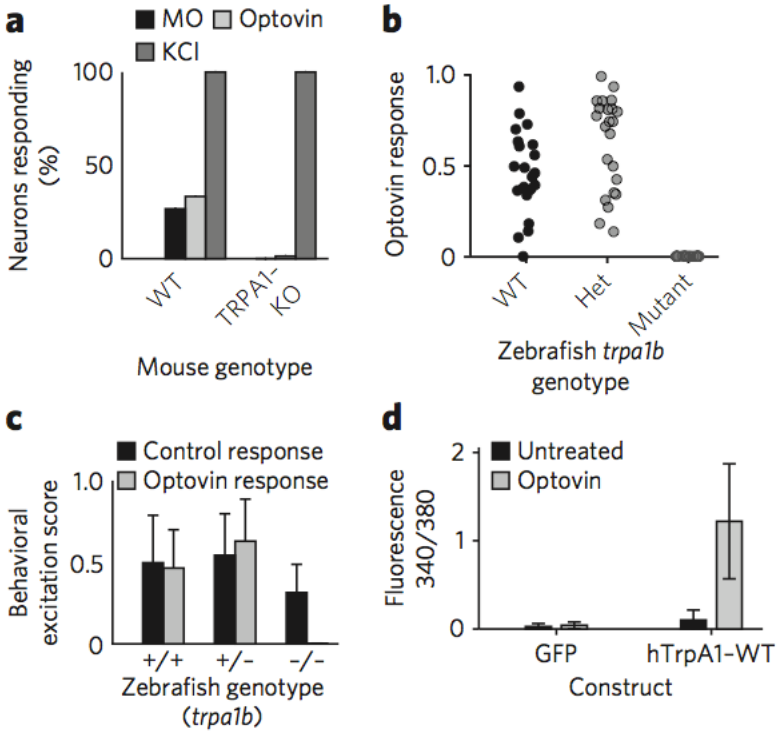

touch response, indicating that the *trpa1b* mutation does not suppress motor behaviors in general (data not shown). These data indicate that *trpa1b* is necessary for the optovin response in zebrafish. To determine whether the gene encoding TRPA1 is also necessary for the optovin response in mice, we analyzed the activity of DRG neurons isolated from *TrpA1* mutant mice[11]. Unlike wild-type controls, *TrpA1* mutant neurons did not respond to either mustard oil or optovin, although they did respond to KCl, a depolarizing agent (**Figure 4.3a**).

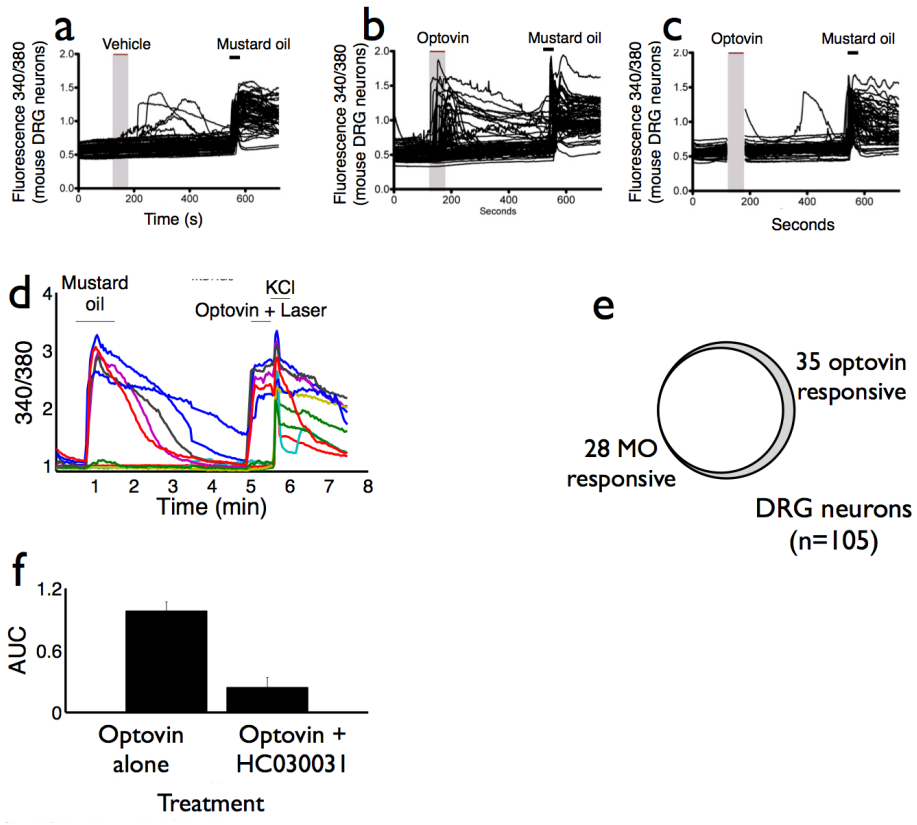

Figure 4.4 - Mustard oil and optovin act on the same subset of DRG sensory neurons. (a-c) Calcium imaging of mouse DRG neurons in response to vehicle (a), optovin and light (b), and optovin without light (c). Black traces indicate calcium indicator fluorescence readings. No readings were recorded during the 1min optovin treatment period in c) when lights were turned off. (d) Fuorescence traces from 10 example cells showing their response to the indicated treatments. (e)Venn diagram showing that 28/35 mustard oil responsive cells also respond to optovin. (f) After Fura-2, AM loading and washing, neurons were loaded with optovin (100 µM) and with either the TRPA1 antagonist, HC-030031 (26 µM, Sigma) (McNamara et al., 2007) or vehicle control (DMSO, 0.025%). After a 10-minute incubation period, the neurons were exposed to a 5-second laser pulse (405 nm), washed, and then activated with mustard oil (100 µM). Responses are presented normalized to the response elicited by mustard oil per

Furthermore, HC-030031, a selective TRPA1 antagonist[35], blocked optovin activity on wild-type mouse DRG neurons (**Figure 4.4f**). Together, these data suggest that TrpA1 is necessary for the optovin response.

Optovin is a reversible photoactivated TRPA1 ligand

Does optovin and light activate TRPA1 in a manner similar to mustard oil, through a few critical cysteine residues? The triple cysteine mutant (3CK) channel is relatively unresponsive to mustard oil, but responsive to carvacrol, another TRPA1 agonist that works through a different mechanism (Bessac et al., 2008). Activation with optovin of this mutant channel was relatively ineffective (**Figure 4.5**). Together, these data suggest that optovin activates TRPA1 channels in a manner similar to mustard oil.

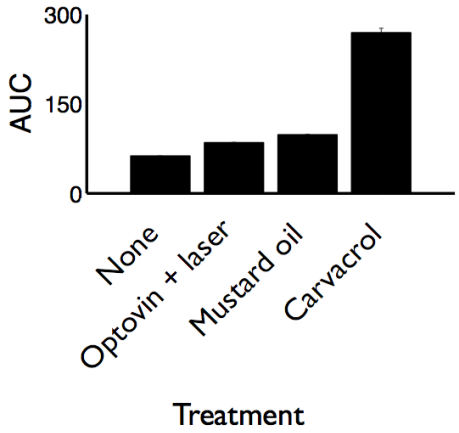

Figure 4.5 - Optovin has no activity on the hTrpA1 3CK triple cysteine mutant. (a) 3CK mutant TRPA1 plasmid (provided by Christian von Hehn) was transfected into HEK- 293 cells and imaged using Fura-2, AM (Life Technologies) the mutations replace the residues on C619, C639, C663, and K708 to serine residues (Escalera et al., 2008). Laser alone, MO alone (100 µM) and optovin (100 µM) and laser combined were used to elicit activation. Carvacrol (100 µM, Sigma-Aldrich) was used as a positive control as it is an agonist of TRPA1 which does not depend on the cysteine residues otherwise critical for MO-based activation (Hinman et al., 2006) (n= 41 cells).

Photochemical control of optovin-treated animals

Optovin's capacity to function in intact adult animals will affect its potential for use in future clinical and research applications. Thus, we analyzed the effects of 405-nm laser illumination on optovin-treated adult animals. In zebrafish, we found that illuminating the dorsal fin elicited rapid and reversible contraction of the fin but did not seem to otherwise disturb the treated animal. To determine whether fin contraction was voluntary or involuntary, we repeated the experiment using spinalized preparations. Optical control of dorsal fin contraction was preserved in spinalized animals treated with optovin (**Figure 4.6a**). Furthermore, we found that carefully controlled laser illumination of specific regions along the body of spinalized zebrafish produced specific dorsal, ventral and lateral tail movements reminiscent of those used by intact fish during swimming (**Figure 4.6b**). Because zebrafish TRPA1 is primarily expressed in sensory neurons, these contractions and swimming behaviors most likely occur via activation of spinal reflex arcs. These data indicate that optovin enables real-time optical control of neurons in adult wild-type vertebrate animals. We found that optovin also elicited head-shaking behaviors in adult mice (**Figure 4.6c**). Thus, optovin shows activity in adult animals in vivo and may be preferable to conventional TRPA1 ligands for achieving high-resolution spatiotemporal control.

DISCUSSION

These studies have identified optovin, a small molecule that enables optical control of endogenous channels and neuronal signaling in wild-type nontransgenic animals. Optovin differs from previously identified photochemical switch compounds in several ways. Optovin acts on TRPA1 channels, which were previously inaccessible via optical techniques. Unlike reversibly caged glutamate and photoswitchable affinity label compounds, optovin is not based on azobenzene photoreactivity. In addition, optovin can be washed out and seems to

be quite selective in its activity, with no substantial activity at dozens of other potential targets tested.

Optovin was discovered in a behavior-based chemical screen. As with most compounds discovered in phenotype-based screens, determining optovin's mechanism of action has been a central focus of our studies. Through genetic, molecular and imaging-based experiments, we have identified that optovin acts on the cation channel TRPA1 most likely in peripheral neurons. Several lines of evidence indicate that TRPA1 channels are both necessary and sufficient for optovin function: (i) Genetic mutation of TrpA1b in zebrafish completely

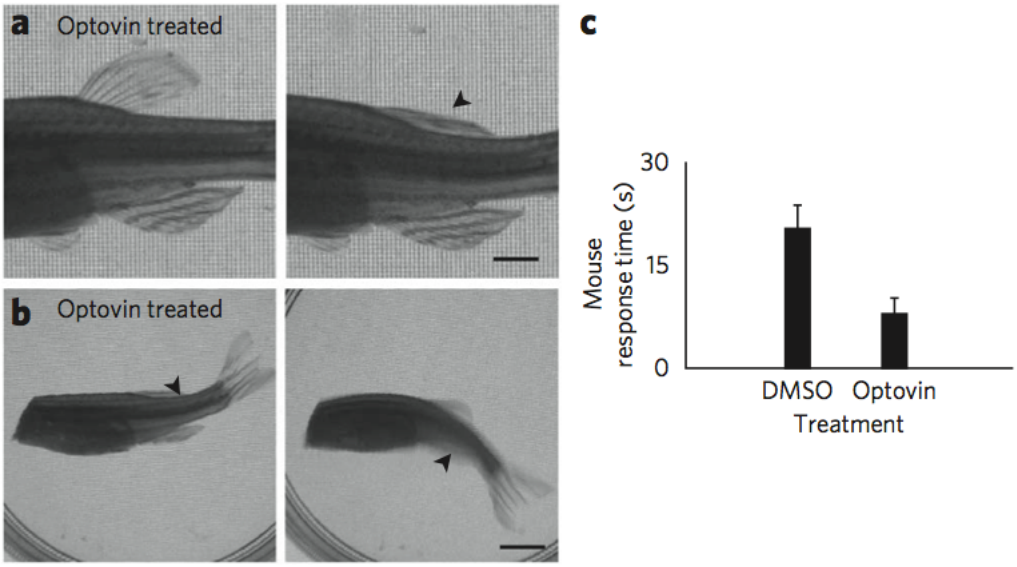

Figure 4.6 - Remote control of optovin-treated animals. (a) Photographs of spinalized zebrafish before and after photo-stimulation of the dorsal fin. Scale bar, 2.5 mm. (b) Photographs of spinalized zebrafish responding to laser photostimulation. Arrowheads indicate approximate location of the 405-nm laser point stimulus. Scale bar, 5 mm. (c) Male C57Bl/6 mice were given an optovin (15 mM) or vehicle (DMSO) swab on one ear. A low-power laser (405 nm) was trained on that ear, and time to a characteristic head shake or head twitch was measured. The difference between groups is significant ($P < 0.05$). Values are averages s.e.m.

eliminates optovin's activity. (ii) In a heterogeneous population of mouse DRG neurons, all optovin-responsive neurons also respond to the TRPA1 agonist mustard oil. (iii) Nonexcitable cultured cells can be rendered light sensitive by transfection with the gene encoding hTrpA1.

Together, these data suggest that optovin specifically targets TRPA1 to enable the light-based control of sensory neurons.

Illumination of many small molecules, including optovin, can produce singlet oxygen or other ROS. Nevertheless, TRPA1 does not seem to simply respond to optovin-generated singlet oxygen because none of the efficient singlet oxygen-generating compounds that we tested caused any behavioral excitation in zebrafish. Instead, we favor the hypothesis that optovin directly binds TRPA1 and forms a photodependent and reversible covalent adduct, perhaps through a radical coupling with a cysteine residue in TRPA1. Olefins such as the one found in optovin's unsaturated rhodanine system are known to react with cysteines under physiological conditions[43,44]. In addition, alterations to optovin or TRPA1 that would prevent cysteine adduct formation reduce optovin activity: methylation of optovin's olefin substantially reduces its activity, as does mutation of presumptive target cysteines in TRPA1. These data are consistent with formation of a thioether linkage between TRPA1 and optovin.

A precedent exists for specific and reversible formation of cysteine adducts between small molecules and their targets. A series of electron-deficient olefins was recently shown to undergo rapid thiol addition reactions with a cysteine in their target kinase. The resultant thioether adducts are short lived, with the reverse reaction (thiol elimination) occurring spontaneously on timescales ranging from subseconds to seconds[44]. In another example that is perhaps even more analogous, flavin mononucleotide (FMN) is bound noncovalently by light, oxygen or voltage (LOV) domain– containing proteins[45]. Illumination with blue light excites FMN to the triplet state such that the C(4a) carbon of FMN reacts with a nearby cysteine in the LOV domain, forms a covalent adduct and alters the protein structure and function. This thioether adduct is also spontaneously reversible on the timescale of seconds.

In both of these examples, noncovalent interactions are necessary to bring the small molecule into close proximity to the target cysteine, where a transient thioether linkage forms spontaneously (electron-deficient olefins) or upon photoactivation (FMN). That structure-directed induced-proximity may also be necessary in the case of optovin is supported by the fact that 171 similar rhodanines in our screening collection did not activate TRPA1 during the screen.

If optovin forms a thioether linkage with TRPA1, it seems to be photodependent and reversible. Its photodependence is suggested by the fact that even high concentrations of optovin do not elicit a behavioral response in zebrafish in the dark. Furthermore, when zebrafish or DRG neurons are treated with optovin and rinsed before illumination, no excitation is observed. Therefore, optovin does not seem to modify TRPA1 in the absence of light. After illumination, excitation is sustained for several seconds, and different optovin derivatives sustain excitation for differing lengths of time after illumination ends, from about 1 s (4g6) to more than 9 s (6b8). These observations are consistent with the idea that termination of excitation is mediated by reversal of the thioether adduct formation and that structural features of the optovin derivatives control the rate of reversal. More extensive analysis will be required to elucidate the factors that influence the reversal rate.

It will be interesting to learn whether optovin-like molecules can be used for controlling endogenous receptors in organisms other than zebrafish and mice. We have shown that optovin activates TRPA1 from zebrafish, mouse and humans and that optovin elicits light-dependent behaviors in zebrafish and mice. Optovin's activity in gating human TRPA1 in transfected cells suggests that it could, in theory, be applied to humans, but development of these compounds for therapeutic applications will require further chemical optimization. For example, rhodanine-containing compounds have been characterized by some as too reactive

for direct clinical development, and only one rhodanine-containing compound is in current clinical use45. Therefore, the safety of optovin-like compounds in humans will need to be evaluated. Nevertheless, the ability to control endogenous TRPA1 channels in vivo raises a number of therapeutic possibilities ranging from pain relief to spinal trauma therapy. Although optovin's activity seems largely restricted to TRPA1-expressing neurons, additional screening may identify next-generation compounds targeting a wide range of targets in different excitable cell types, including cardiac cells. Such tools would have applications ranging from basic neuroscience research to clinical interventions.

METHODS

Aquaculture

A large number of fertilized eggs (up to 5,000 embryos per day) were collected from group mating of Ekkwill or TuAB zebrafish. Embryos were raised in HEPES (10 mM) buffered E3 media in a dark incubator at 28 °C until 30 h.p.f. Groups of approximately eight embryos (28 h.p.f.) were distributed into the wells of flat = bottom black-walled 96-well plates filled with E3 medium (360 l). Embryos were then incubated in a dark incubator at 25 °C for chemical treatment and subsequent experiments. All zebrafish protocols were approved by the Institutional Animal Care and Use Committee at Massachusetts General Hospital.

Chemical libraries and treatments

The Actiprobe library (TimTec) contains 10,000 compounds dissolved in DMSO at a stock concentration of 1mg/ml (~3 mM). The library was screened at a 1:300 dilution in E3 buffer for a final concentration of ~10 μM. Negative controls were treated with an equal volume of DMSO. Stock solutions were added directly to zebrafish in the wells of a 96-well plate, mixed

and allowed to incubate for 2–10 h in the dark before behavioral evaluation in the PMR assay. The library (10,000 compounds) was purchased from the TimTec corporation. The neurotransmitter library (700 compounds; cat. no. 2810) was purchased from Biomol International. Reordered hit compounds were dissolved in DMSO and added to wells as described above. Ordering information: optovin (ST52606; TimTec), analog 6b8 (5707191; Chembridge), 6c1 (6092141; Chembridge), 6c5 (118192; Sigma), 6c7 (6211600; Chembridge), 6c2 (6176046; Chembridge), 6c3 (6206065; Chembridge), 6c4 (7030539; Chembridge), 4g6 (ST025379; TimTec). Reordered compounds were used as received; MS/NMR data were not collected to confirm their identities.

PMR behavioral assay

Animals were exposed to a two-pulse stimulus train with a 10-s interstimulus interval. Exposure to the first pulse was used to trigger the PMR, which has a refractory phase of approximately 10 min. Untreated animals do not respond to the second pulse of light, so motor activity after the second pulse was used to assay for optovin activity. In a typical assay, 1,000 frames of digital video were recorded at 33 f.p.s. using a camera (Hamamatsu ORCA-ER) mounted on a microscope (Nikon TE200) with a 1× objective. Instrument control and data measurement were performed using custom scripts for Metamorph Software (Molecular Devices). Each video was saved for review. Light stimuli were generated with a 300-W xenon bulb housed in a Lambda LS illuminator (Sutter) and delivered to the well 10 s and 20 s after the start of each video. A cold mirror (reflectance between 300 nm and 700 nm) on the illuminator was used to block wavelengths outside of this range. Light intensity was measured using a PM100D power meter attached to a S120VC photodiode power sensor (Thorlabs). Filters were used to restrict the excitation light to the indicated wavelengths.

Spinalized preparations

Adult zebrafish (0.5–1.5 years) were briefly anesthetized in ice water and quickly decapitated with a sharp razor blade. Spinalized preparations were incubated in optovin (50 μM) for 1–2 min before testing with laser light stimuli (405 nm, 400 W mm^{-2}).

Behavioral analysis

To analyze digital video recordings, custom software scripts were used to automatically draw six evenly spaced line segments across each well such that each embryo is likely to be crossed by one of the lines. The software then tracks the average intensity of the pixels for each segment over time. As the embryos move, the light intensity at some of the pixels changes. The motion index was calculated by taking the total absolute difference in pixel intensity between frames. This motion index correlates with the overall amount of motion in the well, both in terms of contraction frequency and number of animals in motion. Behavioral features are quantified by 'excitation scores' that are calculated by taking the 75th percentile of the motion index for 3–5s following the light stimulus. The behavioral profiles were clustered using Euclidean distance and average linkage clustering. All computations and figures were carried out with the MATLAB statistical programming environment.

Statistical analysis

We used one-way ANOVA and the Tukey HSD *post hoc* test to test for significant differences between groups, generate 95% confidence intervals and identify groups with significantly different means. For groups with significant differences, we used the two-tailed *t*-test to test the null hypothesis and calculate the *P* value. Statistical analyses were performed using the anova1, multcompare and ttest2 functions provided by the MATLAB statistics toolbox.

Electrophysiology

HEK293 cells were plated upon polylysine-coated cover slips and transiently transfected with human TRPA1. Voltage clamp recordings were made in the whole-cell configuration 48 h after transfection using glass electrodes with 2-4 MΩ resistance when filled with 140 mM CsCl, 2 mM Mg2ATP3, 2 mM MgCl, 5 mM EGTA and 10 mM HEPES (pH adjusted to 7.2 with CsOH) and while bathed at room temperature in extracellular solution containing 150 mM NaCl, 5.4 mM KCl, 1.8 mM CaCl2, 1 mM MgCl and 5 mM HEPES (pH adjusted to 7.4 with NaOH). A voltage ramp protocol from –80 mV to 80 mV over 400 ms was repeated every second during the follow- ing conditions: while the cell was dialyzed by the pipette, followed by at least 60 s of illumination with 405-nm light, after which optovin (10 μM) containing extracellular solution was perfused into the bath, followed by 1 min of illumination. Current elicited at holding potentials of 70 mV as well as the slope of the current-voltage relation while ramping from 0 to 70 mV were used to characterize TRPA1 activation.

NIMH PDSP profiling

Activity determinations were generously provided by the National Institute of Mental Health's Psychoactive Drug Screening Program, contract no. HHSN-271-2008-00025-C (NIMH PDSP). Complete assay details are found online at http://pdsp.med.unc.edu/UNC-CH%20 Protocol %20Book.pdf.

Calcium imaging methods.

C57Bl/6 male mice (3–4 weeks old) were decapitated, and DRG were dissected into 4°C Hank's Balanced Salt Solution (HBSS; Gibco), then neurons were dissociated using collagenase (1 mg/mL; Worthington) and dispase (5 mg/mL; Gibco) dissolved in HBSS. Neurons were plated in Neurobasal-A medium (Invitrogen), supplemented with B-27 Supplement (Gibco), L-glutamine (Gibco) and penicillin-streptomycin (Gibco). The neurons

were plated onto coverslips coated with 0.1 mg/mL poly-D-lysine (Sigma) and 5 g/mL laminin (Sigma). After 24 h, neurons were washed with assay buffer (HBSS, supplemented with 9 mM HEPES, 11 mM D-glucose, 0.1% fatty-acid free BSA, pH 7.3) and incubated for 1 h with 2 μM Fura2-AM (Invitrogen) with 0.2% pluronic (Invitrogen) in assay buffer in the dark at room temperature. The neurons were then washed with assay buffer and allowed to equilibrate at room temperature for 30 min before imaging. After a 120-s baseline perfusion of assay buffer containing 3.3% DMSO, 100 μM optovin dissolved in the DMSO-assay buffer solution or the DMSO-assay buffer solution alone as a control was perfused onto the neurons for a period of 1 min. Fura-2 is activated with UV light, and the process of imaging Fura-2 was enough to activate the optovin. As a no-light control to ensure that the presence of optovin alone did not cause activation, imaging was stopped for the 1-min period of optovin treatment and resumed once the solution per- fused back onto the neurons. Following this 1-min period, cells were perfused with DMSO-assay buffer to remove the agonist, which was followed by addition of 100 μM mustard oil (in DMSO assay buffer) to determine the total number of TrpA1-expressing neurons present. Images were acquired on a Nikon Eclipse Ti microscope (Nikon, Melville, NY). Neurons were counted as activated if they showed a response during the 1-min activation period. All procedures involving animals for calcium imaging were approved by the Institutional Animal Care and Use Committee at the University of North Carolina at Chapel Hill.

HEK293 cells were plated onto polylysine-coated glass-bottom culture dishes (MatTek Corp) and grown in Dulbecco's Modified Eagle's Medium (DMEM, Sigma) supplemented with 10% FBS and 100 U/mL penicillin and 100 g/ml streptomycin. After 24 h, cells were transfected, according to man- ufacturer's instructions, in Opti-MEM medium, using 4 μl Lipofectamine 2000 (Invitrogen), 0.5 g EGFP in pcDNA and 0.3 g TrpA1 DNA per dish. Medium was replaced after 2 h, and cells were cultured for an additional 17 h. As previously described for neurons,

HEK cells were washed with assay buffer (HBSS Gibco 14025, supplemented with 9 mM HEPES, 11 mM D-glucose, 0.1% fatty acid–free BSA, pH 7.3) and incubated for 1 h with 2 μM Fura2-AM (Invitrogen) with 0.2% pluronic (Invitrogen) in assay buffer in the dark at room temperature. The cells were then washed with assay buffer and allowed to equilibrate at room temperature for 30 min before imaging. At the start of the imaging session for each dish, cells were replaced with DMSO assay buffer. After 50 s of imaging, assay buffer was aspirated by hand and replaced with 100 M optovin dissolved in the DMSO assay buffer solution. Each dish of HEK cells was imaged for a total of 3 min.

Cells were transfected with the hTRPA1 (ref. 38), TRPA1^{C621S} (ref. 38), hTRPA1^{C633S} (ref. 39) and hTRPA1$^{C633S\ C856S}$ (ref. 39) plasmids as described.

Long-term toxicity testing

To determine the long-term effects of optovin exposure on development, behavior and survival, we analyzed the development, behavior and survival of larvae (n = 150) and adult zebrafish (n = 2) exposed to optovin (10 μM) for 96 h. We did not identify any differences between the appearance, touch response, heart rate, fin movements or morphology between the treated and untreated groups.

NIMH PDSP *in vitro* receptor profiling

In vitro receptor profiling was performed by the National Institute of Mental Health's Psychoactive Drug Screening Program, contract no. HHSN-271-2008-00025-C (NIMH PDSP). For primary screening, data represent mean percentage inhibition at the receptor subtypes (n = 4 determinations; Supplementary Table 1). The default primary screening concentration is 10 μM. If >50% inhibition was obtained in the primary screen, K_i determinations were

performed at concentrations ranging from 10 pM to 10 μM. For K_i determinations, data represent K_i (nM) values obtained from nonlinear regression. Complete assay details are found online at http://pdsp.med.unc.edu/UNC-CH%20Protocol%20Book.pdf.

Dissection and culture

Male adult C57Bl/6 mice were purchased from Jackson Laboratories and housed in the animal facilities of Children's Hospital Boston on a 12-h alternating light-dark cycle. Animals for imaging were dissected after 7 weeks of age. TRPA1-KO mice were provided by K. Kwan (Howard Hughes Medical Institute, Harvard Medical School)[11]. After CO_2 asphyxiation and cervical translocation and following spinal laminectomy, the left and right DRG from the whole spine were removed and placed in 4 °C Hank's buffered saline solution without calcium and magnesium (HBSS, Life Technologies). After the DRG were collected and spun down for 3 min at 1,000 r.p.m. (150 *g*), they were placed in a collagenase/dispase solution (3 mg/mL dispase II and 1 mg/mL collagenase A, Roche Applied Science) and allowed to incubate at 37 °C for 90 min. After incubation, the cells were washed in Dulbecco's Modified Eagle's Medium (DMEM, Life Technologies), fortified with 4.5 g L/D- glucose, L-glutamine, 110 mg/L sodium pyruvate, 10% FBS (Life Technologies), penicillin (500 U/mL, Cellgro) and streptomycin (500 g/mL, Cellgro). DNAse (125 U/mL, Sigma) was then added, and the solution was triturated using successively smaller caliber flame-polished Pasteur pipettes. This solution was gently layered onto a bovine serum albumin gradient (10% albumin from bovine serum, Sigma in PBS, Life Technologies) and spun at 150 *g* for 12 min. After removal of the supernatant, the cells were washed again in DMEM; suspended in neurobasal medium (Life Technologies) supplemented with L-glutamine (20 mM, Life Technologies), B-27 supplement (Life Technologies), penicil- lin (500 U/mL, Cellgro) and streptomycin (500 g/mL, Cellgro); plated

onto laminin-treated (1 mg/mL, Sigma) 15-mm glass-bottom dishes (MatTek Corporation); and then placed in an incubator at 37 °C (5% CO_2) overnight. All imaging was performed 1 d after dissection and culture.

Calcium imaging

DRG neurons were imaged on a Nikon Ti Eclipse inverted microscope. Fura-2, AM (Life Technologies) was loaded into the neurons for 30 min (room temperature, 4 μg/mL). After washing with standard extracellular solution (Boston BioProducts), the cells were imaged using a QImaging EXi Aqua cooled camera, and data were collected and analyzed using NIS Elements software (AR 3.10). Neurons were selectively exposed to various solutions via a gravity-assisted perfusion system. Responses were included if they were 20% greater than the baseline.

Mouse behavior

Male adult C57Bl/6 mice were assessed for behavior after 7 weeks of age, purchased from Jackson Laboratories and housed in the animal facilities of Children's Hospital Boston on a 12-h alternating light-dark cycle, with food and water provided *ad libitum*. This behavioral protocol was approved by the Institutional Animal Care and Use Committee at Children's Hospital Boston. After habituation periods in a custom-built behavior chamber, mice were either treated with 20 uL of optovin solution (15 mM in DMSO, Sigma-Aldrich) or vehicle control (DMSO) on the ear. Upon return to the behavior chamber, a laser (405 nm, class 3A, common laser pointer) was trained on the treated ear. Time to activation of a characteristic head-twitch or head-shake response (HSR) was recorded for each animal over five separate trials[47]. The response is a rapid, radial twitch of the head about the dorsal-ventral axis of the head. The time cutoff for laser stimulation was set at 60 s if no response was elicited (four

optovin versus four control animals). One optovin-treated mouse was excluded from the mean analysis because of extreme nonresponsiveness. Average time to response per animal was calculated by a blinded coder using VLC media playback at 0.25× speed who measured the actual time the laser was on the ear. Data were pooled between animals within groups. Error bars represent standard error.

Works Cited

1. Alexander, G.M. *et al.* Remote control of neuronal activity in transgenic mice expressing evolved G protein–coupled receptors. *Neuron* 63, 27–39 (2009).

2. Armbruster, B.N., Li, X., Pausch, M.H., Herlitze, S. & Roth, B.L. Evolving the lock to fit the key to create a family of G protein–coupled receptors potently activated by an inert ligand. *Proc. Natl. Acad. Sci. USA* 104, 5163–5168 (2007).

3. Banghart, M., Borges, K., Isacoff, E., Trauner, D. & Kramer, R. Light-activated ion channels for remote control of neuronal firing. *Nat. Neurosci.* 7, 1381–1386 (2004).

4. Boyden, E.S., Zhang, F., Bamberg, E., Nagel, G. & Deisseroth, K. Millisecond- timescale, genetically targeted optical control of neural activity. *Nat. Neurosci.* 8, 1263–1268 (2005).

5. Deisseroth, K. Optogenetics. *Nat. Methods* 8, 26–29 (2011).

6. Ferguson, S.M. *et al.* Transient neuronal inhibition reveals opposing roles of indirect and direct pathways in sensitization. *Nat. Neurosci.* 14, 22–24 (2011).

7. Szobota, S. *et al.* Remote control of neuronal activity with a light-gated glutamate receptor. *Neuron* 54, 535–545 (2007).

8. Janovjak, H., Szobota, S., Wyart, C., Trauner, D. & Isacoff, E. A light-gated, potassium-selective glutamate receptor for the optical inhibition of neuronal firing. *Nat. Neurosci.* 13, 1027–1032 (2010).

9. Volgraf, M. *et al.* Reversibly caged glutamate: a photochromic agonist of ionotropic glutamate receptors. *J. Am. Chem. Soc.* 129, 260–261 (2007).

10. Wang, S. *et al.* All optical interface for parallel, remote, and spatiotemporal control of neuronal activity. *Nano Lett.* 7, 3859–3863 (2007).

11. Kwan, K.Y. *et al.* TRPA1 contributes to cold, mechanical, and chemical nociception but is not essential for hair-cell transduction. *Neuron* 50, 277–289 (2006).

12. Kramer, R.H., Fortin, D.L. & Trauner, D. New photochemical tools for controlling neuronal activity. *Curr. Opin. Neurobiol.* 19, 544–552 (2009).

13. Callaway, E.M. & Katz, L.C. Photostimulation using caged glutamate reveals functional circuitry in living brain slices. *Proc. Natl. Acad. Sci. USA* 90, 7661–7665 (1993).

14. Dalva, M.B. & Katz, L.C. Rearrangements of synaptic connections in visual cortex revealed by laser photostimulation. *Science* 265, 255–258 (1994).

15. Fortin, D.L. *et al.* Photochemical control of endogenous ion channels and cellular excitability. *Nat. Methods* 5, 331–338 10.1038/nmeth.1187 (2008).

16. Fortin, D.L. *et al.* Optogenetic photochemical control of designer K^+ channels in mammalian neurons. *J. Neurophysiol.* 106, 488–496 (2011).

17. Noguchi, J. *et al. In vivo* two-photon uncaging of glutamate revealing the structure-function relationships of dendritic spines in the neocortex of adult mice. *J. Physiol. (Lond.)* 589, 2447–2457 (2011).

18. Volgraf, M. *et al.* Allosteric control of an ionotropic glutamate receptor with an optical switch. *Nat. Chem. Biol.* 2, 47–52 (2006).

19. Wieboldt, R. *et al.* Photolabile precursors of glutamate: synthesis, photochemical properties, and activation of glutamate receptors on a microsecond time scale. *Proc. Natl. Acad. Sci. USA* 91, 8752–8756 (1994).

20. Mourot, A. *et al.* Rapid optical control of nociception with an ion-channel photoswitch. *Nat. Methods* 9, 396–402 (2012).

21. Brain, S.D. TRPV1 and TRPA1 channels in inflammatory pain: elucidating mechanisms. *Ann. NY Acad. Sci.* 1245, 36–37 (2011).

22. Jordt, S.E. & Ehrlich, B.E. TRP channels in disease. *Subcell. Biochem.* 45, 253–271 (2007).

23. Kremeyer, B. *et al.* A gain-of-function mutation in TRPA1 causes familial episodic pain syndrome. *Neuron* 66, 671–680 (2010).

24. Schwartz, E.S. *et al.* Synergistic role of TRPV1 and TRPA1 in pancreatic pain and inflammation. *Gastroenterology* 140, 1283–1291 (2011).

25. MacRae, C.A. & Peterson, R.T. Zebrafish-based small molecule discovery. *Chem. Biol.* 10, 901–908 (2003).

26. Zon, L.I. & Peterson, R.T. *In vivo* drug discovery in the zebrafish. *Nat. Rev. Drug Discov.* 4, 35–44 (2005).

28. Schmitt, E.A. & Dowling, J.E. Early retinal development in the zebrafish, *Danio rerio*: light and electron microscopic analyses. *J. Comp. Neurol.* 404, 515–536 (1999).

30. Dhaka, A., Viswanath, V. & Patapoutian, A. TRP ion channels and temperature sensation. *Annu. Rev. Neurosci.* 29, 135–161 (2006).

31. Bandell, M. *et al.* Noxious cold ion channel TRPA1 is activated by pungent compounds and bradykinin. *Neuron* 41, 849–857 (2004).

32. Moran, M.M., Xu, H. & Clapham, D.E. TRP ion channels in the nervous system. *Curr. Opin. Neurobiol.* 14, 362–369 (2004).

33. Escalera, J., von Hehn, C.A., Bessac, B.F., Sivula, M. & Jordt, S.E. TRPA1 mediates the noxious effects of natural sesquiterpene deterrents. *J. Biol. Chem.* 283, 24136–24144 (2008).

34. Prober, D.A. *et al.* Zebrafish TRPA1 channels are required for chemosensation but not for thermosensation or mechanosensory hair cell function. *J. Neurosci.* 28, 10102–10110 (2008).

35. Eid, S.R. *et al.* HC-030031, a TRPA1 selective antagonist, attenuates inflammatory- and neuropathy-induced mechanical hypersensitivity. *Mol. Pain* 4, 48 (2008).

36. Laustriat, G. Molecular mechanisms of photosensitization. *Biochimie* 68, 771–778 (1986).

37. Ouannes, C. & Wilson, T. Quenching of singlet oxygen by tertiary aliphatic amines. Effect of DABCO (1,4-diazabicyclo [2.2.2]octane). *J. Am. Chem. Soc.* 90, 6527–6528 (1968).

38. Macpherson, L.J. *et al.* Noxious compounds activate TRPA1 ion channels through covalent modification of cysteines. *Nature* 445, 541–545 (2007).

39. Takahashi, N. *et al.* TRPA1 underlies a sensing mechanism for O_2. *Nat. Chem. Biol.* 7, 701–711 (2011).

40. Hinman, A., Chuang, H.H., Bautista, D.M. & Julius, D. TRP channel activation by reversible covalent modification. *Proc. Natl. Acad. Sci. USA* 103, 19564–19568 (2006).

43. Patch, R.J. *et al.* Identification of diaryl ether–based ligands for estrogen- related receptor alpha as potential antidiabetic agents. *J. Med. Chem.* 54, 788–808 (2011).

44. Serafimova, I.M. *et al.* Reversible targeting of noncatalytic cysteines with chemically tuned electrophiles. *Nat. Chem. Biol.* 8, 471–476 (2012).

45. Herrou, J. & Crosson, S. Function, structure and mechanism of bacterial photosensory LOV proteins. *Nat. Rev. Microbiol.* 9, 713–723 (2011).

47. Corne, S.J., Pickering, R.W. & Warner, B.T. A method for assessing the effects of drugs on the central actions of 5-hydroxytryptamine. *Br. J. Pharmacol. Chemother.* 20, 106–120 (1963).

Chapter 5: Activity-dependent silencing reveals functionally distinct itch-generating sensory neurons* **

ABSTRACT

The peripheral terminals of primary sensory neurons detect histamine and non-histamine itch-provoking ligands through molecularly distinct transduction mechanisms. It remains unclear, however, whether these distinct pruritogens activate the same or different afferent fibers. Using a strategy of reversibly silencing specific subsets of murine pruritogen-sensitive sensory axons by targeted delivery of a charged sodium-channel blocker, we found that functional blockade of histamine itch did not affect the itch evoked by chloroquine or SLIGRL-NH2, and vice versa. Notably, blocking itch-generating fibers did not reduce pain-associated behavior. However, silencing TRPV1$^+$ or TRPA1$^+$ neurons allowed allyl isothiocyanate or capsaicin, respectively, to evoke itch, implying that certain peripheral afferents may normally indirectly inhibit algogens from eliciting itch. These findings support the presence of functionally distinct sets of itch-generating neurons and suggest that targeted silencing of activated sensory fibers may represent a clinically useful anti-pruritic therapeutic approach for histaminergic and non-histaminergic pruritus.

INTRODUCTION

---

* The behavior work was performed by David Roberson in the Woolf laboratory. I performed calcium imaging experiments showing the population connections between TRPV1/histamine and TRPA1/ chloroquine after dissecting and culturing DRG neurons, demonstrating an anatomical distinction between the histamine-independent and dependent itch neurons in trigeminal neurons.

** This chapter is a modified version of an article previously published as: Roberson, D. P., Gudes, S., Sprague, J. M., Patoski, Haley A. W., Robson, V. K., Blasl, F., Duan, B., Oh, S. B., Bean, B. P., Ma, Q., Binshtok, A. M., & Woolf, C. J. Activity-dependent silencing reveals functionally distinct itch-generating sensory neurons. Nat. Neurosci. 16, 910–8 (2013).

Itch is a complex unpleasant cutaneous sensation that in some respects resembles pain, yet is different in terms of its intrinsic sensory quality and the urge to scratch. Histamine-mediated itch, as in patients with urticaria, can be effectively treated using histamine receptor antagonists[1]. However, itch accompanying most chronic pruritic diseases, including atopic dermatitis (eczema)[2], allergic itch[3] and dry skin itch[4], is not predominantly mediated by histamine[5]. The G protein–coupled receptors responsive to specific itch-generating ligands are distinct, although, at a cellular level, there is overlapping responsiveness of trigeminal and dorsal root ganglia (DRG) neurons to itch-producing pruritogens and pain-producing algogens[6–9]. Histamine-sensitive H1 receptors (H1Rs) generate histamine itch and are expressed by TRPV1$^+$ phospholipase-β3 (PLCβ3)$^+$ fibers[10,11]. Itch evoked by chloroquine is mediated by Mas-related G protein–coupled receptor (Mrgpr) A3 (refs. 6,12), whereas MrgprC11 is sensitized in dry skin itch[9,13] and activated by pruritogens released from mast cells during allergic itch[3]. Notably, co-activation of TRPV1 and H1R is required to produce histamine itch[14], whereas MrgprA3- or MrgprC11-mediated itch requires co-activation of TRPA1[12], even though each of these TRP channels are canonical nociceptor transducers. *In vitro* calcium-imaging experiments have shown that neurons expressing MrgprA3 also respond to histamine, which has been interpreted as indicating a single neuronal path for histaminergic and MrgprA3- dependent itch[6]. Supporting this, ablation of neurons expressing MrgprA3 reduces the scratching evoked by histamine, chloroquine, dry skin and allergic inflammation[15]. However, others report separate neural pathways mediating histamine and certain types of non-histamine itch[16,17]. Furthermore, although primary sensory neurons of juvenile mice respond to multiple itch mediators, this nonspecificity decreases with age[18].

Thus, it remains controversial whether there are separate afferents in the adult that mediate histamine itch and MrgprA3-dependent non-histamine itch. This distinction is clinically important, as therapies targeting histaminergic itch fibers might be ineffective for treating non-histaminergic itch if the neurons mediating the two itches are functionally distinct in the adult.

To study whether histaminergic and non-histaminergic itch are functionally distinct, we adapted a method originally designed for achieving a pain-specific peripheral nerve block[19,20] to selectively silence the peripheral terminals of different subsets of pruritogen- and algogen-responsive primary afferents in an activity-dependent manner. To do this, we targeted the charged, membrane-impermeable lidocaine derivative *N*-ethyl-lidocaine (QX-314, a sodium channel blocker) through large pore ion channels activated specifically by different algogens and pruritogens.

METHODS

Cell culture. Trigeminal neuron cultures were prepared from adult (2–3 month old) CD-1 mice[44]. In short, trigeminal neurons were removed and placed into Hank's balanced salt solution and 1% penicillin-streptomycin (vol/vol, Sigma), then digested in 5 mg ml^{-1} collagenase and 1 mg ml^{-1} Dispase II (Roche). Cells were triturated in the presence of DNAse I inhibitor (50U) and centrifuged through 10% BSA (vol/vol, Sigma). The cell pellet was resuspended in 1 ml Neurobasal (Sigma) containing B27 supplement (Invitrogen), penicillin and streptomycin (Sigma), 10 μM AraC. Cells were plated onto poly-d-lysine–coated (500 μg ml^{-1}) and laminin-coated (5 mg ml^{-1}) 35-mm tissue culture dishes (Becton Dickinson) at 8,000–9,000 per dish, at 37 °C, in 5% carbon dioxide.

Calcium imaging experiments. All dissections were performed on adult (2–4 month old) male CD-1 mice. The calcium-indicator dye Fura-2 a.m. was introduced at 2 μg ml^{-1} for 30 min at 22±2 °C, washed and analyzed on a Nikon Eclipse Ti inverted microscope with exi-aqua CCD camera and NIS-elements AR 3.10 software. Each cell was given 3 min to recover from each pruritogen exposure and 8 min to recover between exposure to AITC and capsaicin. Each exposure lasted for 60 s, except for capsaicin, which was exposed for 10 s. Pruritogens were locally applied, with the perfusion opening placed approximately 150 μm from the field of view, and preliminary exposure to standard extracellular solution was employed before exposure to reagents made in SES. Pruritogen order was assigned at random (coin toss) for each plate, and no order effects were observed between differently ordered groups.

Behavioral studies. All animal procedures were approved by the Boston Children's Hospital Animal Care and Use Committee. Naive adult (2–4 month old) male CD-1 mice (Charles River Laboratories) housed in groups of five mice using a normal 12-h light/dark cycle were used. Mice were fully habituated to handling before all experimental procedures and were randomly assigned to experimental groups. The day before beginning itch experiments, mice were briefly anesthetized by inhalation of 1–2% isofluorane (vol/vol) and a ~1-cm^2 area of hair was shaved on the right cheek of each mouse. Capsaicin (Sigma-Aldrich) was freshly prepared by dilution in vehicle (20% ethanol (vol/vol), 5% Tween 20 (vol/vol), in saline, 10 ml). All other drug solutions were prepared fresh in normal saline (0.9% NaCl, wt/vol).

Itch assay. Mice received intradermal microinjections of pruritogen, algogen, QX-314, vehicle or a combination of pruritogen or algogen together with QX-314 intradermally in the cheek. To ensure proper intradermal injection, needle puncture with a 28-gauge needle was initiated bevel-up at 5° to the plane of taut skin until initial penetration, then inserted horizontally until the needle tip was 0.5 cm beyond the point of insertion before intradermal evacuation of

syringe contents. Correct injection was confirmed by presence of a slightly domed bulla immediately following removal of needle. For sequential injection experiments, the intradermal bullae of the conditioning (first) injection were outlined with fine-tip permanent marker to denote the extent of intradermal drug distribution, thereby providing visible drug distribution boundaries for subsequent injections. Mice not receiving proper drug injections were noted and excluded from the study before observation. Immediately after conditioning injection, mice were placed in a custom-built itch observation apparatus and video recorded during the mouse dark cycle as previously described[26]. Scratches and/or wipes were subsequently quantified by blinded observers.

Statistical analysis. Sample sizes for all experiments were chosen according to standard practice in the field. For electrophysiological experiments, the significance of the effect was calculated using two-way ANOVA non-parametric test followed by Bonferroni post-test. Comparison of group means for behavior studies was performed using Student's *t* test. All bar graphs are plotted as mean s.e.m. For behavioral studies, *n* represents the total number of mice used in each group.

RESULTS

Selective silencing of pruriceptors *in vivo*

To determine whether we could selectively silence pruriceptors *in vivo*, we used intradermal cheek injections of pruritogens and QX- 314, and then characterized pruriceptor function by quantifying ensuing behavioral responses related to itch (hindlimb scratching of cheek) or pain (forelimb wiping of cheek)[26]. Intradermal injection of histamine (100 μg per 20 μl) produced scratching (64.3 ± 7.5 bouts, n = 6 mice) that fully resolved in 30 min. There was no significant

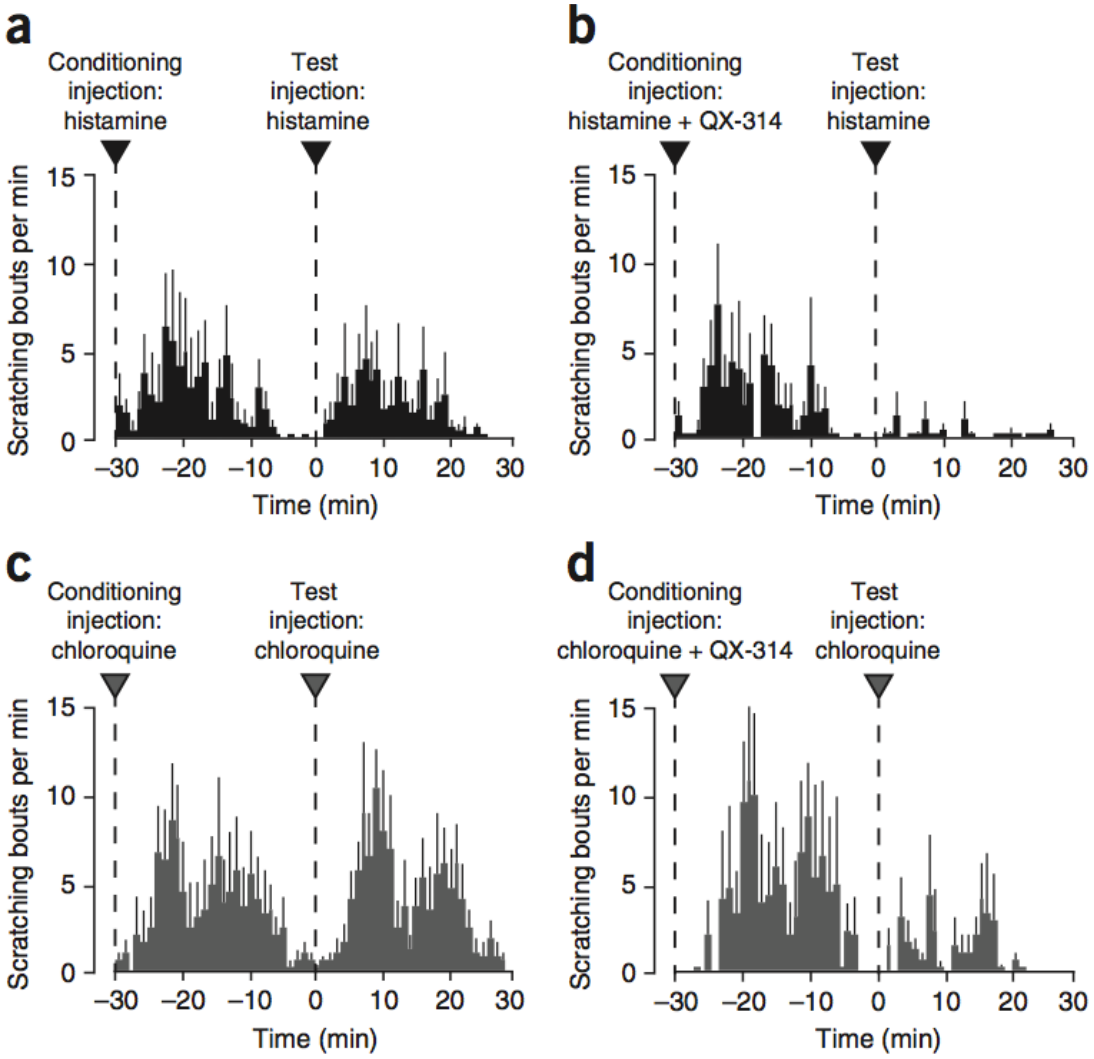

Figure 5.1 - Co-administration of QX-314 and pruritogens inhibits subsequent pruritogen-evoked scratching. (**a**,**c**,**e**) Sequential pruritogen cheek injections at 30-min inter-stimulus intervals evoked similar levels of cheek scratching (itch) bouts. (**b**,**d**,**f**) Pruritogen-evoked scratching was inhibited 30-min after conditioning injection of pruritogen and 1% QX-314. (**a**) Conditioning injection: histamine (100 μg per 20 μl), total scratching bouts in 30 min (TSB) = 64.3±7.5 bouts. Test injection: histamine (100 μg per 10 l), TSB = 49.2±9.7, $P > 0.05$, $n = 6$ mice, degrees of freedom (df) = 10. (**b**) Conditioning injection: histamine (100 μg per 20 μl) + 1% QX-314, TSB = 56.0±8.3. Test injection: histamine (100 μg per 10 μl), TSB = 7.5±3.8, $P < 0.001$, $n = 6$ mice, df = 10. (**c**) Conditioning injection: chloroquine (50 μg per 20 μl), TSB min = 103.0±19.1. Test injection: chloroquine (50 μg per 10 μl), TSB = 109.0±20.8, $P > 0.05$, $n = 7$ mice, df = 12. (**d**) Conditioning injection: chloroquine (50 μg per 20 μl) + 1% QX-314, TSB = 110.0±13.7. Test injection: chloroquine (50 μg per 10 μl), TSB = 31.8±13.3, $P < 0.01$, $n = 6$ mice, df = 10. Data are presented as mean s.e.m. of total scratching bouts per minute for 30 min after conditioning injection and test injection. *P* values represent comparison of value of mean total scratching bouts in 30 min evoked by test injection to those evoked by conditioning injection.

change in scratching (56.0 ± 8.3 bouts, $n = 6$ mice, $P > 0.05$) when histamine was injected with 1% QX-314. On the basis of the delayed time course of nociceptor block *in vivo* in response to a combination of capsaicin and QX-314 (ref. 19), and considering the gradual development of full sodium current block *in vitro* after QX-314 and histamine co-administration (data not shown), we hypothesized that the short duration of histamine-evoked scratching behavior (~25 min) was too brief to detect the slow-onset blocking effects generated by co-administration of histamine with QX-314. To test this, we devised a behavioral model using two sequential intradermal injections, 30 min apart, of a pruritogen into the same intradermal cheek injection site. Identical pruritogen doses were used in each injection. Only behavior evoked by the test (second) injection was compared with behavior evoked by other identical test injections, with the experimental variable being the identity of the conditioning (first) injection given 30 min earlier.

When histamine alone was given for the conditioning injection (100 μg per 20 μl) and again 30 min later for the test injection (100 μg per 10 μl) at the same site, the amount of scratching evoked by the two injections was not significantly different ($P > 0.05$; **Figure 5.1a**). However, histamine-evoked scratching was effectively abolished 30 min after a conditioning injection of both histamine and QX-314 (**Figure 5.1b**), but not when it was preceded by an injection of QX-314 alone (**Figure 5.2a**). We conclude that histamine-mediated activation of large pore channels, such as TRPV1 (ref. 14), permitted uptake of QX-314 and produced a slow (<30 min) onset electrical silencing of the histamine-responsive sensory fibers, which then blocked the response to subsequent injection of histamine (**Figure 5.1b**).

We further hypothesized that intradermal administration of chloroquine with QX-314 could block chloroquine itch by permitting selective uptake of QX-314 through chloroquine-mediated activation of a large-pore ion channel, likely TRPA1 (ref. 12). Co-injection of QX-314 together

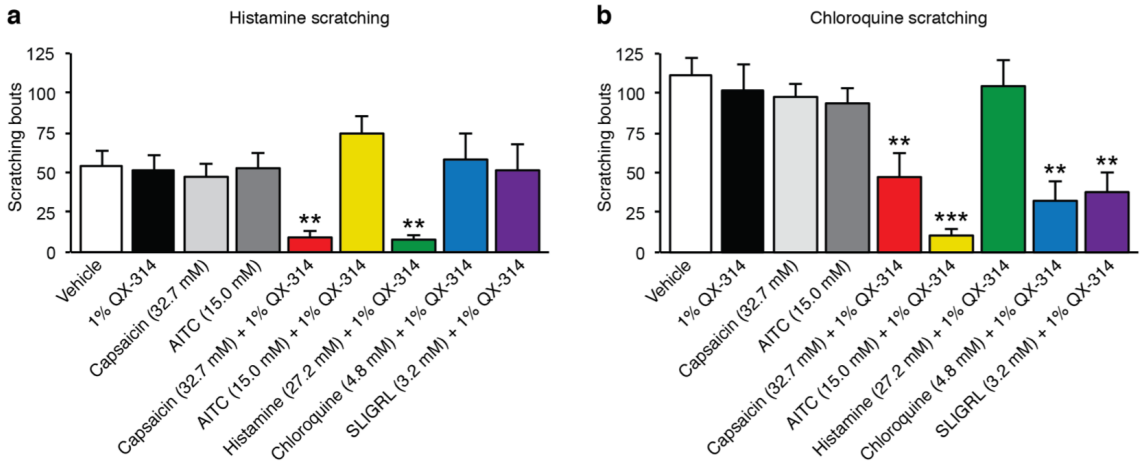

Figure 5.2 - Pruritogen and algogen- mediated scratching measured 30 minutes after conditioning injections (indicated at the x-axes). **(a)** Histamine-evoked hindlimb scratching bouts. **(b)** Chloroquine-evoked hindlimb scratching bouts. P-value annotations represent comparison of value of annotated column to vehicle conditioning injection value (No annotation, $P > 0.05$; *, $P < 0.05$; **, $P < 0.01$; ***, $P < 0.001$). Error bars represent SEM.

with chloroquine (50 μg per 20 μl) inhibited scratching produced by subsequent chloroquine (50 μg per 10 μl) test injection, whereas injection of chloroquine alone or QX-314 alone did not (**Figure 5.1c**,**d** and **Figure 5.2b**). We conclude that large-pore channels downstream of chloroquine-evoked MrgprA3 activation, possibly TRPA1 (ref. 12), permit selective uptake of QX-314 and subsequent electrical silencing of chloroquine-sensitive afferent fibers.

Distinct fibers mediate histamine and non-histamine itch

We next used the silencing strategy to reveal whether different pruritogens activate the same or unique peripheral afferent pathways by administering test injections (10 μl) of histamine (100 μg) or chloroquine (50 μg) 30 min after conditioning injections (20 μl) of histamine (100 μg), chloroquine (50 μg) or SLIGRL (50 μg) with or without QX-314. We hypothesized that if histaminergic and non-histaminergic itch are transmitted by different subsets of afferent fibers,

application of both histamine and QX-314 will block histaminergic itch, whereas chloroquine itch will remain intact, and vice versa.

We first examined whether histamine-evoked scratching is affected by the targeted silencing of chloroquine-activated pruriceptors. Histamine-evoked scratching was unchanged 30 min after a conditioning injection of both chloroquine and QX-314 (**Figure 5.3a**), even though this treatment blocked subsequent chloroquine itch (**Figures 5.1b** and **5.3b**). Similarly, conditioning injection of SLIGRL and QX-314 (which reverses later SLIGRL-evoked scratching) did not reduce subsequent histamine (100 μg per 10 μl) itch (**Figure 5.3a**).

We then asked whether chloroquine itch is affected following silencing of histamine- or SLIGRL-sensitive itch fibers by injecting chloroquine 30 min after administration of QX-314 and either histamine or SLIGRL. Chloroquine-evoked itch was blocked after co-injection of SLIGRL and QX-314, but not by co-administration of histamine and QX-314 (**Figure 5.3b**).

It appears that a common afferent population mediates chloroquine and SLIGRL itch, but this population is functionally distinct from the neurons responsible for histamine itch. These findings contrast, however, with prior *in vitro* data showing that all chloroquine-responsive DRG neurons respond to histamine[6]. A possible explanation for this discrepancy is that peripheral terminals of trigeminal neurons differ from DRG neuron cell bodies in terms of their responsiveness to multiple pruritogens. To explore this, we repeated the same silencing strategy on the back below the neck. Treatment with both histamine and QX-314 did not reduce subsequent chloroquine-evoked scratching when compared with treatment with vehicle, whereas intradermal injection of both chloroquine and QX-314 inhibited subsequent chloroquine-evoked scratching (data not shown), indicating that facial and somatic itch appear to be similar in terms of the functional independence of histamine and non-histamine itch.

Another possibility is that different pruriceptor subsets exist with high or low sensitivity to either histamine or non-histamine pruritogens. To investigate this, we varied the dose of pruritogen given with 1% QX-314 (20 μl) for conditioning injections. Application of a lower dose of histamine (10 μg) together with QX-314 inhibited subsequent histamine-evoked scratching without reversing chloroquine (50 μg) scratching (**Figure 5.3a**,**b**), which was essentially the same as the observed effects following a higher dose of histamine (100 μg) with QX-314. However, increasing the concentration of histamine to 108.7 mM (400 μg per 20 μl) with QX-314 for conditioning injections blocked scratching evoked by both histamine and chloroquine (**Figure 5.3a**,**b**), indicating that an overlap manifests only at very high doses of histamine. Higher doses of chloroquine (200 or 400 μg) and QX-314 blocked later chloroquine itch behavior, but not scratching evoked by histamine. However, using 96.9 mM chloroquine (1 mg per 20 μl) together with QX-314 for conditioning injections blocked subsequent histamine- and chloroquine-evoked scratching (**Figure 5.3a**,**b**). These data suggest that histamine and

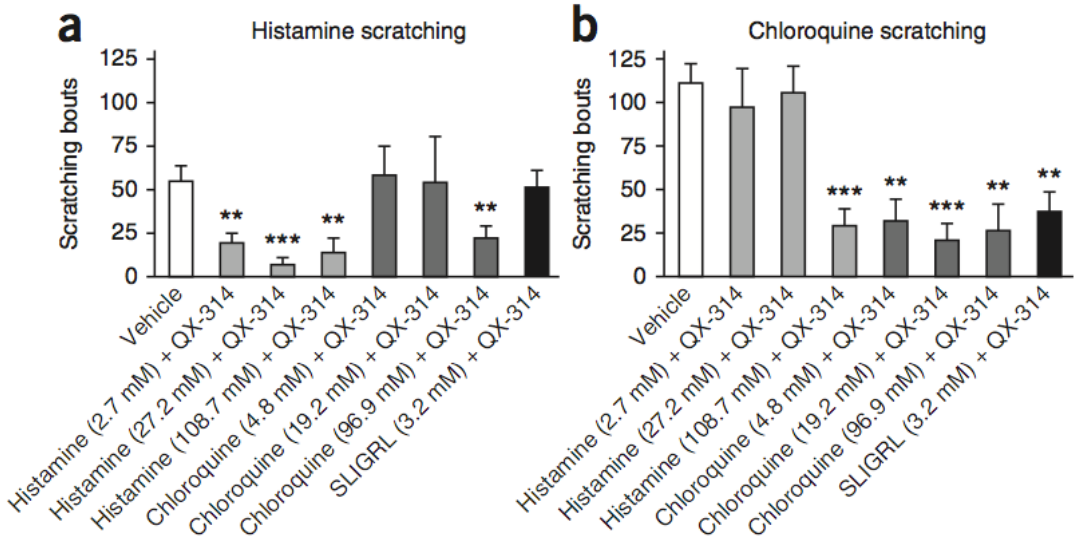

Figure 5.3 - Distinct primary afferents mediate histaminergic itch and non-histaminergic itch. Pruritogen-evoked cheek scratching (itch) bouts 30 min after different conditioning injections, indicated at the *x* axes, are shown. (**a**–**c**) Intradermal test injection of histamine (100 μg per 10 μl) alone (**a**), or chloroquine (CQ, 50 μg per 10 μl) alone (**b**) Error bars represent s.e.m. (n = 5–7 mice for all groups).

chloroquine generally activate functionally distinct pruriceptor populations, but these fibers can respond to multiple pruritogens, either directly or indirectly, when they are presented at very high, presumably non-physiological[29,30], concentrations (histamine, 107.8 mM; chloroquine, 96.9 mM).

Histamine and chloroquine act on different sets of neurons

The responsiveness of DRG neurons to multiple pruritogens decreases with age[18]. In juvenile mice, 60–100% of all chloroquine-responsive DRG cells also respond to histamine[6,18], whereas only half of chloroquine-responsive DRG neurons respond to histamine in adolescent mice[18]. We asked whether distinct chloroquine- and histamine- sensitive neuronal populations could be revealed in adult (2–4 months old) mice by their sensitivity to pruritogens *in vitro*. MrgprA3 receptors are activated by 10 μM chloroquine and maximally activated by 1 mM chloroquine in HEK293 cells[6]. Murine DRG neurons respond to histamine at doses as low as 10 μM[14]. We examined coincident calcium responses of 564 cultured trigeminal neurons to 10 μM histamine and 10 μM chloroquine. Histamine activated 4.1% (23 of 564) of trigeminal neurons, whereas 3.0% (17 of 564) responded to chloroquine (**Figure 5.4a**). A majority of chloroquine- and histamine- responding trigeminal neurons responded to only one pruritogen. Among chloroquine-activated cells, 76.5% (13 of 17) responded to chloroquine, but not to histamine, whereas the remaining 23.5% (4 of 17) responded to both 10 μM histamine and 10 μM chloroquine. Likewise, trigeminal neurons responding to histamine were largely unresponsive to chloroquine: 82.6% (19 of 23) responded to histamine, but not chloroquine, and 17.4% (4 of 23) responded to both histamine and chloroquine.

To determine whether responsiveness of adult trigeminal neurons to chloroquine or histamine is dependent on pruritogen dose, we further explored coincident calcium responses to 100 μM histamine and 100 μM chloroquine. Most trigeminal neurons that responded to either 100 μM histamine (4.8% of all cells) or 100 μM chloroquine (4.3% of all cells) did not respond to both (0.9% of all cells) (**Figure 5.5a**). Moreover, we also found that the populations of fibers responding to chloroquine and histamine in DRG neurons from adult mice were, as in the trigeminal ganglia, largely distinct (**Figure 5.5b**). These data indicate that primary afferent populations responding to histamine and chloroquine are largely distinct in adult mice.

The requisite expression of TRPV1 for histaminergic itch[14] and TRPA1 for chloroquine-evoked itch[12] raises the question of whether relative expression patterns of TRPA1 and TRPV1 differ among chloroquine- and histamine-sensitive neuronal populations. To answer this, we exposed cultured trigeminal neurons to 100 μM AITC and 1 μM capsaicin and measured the coincident responses of neurons to both agents. Consistent with the described receptor expression patterns for neurons that mediate histamine itch (for example, H1R and TRPV1)[10,14] and chloroquine itch (for example, MrgprA3 and TRPA1)[6,12], we found that a majority (16 of 23, 69.6%) of histamine- responsive cells responded to capsaicin (**Figure 5.4b**) and most (9 of 17, 52.9%) of the chloroquine-activated neurons were sensitive to AITC (**Figure 5.4c**). The inverse relationships were also true; most (14 of 23 neurons, 60.8%) histamine-responsive trigeminal cells did not respond to AITC (**Figure 5.4d**), and capsaicin failed to activate a majority (12 of 17, 70.6%) of chloroquine-activated neurons (**Figure 5.4e**).

Roles of TRP channels in histamine and non-histamine itch

The different expression patterns of TRPV1 and TRPA1 among histamine- and chloroquine-sensitive neurons *in vitro* (**Figure 5.4**) suggest that targeted silencing of TRPV1 or TRPA1

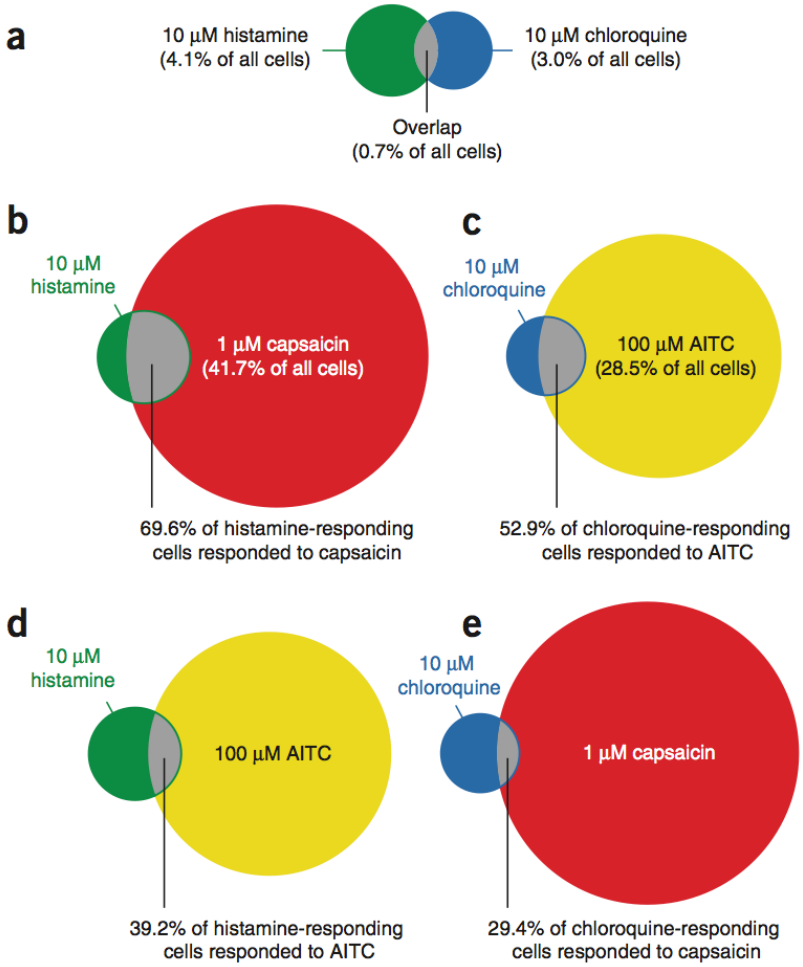

Figure 5.4 - Proportional representation of coincident trigeminal cell responses to low-dose chloroquine and histamine and their overlapping responsiveness with capsaicin and AITC. Shown are Venn diagrams of calcium responses of 564 cultured trigeminal neurons to 10 μM histamine, 10 μM chloroquine, 1 μM capsaicin and 100 μM AITC. (**a**) Histamine (10 μM) activated 23 of 564 trigeminal neurons, whereas 17 neurons responded to 10 μM chloroquine. Among histamine-activated cells, 19 of 23 responded to histamine, but not chloroquine, and 4 of 23 responded to both histamine and chloroquine. For trigeminal cells responding to chloroquine, 13 of 17 responded to chloroquine, but not histamine. (**b**) Capsaicin activated 235 of 564 cells. Among the histamine-responsive cells, 16 of 23 also responded to capsaicin. (**c**) AITC activated 161 of 564 trigeminal neurons, and more than half of chloroquine-responding cells (9 of 17) responded to AITC. (**d**) AITC activated 9 of 23 of histamine-responding cells. (**e**) Capsaicin

fibers may differently affect histamine itch and chloroquine itch. To explore this, we administered 20-μl conditioning injections of capsaicin (0.1%) or AITC (0.15%), with or without QX-314, and then administered 10-μl test injections of the pruritogens histamine (100 μg),

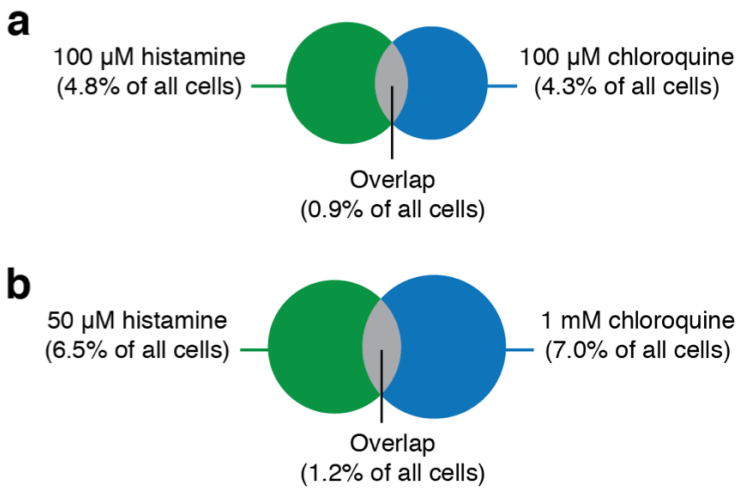

Figure 5.5 - Venn representation of relative populations of trigeminal and DRG neurons defined by their calcium responses to histamine and chloroquine. **(a)** Histamine (100 µM) activated 10 of 208 trigeminal neurons, while 9 responded to 100 µM chloroquine. Among histamine-activated cells 8 of 10 responded to histamine but not chloroquine. For chloroquine-responsive neurons, 7 of 9 responded to chloroquine alone. 2 cells responded to both histamine and chloroquine. **(b)** Among 417 cultured DRG neurons, 32 cells responded 50 µM histamine and 34 were activated by 1 mM chloroquine. Among histamine responsive cells, 27 of 32 responded to histamine alone. Chloroquine, but not histamine, activated 29 of 34 chloroquine responders. 5 cells responded to histamine and chloroquine.

chloroquine (50 μg) or SLIGRL (50 μg) 30 min later at the same site. Injection of capsaicin alone did not significantly reduce histamine- or chloroquine- evoked scratching ($P > 0.05$; **Figure 5.2**). However, when the conditioning injection of capsaicin was administered together with QX-314, the scratching evoked by subsequent histamine injection was abolished (**Figure 5.6a**). Administration of capsaicin with QX-314 also significantly reduced, but did not eliminate, scratching produced by subsequent injections of chloroquine ($P < 0.01$; **Figure 5.6b**), even though only a third of chloroquine neurons were capsaicin sensitive (**Figure 5.4e**), implying that the TRPV1$^+$ subset of chloroquine- sensitive neurons may have a particularly prominent role in eliciting behavioral itch responses.

Chloroquine-evoked scratching was virtually abolished 30 min after injection of QX-314 together with AITC (**Figure 5.6b**). In contrast, injection of QX-314 with AITC did not reduce subsequent histamine-evoked scratching (**Figure 5.6a**). In summary, chloroquine-evoked scratching is effectively blocked when TRPA1$^+$ (AITC responsive) fibers are electrically silenced. Histamine-evoked scratching, on the contrary, is largely abolished when TRPV1$^+$ fibers are electrically silenced, but is unaffected when TRPA1$^+$ (AITC responsive) fibers are blocked. Histamine itch is predominantly associated with TRPV1$^+$ pruriceptor fibers, and non-histamine itch is associated with TRPA1$^+$ fibers.

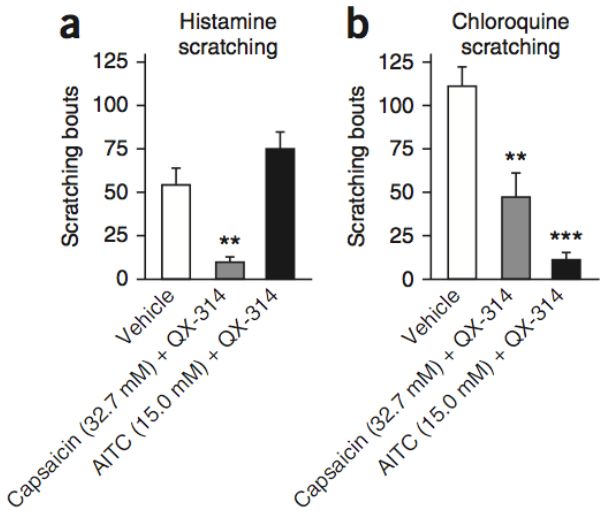

Figure 5.6 - Selective silencing of nociceptor populations differentially inhibits histamine itch and non-histamine itch. (**a** and **b**) Cheek scratching (itch) following intradermal test injection of histamine (100 μg per 10 μl) alone (n = 6 mice, **a**) and chloroquine (CQ, 50 μg per 10 μl) alone (n = 6–7 mice, **b**) 30 min after a conditioning injection of vehicle (0.9% NaCl, 20 μl) or 1% QX-314 together with capsaicin or AITC. P values represent comparison to vehicle (white column) value (not significant, $P > 0.05$; $^{**}P < 0.01$, $^{***}P < 0.001$). Error bars represent s.e.m.

DISCUSSION

We selectively inhibited pain- and itch-related behaviors by targeting the membrane-impermeant sodium channel blocker QX-314 into peripheral axon terminals of distinct populations of trigeminal pruriceptors or nociceptors. The specific population silenced was determined by the pattern of activation of particular large pore channels by different pruritogens or algogens; TRPV1 for capsaicin and histamine, TRPA1 for AITC and chloroquine. Our approach differs from interventions that only block a particular receptor (for example, H1R and H4R)[33] or channel (for example, TRPA1)[34] in that it targets action potential generation and conduction of the activated axon, and differs from genetic targeted ablation of different sensory neuronal subtypes[35] in that it is temporary, with no known compensatory changes.

Using this selective silencing strategy, we found that the fibers that mediate histamine and non-histamine itch are functionally separable. Our *in vitro* data confirm the presence of adult sensory neurons that respond only to histamine or only to chloroquine.

Separate afferent lines have been described for histamine and cowhage itch[16,36] and a distinct non-histamine itch pathway activated by β-alanine[17]. Our data support separate functional pathways for histamine itch and itch mediated by the MrgprA3 and MrgprC11 ligands chloroquine and SLIGRL, respectively. The separation of these afferents on the basis of the silencing approach was defined for a broad range of pruritogen concentrations for targeting QX-314 into afferent terminals through activated TRP channels. At extremely high concentrations (>90 mM) of pruritogen *in vivo*, however, an overlap did occur between histamine and chloroquine populations. This cross-activation between the two populations

could be secondary to release of endogenous mediators from keratinocytes, mast cells or other non-neuronal cells activated secondary to high-dose pruritogen administration, or it could reflect a very limited sensitivity of the peripheral terminals of histaminergic pruriceptors to chloroquine and SLIGRL and of the non-histaminergic terminals to histamine. Given that the high concentrations of the opposing pruritogen required to co-activate the separate histamine or non-histamine responsive set of afferents are unlikely to be found in most natural conditions[29,30], we consider it probable that the two sets are functionally distinct and normally act independently.

Our calcium imaging data also confirm the existence of distinct trigeminal and DRG neuron populations that respond to either chloroquine or histamine at a range of doses in adult mice. Prior *in vitro* experiments have shown that MrgprA3 lineage DRG neurons in juvenile (4 week old) mice respond both to chloroquine (1 mM) and histamine (50 μM)[6]. Similarly, ablation of MrgprA3$^+$ neurons in 5-week-old mice substantially attenuates both chloroquine- and histamine-evoked scratching behavior[15]. However, a recent study found that the proportion of DRG neurons responding to both histamine and chloroquine was markedly less in 7–9-week-old mice compared with 3–4-week-old mice[18]. We interpret these collective data as suggesting that, in adult (2–4 month old) mice, Mrgpra3$^+$ neurons are likely composed of pruriceptors with a differential sensitivity to, but not absolute selectivity for, chloroquine, and that these afferents normally contribute primarily to non-histaminergic itch. Microneurographic studies in humans have identified a distinct set of histamine-insensitive fibers that are activated during cowhage-evoked itch[16]. The finding that cowhage spicules activate MrgprA3$^+$ neurons suggests that a common pathway may mediate chloroquine and cowhage itch[15]. However, cowhage spicules

act nondiscriminatively on many nociceptor subtypes and may instead trigger itch nonspecifically through focal activation of superficial nociceptor terminals[37].

H1R and MrgprA3 receptors rely on downstream activation of TRPV1 or TRPA1 channels, respectively, to generate itch behavior[11,12,14], which is somewhat counterintuitive, as these TRP channels are also activated by algogens (capsaicin and AITC) that normally produce pain. This raises questions as to whether there are different subsets of $TRPV1^+$ or $TRPA1^+$ neurons involved in processing pain or itch and why pain normally predominates. Our data indicate that histamine itch is mediated by $TRPV1^+$ fibers that do not express appreciable levels of TRPA1, as histamine itch is inhibited by silencing capsaicin-activated fibers, but not by silencing AITC-activated fibers. This correlates with the coincidence of capsaicin and histamine responsiveness in most histamine-responsive trigeminal neurons. In contrast, chloroquine itch appears to be mediated mainly by $TRPA1^+$ fibers. However, using capsaicin-induced silencing and trigeminal neuron calcium imaging, we found that a subset of these fibers also co-expressed TRPV1. TRPV1 is therefore broadly expressed in nociceptors and both histaminergic and non- histaminergic pruriceptors.

Our findings suggest that primary afferent itch-generating neurons encode functionally distinct histamine and chloroquine itch pathways. In addition to revealing modality specificity and functional specialization of somatosensory afferents, our findings could also help to direct development of new treatments for itch. Administration of QX-314 may be an effective treatment for pruritus caused by either histamine or non-histamine pruritogens if they are associated with sufficient activation of TRPV1 or TRPA1. Alternatively, given that large-pore channels are present in both histamine- and chloroquine-sensitive pruriceptors, broadly targeting QX-314 into these fibers via co-activation of both TRPV1 and TRPA1 channels, for

example, by using a non-pungent TRPV1/TRPA1 co-activator[23,24,43], may have therapeutic promise for preventing or blocking both histamine-evoked itch and histamine-independent itch, albeit at the expense of also producing analgesia.

Works Cited

1. Grundmann, S. & Stander, S. Chronic pruritus: clinics and treatment. *Ann. Dermatol.* 23, 1–11 (2011).

2. Yosipovitch, G. & Papoiu, A.D. What causes itch in atopic dermatitis? *Curr. Allergy Asthma Rep.* 8, 306–311 (2008).

3. Lee, M.G. *et al.* Agonists of the MAS-related gene (Mrgs) orphan receptors as novel mediators of mast cell-sensory nerve interactions. *J. Immunol.* 180, 2251–2255 (2008).

4. Akiyama, T., Carstens, M.I. & Carstens, E. Enhanced scratching evoked by PAR-2 agonist and 5-HT but not histamine in a mouse model of chronic dry skin itch. *Pain* 151, 378–383 (2010).

5. Papoiu, A.D., Tey, H.L., Coghill, R.C., Wang, H. & Yosipovitch, G. Cowhage-induced itch as an experimental model for pruritus. A comparative study with histamine- induced itch. *PLoS ONE* 6, e17786 (2011).

6. Liu, Q. *et al.* Sensory neuron–specific GPCR Mrgprs are itch receptors mediating chloroquine-induced pruritus. *Cell* 139, 1353–1365 (2009).

7. Akiyama, T., Carstens, M.I. & Carstens, E. Facial injections of pruritogens and algogens excite partly overlapping populations of primary and second-order trigeminal neurons in mice. *J. Neurophysiol.* 104, 2442–2450 (2010).

8. Patel, K.N. & Dong, X. Itch: cells, molecules and circuits. *ACS Chem. Neurosci.* 2, 17–25 (2011).

9. Liu, Q. *et al.* The distinct roles of two GPCRs, MrgprC11 and PAR2, in ich and hyperalgesia. *Sci. Signal.* 4, 45 (2011).

10. Han, S.-K., Mancino, V. & Simon, M.I. Phospholipase Cbeta 3 mediates the scratching response activated by the histamine H1 receptor on C-fiber nociceptive neurons. *Neuron* 52, 691–703 (2006).

11. Imamachi, N. *et al.* TRPV1-expressing primary afferents generate behavioral responses to pruritogens via multiple mechanisms. *Proc. Natl. Acad. Sci. USA* 106, 11330–11335 (2009).

12. Wilson, S.R. *et al.* TRPA1 is required for histamine-independent, Mas-related G protein–coupled receptor–mediated itch. *Nat. Neurosci.* 14, 595–602 (2011).

13. Akiyama, T., Carstens, M.I. & Carstens, E. Enhanced responses of lumbar superficial dorsal horn neurons to intradermal PAR-2 agonist but not histamine in a mouse hindpaw dry skin itch model. *J. Neurophysiol.* 105, 2811–2817 (2011).

14. Shim, W.-S. *et al.* TRPV1 mediates histamine-induced itching via the activation of phospholipase A2 and 12-lipoxygenase. *J. Neurosci.* 27, 2331–2337 (2007).

16. Namer, B. *et al.* Separate peripheral pathways for pruritus in man. *J. Neurophysiol* 100, 2062–2069 (2008).

17. Liu, Q. *et al.* Mechanisms of itch evoked by beta-alanine. *J. Neurosci.* 32, 14532–14537 (2012).

18. Akiyama, T. *et al.* Cross-sensitization of histamine-independent itch in mouse primary sensory neurons. *Neuroscience* 226, 305–312 (2012).

19. Binshtok, A.M., Bean, B.P. & Woolf, C.J. Inhibition of nociceptors by TRPV1- mediated entry of impermeant sodium channel blockers. *Nature* 449, 607–610 (2007).

20. Brenneis, C. *et al.* Phenotyping the function of TRPV1-expressing sensory neurons by targeted axonal silencing. *J. Neurosci.* 33, 315–326 (2013).

21.Kim, H.Y. *et al.* Selectively targeting pain in the trigeminal system. *Pain* 150, 29–40 (2010).

22. Puopolo, M. *et al.* Permeation and block of TRPV1 channels by the cationic lidocaine derivative QX-314. *J. Neurophysiol.* 109, 1704–1723 (2013).

23. Binshtok, A.M. *et al.* Coapplication of lidocaine and the permanently charged sodium channel blocker QX-314 produces a long-lasting nociceptive blockade in rodents. *Anesthesiology* 111, 127–137 (2009).

24. Roberson, D.P., Binshtok, A.M., Blasl, F., Bean, B.P. & Woolf, C.J. Targeting of sodium channel blockers into nociceptors to produce long-duration analgesia: a systematic study and review. *Br. J. Pharmacol.* 164, 48–58 (2011).

25. Chen, J. *et al.* Pore dilation occurs in TRPA1 but not in TRPM8 channels. *Mol. Pain* 5, 3 (2009).

26. Shimada, S.G. & LaMotte, R.H. Behavioral differentiation between itch and pain in mouse. *Pain* 139, 681–687 (2008).

29. Petersen, L.J. Quantitative measurement of extracellular histamine concentrations in intact human skin *in vivo* by the microdialysis technique: methodological aspects. *Allergy* 52, 547–555 (1997).

30. Khalil, I.F. *et al.* Development of ELISA-based methods to measure the anti-malarial drug chloroquine in plasma and in pharmaceutical formulations. *Malar. J.* 10, 249 (2011).

31. Akiyama, T., Carstens, M.I. & Carstens, E. Differential itch- and pain-related behavioral responses and micro-opoid modulation in mice. *Acta Derm. Venereol.* 90, 575–581 (2010).

33. Ohsawa, Y. & Hirasawa, N. The antagonism of histamine H1 and H4 receptors ameliorates chronic allergic dermatitis via anti-pruritic and anti-inflammatory effects in NC/Nga mice. *Allergy* 67, 1014–1022 (2012).

34. Liu, T. & Ji, R.R. Oxidative stress induces itch via activation of transient receptor potential subtype ankyrin 1 in mice. *Neurosci. Bull.* 28, 145–154 (2012).

36. Schmelz, M. *et al.* Chemical response pattern of different classes of C-nociceptors to pruritogens and algogens. *J. Neurophysiol.* 89, 2441–2448 (2003).

37. Namer, B. & Reeh, P. Scratching an itch. *Nat. Neurosci.* 16, 117–118 (2013).

41. Koppert, W., Reeh, P.W. & Handwerker, H.O. Conditioning of histamine by bradykinin alters responses of rat nociceptor and human itch sensation. *Neurosci. Lett.* 152, 117–120 (1993).

43. Leffler, A. *et al.* The vanilloid receptor TRPV1 is activated and sensitized by local anesthetics in rodent sensory neurons. *J. Clin. Invest.* 118, 763–776 (2008).

44. Malin, S.A., Davis, B.M. & Molliver, D.C. Production of dissociated sensory neuron cultures and considerations for their use in studying neuronal function and plasticity. *Nat. Protoc.* 2, 152–160 (2007).

Conclusion

The research I have been privileged to participate in has broadly focused on the mechanisms and pathways of nociception. Nociception as a biological process is still quite mysterious in many ways. Additional tools, compounds, molecules and approaches are necessary to delve further into these mysteries. It is a process I have been enjoyed being a part of.

In spite of clinical and experimental setbacks to developing antagonists to TRPV1, TRPV1 is still an important target for analgesia-development. Using an innovative method to look at TRPV1 sensitization could open another pathway to efficiently finding modulators of TRPV1 sensitization. Using the FDSS7000EX (Hamamatsu) for examining TRPV1 sensitization makes it possible to look at many different compounds and examine these in a more native environment than in heterologous expression systems. I think there is much promise in the modulation of TRPV1 sensitization/desensitization if competitive antagonists of the heat modality are not as safe clinically. I also think non-competitive antagonists could play a valuable role in developing TRPV1-targeted analgesia. Fortunately, this research has led to many additional questions to ask about TRPV1 function in general. Showing that TRPV1 is sensitized by bortezomib, a proteasome inhibitor could lead to understanding about TRPV1 biology if it doesn't lead to analgesic potential in the clinic. So, there are broad implications about the role of TRPV1 still to follow up on. Is TRPV1 actively contributing to nerve damage following bortezomib treatment? Is TRPV1 merely a sensor for the damage that is occurring, or is it both? TRPV1 sensitization is still a critically important research topic.

Teasing apart the pathways in itch using the trigeminal system has shown that itch fibers responsive to chloroquine are distinct from those fibers which respond to histamine. This is an important contribution to the labeled-line debate as well as a nice demonstration of the utility of the QX-314 silencing strategy in probing biology. By examining cultured trigeminal neurons, I confirmed that these cells are largely separate and that they are preferentially connected with TRPA1 (chloroquine) or TRPV1 (histamine). Not only does this study demonstrate the anatomical separation of these cells, but by so doing exhibits a potential approach to treating pruritic conditions. QX-314 will only enter those neurons which are actively firing through TRPA1 or TRPV1, keeping its action specific.

The study on Optovin was a particularly unique opportunity. The pharmacological tools for TRPA1 are still far behind those for TRPV1, although in the particular case of optovin, TRPA1 has the advantage. Optovin is a light-sensitive TRPA1 activator. We showed that it works on TRPA1 expressed in HEK cells, that it is not operative in TRPA1 knockout cells, and that it likely interacts with TRPA1 on a site similar to where mustard oil acts using a 3CK TRPA1 mutant. The potential benefits of this tool are just waiting to be explored.

There are additional variations on the themes mentioned in this dissertation that are worth mentioning. An additional project that I worked on was the role of endothelin-1 in the sensitization of P2X receptors, utilizing a similar approach that we are using in the hamamatsu-based experiments. Additionally, our lab has culturing nociceptors from mouse-embryonic fibroblasts. The TRPA1 and TRPV1 responses of these cells are quite similar to primary sensory neurons, which is quite remarkable. It is conceivable that we should be able to culture enough cells to replace our primary sensory neurons in a 384-well plate and even examine human-derived nociceptors for tendencies to be sensitized or desensitized in a

very interesting and novel model of nociception. In the meantime, we are making attempts to increase the efficiency of our sensitization models in the high-throughput system by utilizing GCaMP3-loxp X $Na_V1.8$-cre animals to either look at *in vivo* sensitization of TRPV1 or increase the signal in our setup relative to noise in the absence of dyes.

Our work on TRPV1 sensitization in an unbiased high-throughput manner is a unique approach. We focus on one phenotypic outcome in native cells after manipulating various signaling pathways with bioactive molecules. There are still many other leads to follow up on and more thoroughly analyze. But in all cases, we are able to look backwards to begin to paint a more solid picture of the nodes and pathways leading to sensitization of TRPV1 in primary sensory neurons.

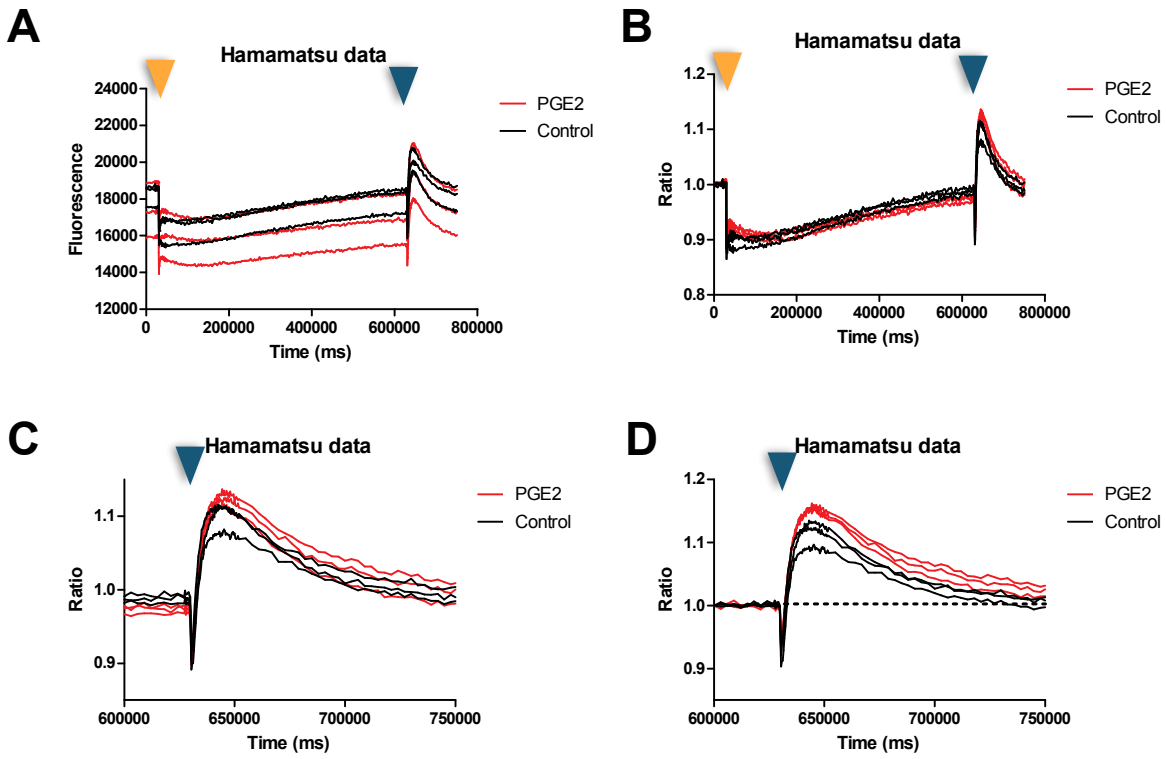

Supplementary Figure 2.1 - Demonstration of raw data from FDSS 7000EX apparatus. **(A)** Raw activation of individual wells. Orange arrow indicates the addition of either 30 μM PGE_2 (red line) or vehicle control (black). The blue arrow indicates the addition of 100 nM capsaicin. **(B)** Same data as in **(A)** only normalized by the first fluorescence value of each well (Ratio - X_n/X_1). **(C)** Showing a closeup of the ratio response with the addition of 100 nM capsaicin where the ratio measurement is set to prior to the addition of the compound. **(D)** A closeup of the ratio response where the ratio standard denominator is adjusted to the 10 minute mark (600000 ms).

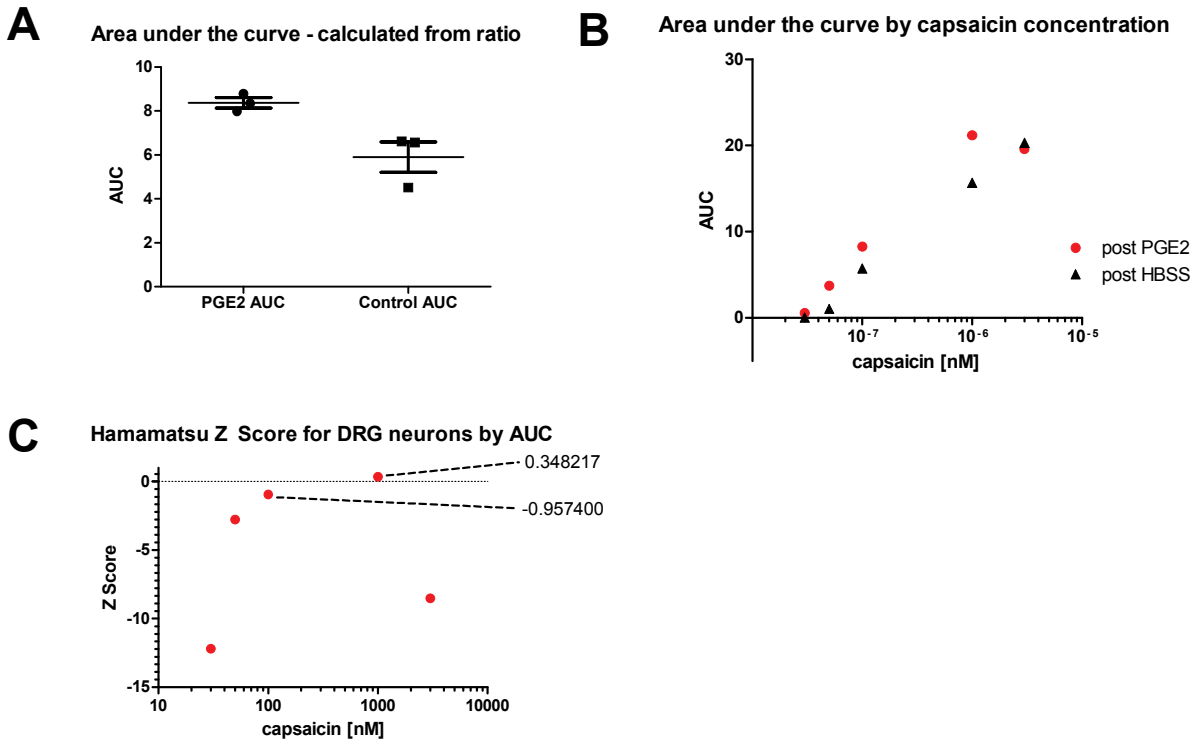

Supplementary Figure 2.2 - Calculation of Z-scores from raw data in FDSS 7000EX apparatus. **(A)** Calculated area under the curve for 60 second time period from the beginning of uniform addition of capsaicin (100 nM) to each well, some treated, some untreated. Showing mean and standard error. **(B)** Concentration response curve for capsaicin following 10 minute treatment with PGE_2 or HBSS (Control) demonstrating increased response at 100 nM and 1 μM capsaicin. **(C)** Z-score calculated by using area under the curve showing the optimal zone of capsaicin concentration for the experiment to be between 100 nM and 1 μM.

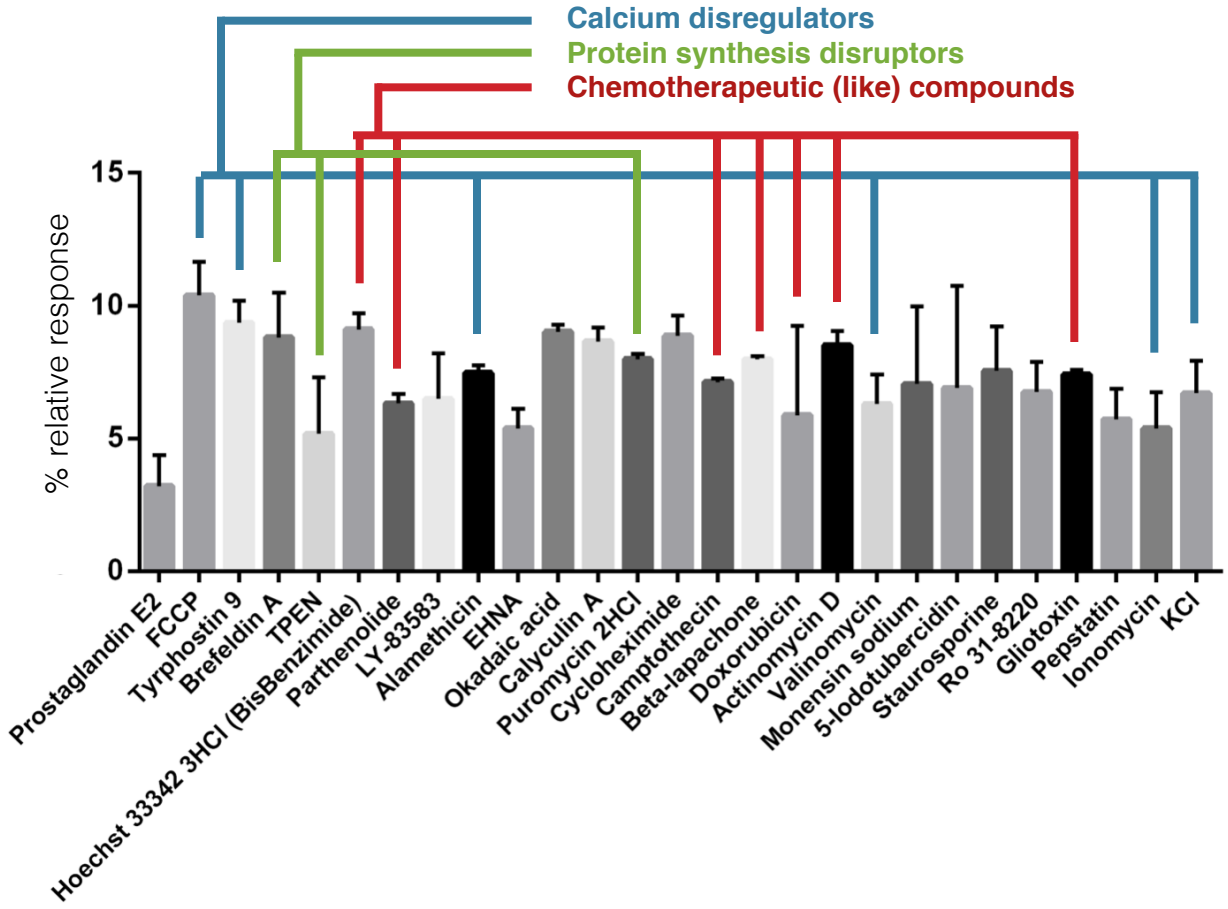

Supplementary Figure 3.1 - Top hits from BioMol screen for TRPV1 sensitization. All compounds are sorted by Fisher's unprotected LSD test, all with P values < 0.05. Prostaglandin E_2 is a positive control. Different mechanistic and therapeutic classes of compounds are represented by colored bars.